Non-methane volatile organic compounds in Africa: a vew from space

Citation

Marais, Eloise Ann. 2014. Non-methane volatile organic compounds in Africa: a vew from space. Doctoral dissertation, Harvard University.

Permanent link

http://nrs.harvard.edu/urn-3:HUL.InstRepos:12274545

Terms of Use

Share Your Story

Non-methane volatile organic compounds in Africa: a view from space

A dissertation presented

by

Eloïse Ann Marais

to

The Department of Earth and Planetary Sciences

in partial fulfillment of the requirements

for the degree of

Doctor of Philosophy

in the subject of

Earth and Planetary Sciences

Harvard University

Cambridge, Massachusetts

February 2014

Dissertation Advisor: Professor Daniel J. Jacob   Eloïse Ann Marais

Non-methane volatile organic compounds in Africa: a view from space

Abstract

Isoprene emissions affect human health, air quality, and the oxidative capacity of the atmosphere. Globally anthropogenic non-methane volatile organic compounds (NMVOC) emissions are lower than that of isoprene, but local hotspots are hazardous to human health and air quality. In Africa the tropics are a large source of isoprene, while Nigeria appears as a large contributor to regional anthropogenic NMVOC emissions. I make extensive use of space-based formaldehyde (HCHO) observations from the Ozone Monitoring Instrument (OMI) and the chemical transport model (CTM) GEOS-Chem to estimate and examine seasonality of isoprene emissions across Africa, and identify sources and air quality consequences of anthropogenic NMVOC emissions in Nigeria.

To estimate isoprene emissions I first developed a filtering scheme to remove (1) contamination from biomass burning and anthropogenic influences; and (2) displacement of HCHO from the isoprene emission source diagnosed with the GEOS-Chem CTM. Conversion to isoprene emissions is with NO_x-dependent GEOS-Chem HCHO yields, obtained as the local sensitivity S of the HCHO column Ω_{HCHO} to a perturbation Δ in isoprene emissions E_{ISOP} ($S = \Delta\Omega_{HCHO}/\Delta E_{ISOP}$). The error in OMI-derived isoprene emissions is 40% at low levels of NO_x and 40-90% under high-NO_x conditions and is reduced by spatial and temporal averaging to the extent that errors are random. Weak isoprene emission seasonality in equatorial forests is driven predominantly by temperature, while large seasonality in northern and southern savannas is driven by temperature and leaf area index. The largest contribution of African isoprene emissions

to surface ozone and particulate matter, determined with GEOS-Chem, of 8 ppbv and 1.5 μg m^{-3}, respectively, is over West Africa.

The OMI HCHO data feature a large enhancement over Nigeria that is due to anthropogenic NMVOC emissions. With the OMI HCHO data, coincident satellite observations of atmospheric composition, aircraft measurements, and GEOS-Chem I estimate Nigerian NMVOC emissions that are higher per capita than China (5.7 Tg C a^{-1}). Should Nigeria develop its electricity sector to sustain economic growth with local natural gas and coal reserves NO$_x$ emissions will exacerbate wintertime (December-February) surface ozone pollution that exceeds 90 ppbv due to poor ventilation and the Harmattan inversion layer.

Table of Contents

Chapter 3: Improved model of isoprene emissions in Africa using OMI satellite observations of formaldehyde: implications for oxidants and particulate matter

Chapter 4: Anthropogenic emissions in Nigeria and air quality implications: a view from space

Appendix

List of Tables

List of Figures

Emva koku nyuka intaba enkulu, umntu uzibona seyejongene nezinye iintaba ekufuneka eziqabele.

"After climbing a great hill, one only finds that there are many more hills to climb"

-Nelson Rolihlahla Mandela

This thesis is dedicated to my mother, Sandra Ann Baxter Marais, whose circumstances prevented her from pursuing a scholarship in the US.

Chapter 1. Overview

Non-methane volatile organic compounds (NMVOCs) are important precursors of tropospheric ozone (Trainer et al., 1987), secondary organic aerosols (SOA) (Claeys et al., 2004), and nitrogen oxide radicals ($NO_x \equiv NO + NO_2$) reservoir species such as organic nitrates (Paulot et al., 2012) and peroxyacetyl nitrates (Pfister et al., 2008). Consequently NMVOCs have local and global impacts on the oxidative capacity of the atmosphere, air quality, climate, and human health. Natural sources of NMVOCs are dominated by isoprene produced in the chloroplasts of plants and released to the atmosphere via the stomata of leaves (Sharkey and Yeh, 2001; Guenther et al., 2006). A wide range of anthropogenic NMVOCs are emitted, some of which are directly harmful to human health. Large sources of anthropogenic NMVOCs include energy use (e.g. fuelwood burning, natural gas flaring) and industrial processes (e.g. solvent evaporation) (Barletta et al., 2005). Field campaigns in Africa have historically focused on NMVOCs from biomass burning (Andreae and Merlet, 2001), but Africa is a large source of isoprene emissions (Stavrakou et al., 2009a) and anthropogenic NMVOCs (Hopkins et al., 2009) and has thus far received little attention due in part to limited ground-based observations.

1.1 NMVOCs in Africa

Isoprene, the dominant biogenic NMVOC emitted from African biomes (Otter et al., 2003), is a larger source contributor than biomass burning to global tropospheric O_3 due to convective uplift of isoprene and its oxidation products in the tropics (Aghedo et al., 2007; Bechara et al., 2010; Bouarar et al., 2011). The tropics appear as a major source region of isoprene from global formaldehyde (HCHO) satellite data (Meyer-Arnek et al., 2005; De Smedt et al., 2008), but emission

estimates from the widely used Model of Emissions of Gases and Aerosols from Nature (MEGAN) inventory are uncertain by a factor of 5 in equatorial Africa (Pfister et al., 2008).

The largest oil and gas industry and only megacity (Lagos: 21 million people) on the continent are located in Nigeria. In Lagos pollution from vehicle exhausts is exacerbated by inefficient vehicles, disorganized road networks, traffic congestion, and unregulated fuel (Assamoi et al., 2010). Benzene levels in Lagos, measured during a field campaign in the 1990s, are 8 times higher than maximum levels measured in Chinese cities (Baumbach et al., 1995; Barletta et al., 2005). More recently high levels of aromatics, alkenes, and alkanes over Lagos, obtained from aircraft measurements of NMVOCs during the African Monsoon Multidisciplinary Analysis (AMMA) field campaign in West Africa in July-August 2006, were attributed to vehicle exhaust emissions, natural gas leakage, and solvent evaporation (Hopkins et al., 2009). A 13-year record of HCHO satellite observations indicates a positive trend in Lagos NMVOC emissions (De Smedt et al., 2010). In the Niger Delta, where oil and gas extraction is concentrated, polycyclic aromatic hydrocarbon (PAH) levels are amongst the highest in the world (Ana et al., 2012), suggesting large NMVOC emissions in the Delta.

Africa is anticipated to experience the highest population growth in the 21st century, with the largest contribution from Nigeria, where currently one in five Africans resides. Economic growth in Nigeria is amongst the highest in the world, due predominantly to the oil and gas industry, and continued economic growth could place Nigeria amongst the top 20 world economies by 2050 (PwC, 2013). Large changes in land cover are expected for Africa over the coming decades due not only to population pressure but also climate change (Boko et al., 2007). Ground-based observations in Africa are scarce, so that low Earth orbit satellites can provide measurements of atmospheric composition for

improved understanding of the sources, spatial distribution, seasonality, and impact on local and regional air quality of biogenic and anthropogenic NMVOCs in Africa.

1.2 Top-down constraints on NMVOCs

Slant columns of HCHO are obtained by spectral fitting of backscattered solar radiation in the 330-360 nm window (Chance et al., 2000). Conversion to the true vertical columns is achieved by applying an air mass factor to the slant columns that accounts for satellite viewing geometry, atmospheric scattering, and sensitivity to the vertical distribution of HCHO (Palmer et al., 2001). Space-based sensors with operational HCHO products include GOME (launched in 1995), SCIAMACHY (2002), OMI (2004), and the two GOME-2 instruments (2006; 2012).

Oxidation of methane and long-lived NMVOCs contribute to background HCHO, while local enhancements in HCHO are from oxidation of reactive NMVOCs. Space-based observations of HCHO have been used to estimate reactive NMVOC emissions and evaluate emission inventories regionally over North America (Palmer et al., 2003, 2006; Millet et al., 2008), South America (Barkley et al., 2008), Europe (Dufour et al., 2009; Curci et al., 2010), and Southeast Asia (Fu et al., 2007), and globally (Stavrakou et al., 2009a, 2009b; Shim et al., 2005). De Smedt et al. (2010) identified large positive trends in anthropogenic NMVOC emissions in megacities by stitching together a 13-year record of space-based observations of HCHO. Previous estimates of above-canopy isoprene emissions are based on the method developed by Palmer et al. (2003) for North America in which an effective HCHO yield S is obtained as the slope of the linear relationship between the HCHO column Ω_{HCHO} and isoprene emissions E_{ISOP} ($\Omega_{HCHO} = S \times E_{ISOP} + B$), where B is background HCHO. Yields of HCHO increase with increasing NO_x, so that in Africa variable NO_x levels may limit the applicability of a uniform value of S to estimate E_{ISOP} from OMI Ω_{HCHO}. More explicit Bayesian (Shim et al., 2005) and

adjoint (Stavrakou et al., 2009b) inversion methods have been applied to global space-based observations of HCHO, but these estimates are hampered by uncertainties in time-dependent yields of HCHO from isoprene oxidation at low levels of NO_x, and coupling between transport and chemistry at timescales relevant to boundary-layer mixing and mesoscale motions.

1.3 Research objectives and approach

This thesis aims to exploit space-based observations of chemical composition over a continent with sparse ground-based observations to better understand the sources, seasonal and spatial variability, and impact of biogenic and anthropogenic NMVOCs on local and regional air quality. As part of the thesis I address the following specific objectives:

- Estimate isoprene emissions under particularly challenging conditions in Africa with space-based observations of HCHO, and the GEOS-Chem chemical transport model updated to include improved treatment of isoprene oxidation.

- Examine the seasonality, identify dominant environmental drivers, and evaluate regional air quality implications of African isoprene emissions with satellite-derived isoprene emissions and GEOS-Chem.

- Use coincident space-based observations of atmospheric composition, sparse aircraft data, and GEOS-Chem to identify and quantify anthropogenic NMVOC emission sources in Nigeria, and assess current and future impacts on local air quality.

To achieve these goals I use HCHO observations from the OMI sensor that offers the advantage over other sensors of high spatial resolution (13×24 km^2 at nadir) that reduces data loss from cloud contamination and decreases errors in the vertical column to the extent that the errors are random.

To estimate isoprene emissions I develop a filtering scheme that uses coincident satellite data to remove scenes contaminated with biomass burning and anthropogenic HCHO. I generate NO_x-dependent yields of HCHO with the GEOS-Chem chemical transport model updated to include improved treatment of isoprene oxidation (Paulot et al., 2009a, 2009b).

In Nigeria I evaluate anthropogenic NMVOC sources with OMI Ω_{HCHO} along with space-based observations of carbon monoxide (CO), nitrogen dioxide (NO_2), methane (CH_4), glyoxal (CHOCHO), and aerosol optical depth (AOD), aircraft observations of anthropogenic emissions, and GEOS-Chem.

1.4 Summary of results

Chapter 2 presents a method for estimating above-canopy isoprene emissions from space-based observations of HCHO from OMI in Africa. HCHO enhancements are from biomass burning, anthropogenic activity, and isoprene emissions. We exclude biomass burning HCHO with satellite observations of fire counts from MODIS and absorbing AOD from OMI. Enhanced HCHO from anthropogenic NMVOC emissions in Nigeria (Chapter 4) is removed with gas flare hotspots observed with the ATSR satellite sensor series. The resulting biogenic slant columns are converted to the true vertical columns with an air mass factor (AMF) that accounts for atmospheric scattering. The local NO_x-dependent sensitivity, S, of the HCHO column Ω_{HCHO} to a perturbation Δ in isoprene emissions E_{ISOP} ($S = \Delta\Omega_{HCHO}/\Delta E_{ISOP}$), determined with GEOS-Chem, is applied to OMI observations of NO_2 and OMI Ω_{HCHO} to estimate above-canopy isoprene emissions. The resulting isoprene emissions are spatially consistent with the distribution of vegetation in Africa and errors in the satellite-derived isoprene emissions are 40% at high levels of NO_x and 40-90% under low-NO_x conditions.

We use our OMI-derived isoprene emissions to investigate the factors controlling African isoprene emissions and investigate implications for atmospheric oxidants and particulate matter in Chapter 3. Large seasonality over savannas is driven by temperature and leaf area index (LAI) and weaker seasonality over equatorial forests is modulated by temperature. OMI-derived isoprene emissions appear biased high compared to limited above-canopy relaxed-eddy accumulation flux measurements from field campaigns in Africa, but the commonly used MEGAN inventory is much worse. MEGAN isoprene emissions are obtained as the product of leaf-level isoprene emissions E_o, LAI, and environmental activity factors. The discrepancy in MEGAN is largely due to E_o, as MEGAN reproduces seasonality over savannas and equatorial forests. An update to MEGAN inventory values of E_o is achieved by obtaining OMI-derived E_o with MEGAN environmental activity factors and OMI isoprene emissions. OMI-derived values of E_o are in good agreement with leaf-level flux measurements for African field sites ($r = 0.55$; bias = -19%) and when implemented in MEGAN leads to a decrease in African isoprene emissions from 104 to 77 Tg C a^{-1}. A GEOS-Chem simulation with the updated MEGAN inventory indicates annual mean increases in surface ozone and particulate matter of up to 8 ppbv and 1.5 μg m^{-3}, respectively, relative to a simulation without African isoprene emissions.

The OMI HCHO data, prior to isolating biogenic HCHO, feature a large HCHO enhancement in Nigeria – more than can be explained by isoprene and biomass burning emissions. HCHO is a high-yield oxidation product of anthropogenic NMVOCs and in Chapter 4 OMI HCHO data over Nigeria are examined with an ensemble of space-based observations of CO, NO_2, CHOCHO, AOD, and CH_4. Emissions of NMVOCs are dominated by aromatics in Lagos with contributions from natural gas leakage, as determined with space-based CHOCHO and HCHO, and aircraft data from the AMMA campaign. In the Niger Delta alkanes from

extensive natural gas leakage is evident from high levels of HCHO and CH_4. GEOS-Chem reproduces satellite HCHO, CHOCHO and CH_4 levels with a 3.5 fold increase in NMVOC emissions to 5.7 Tg C a^{-1} (higher per capita than China) and a 50% increase in CH_4 emissions to 12 Tg CH_4 a^{-1}. Levels of CO, NO_2, and AOD are not particularly high and are dominated by seasonal open fires. GEOS-Chem surface ozone in 2006 is low in summer (June-August) as coastal Nigeria is ventilated by the West African Monsoon. In winter (December-February) ozone exceeds 80 ppbv in south central Nigeria as onshore winds are low and convection is restricted by the Harmattan inversion layer. Should Nigeria develop its electricity sector to sustain current economic growth without emission controls December-February ozone may exceed 100 ppbv.

References:

Aghedo, A. M., Schultz, M. G., and Rast, S.: The influence of African air pollution on regional and global tropospheric ozone, Atmos. Chem. Phys., 7, 1193-1212, 2007.

Ana, G. R. E. E., Sridhar, M. K. C., and Emerole, G. O.: Polycyclic aromatic hydrocarbon burden in ambient air in selected Niger Delta communities in Nigeria, *J. Air Waste Manage*, 62, 18-25, doi:10.1080/10473289.2011.628900, 2012.

Andreae, M. O., and Merlet, P.: Emission of trace gases and aerosols from biomass burning, Global Biogeochem. Cy., 15, 955-966, 2001.

Assamoi, E-M., and Liousse, C.: A new inventory for two-wheel vehicle emissions in West Africa for 2002, *Atmos. Environ.*, 44, 3985-3996, doi:10.1016/j.atmosenv.2010.06.048, 2010.

Barkley, M. P., Palmer, P. I., Kuhn, U., Kesselmeier, J., Chance, K., Kurosu, T. P., Martin, R. V., Helmig, D., and Guenther, A.: Net ecosystem fluxes of isoprene over tropical South America inferred from Global Ozone Monitoring Experiment (GOME) observations of HCHO columns, J. Geophys. Res., 113, D20304, doi:10.1029/2008JD009863, 2008.

Barletta, B., Meinardi, S., Rowland, F. S., Chan, C.-Y., Wang, X., Zou, S., Chan, L. Y., Blake, D. R.: Volatile organic compounds in 43 Chinese cities, *Atmos. Environ.*, 39, 5979-5990, doi:10.1016/j.atmosenv.2005.06.029, 2005.

Baumbach, G., Vogt, U., Hein, K. R. G., Oluwole, A. F., Ogunsola, O. J., Olaniyi, H. B., and Akeredolu, F. A.: Air pollution in a large tropical city with a high traffic density – results of measurements in Lagos, Nigeria, *Sci. Total Environ.*, 169, 25-31, 1995.

Bechara, J., Borbon, A., Jambert, C., Colomb, A., and Perros, P. E.: Evidence of the impact of deep convection on reactive Volatile Organic Compounds in the upper tropical troposphere during the AMMA experiment in West Africa, Atmos. Chem. Phys., 10, 10321-10334, 2010.

Boko, M. et al., *Climate Change 2007: Impacts, Adaptation and Vulnerability. Contribution of Working Group II to the Fourth Assessment Report of the IPCC*, Cambridge University Press, Cambridge, UK, 433-467, 2007.

Bouarar, I., Law, K. S., Pham, M., Liousse, C., Schlager, H., Hamburger, T., Reeves, C. E., Cammas, J.-P., Nédélec, P., Szopa, S., Ravegnani, F., Viciani, S., D'Amato, F., Ulanovsky, A., and Richter, A.: Emission sources contributing to tropospheric ozone over Equatorial Africa during the summer monsoon, Atoms. Chem. Phys., 11, 13395-13419, 2011.

Bowman, K., and Henze, D. K.: Attribution of direct ozone radiative forcing to spatially resolved emissions, *Geophys. Res. Lett.*, 39, L22704, doi:10.1029/2012GL053274, 2012.

Chance, K., Palmer, P. I., Spurr, R. J. D., Martin, R. V., Kurosu, T. P., and Jacob, D. J.: Satellite observations of formaldehyde over North America from GOME, Geophys. Res. Lett., 27, 3461–3464, doi:10.1029/2000GL011857, 2000.

Claeys, M., Graham, B., Vas, G.,Wang,W., Vermeylen, R., Pashynska, V., Cafmeyer, J., Guyon, P., Andreae, M. O., Artaxo, P., and Maenhaut, W.: Formation of secondary organic aerosols through photooxidation of isoprene, Science, 303, 1173–1176, 2004.

Curci, G., Palmer, P. I., Kurosu, T. P., Chance, K., and Visconti, G.: Estimating European volatile organic compound emissions using satellite observations of formaldehyde from the Ozone Monitoring Instrument, Atmos. Chem. Phys., 10, 11501–11517, doi:10.5194/acp-10-11501-2010, 2010.

De Smedt, I., Müller, J.-F., Stavrakou, T., van der A, R., Eskes, H., and Van Roozendael, M.: Twelve years of global observations of formaldehyde in the troposphere using GOME and SCIAMACHY sensors, Atmos. Chem. Phys., 8, 4947–4963, doi:10.5194/acp-8-4947-2008, 2008.

De Smedt, I., Stavrakou, T., Müller, J.-F., van der A, R. J., and van Roozendael, M.: Trend detection in satellite observations of formaldehyde tropospheric columns, Geophys. Res. Lett., 37, L18808, doi:10.1029/2010GL044245, 2010.

Dufour, G., Wittrock, F., Camredon, M., Beekmann, M., Richter, A., Aumont, B., and Burrows, J. P.: SCIAMACHY formaldehyde observations: constraint for isoprene emission estimates over Europe?, Atmos. Chem. Phys., 9, 1647–1664, doi:10.5194/acp-9-1647-2009, 2009.

Fu, T.-M., Jacob, D. J., Palmer, P. I., Chance, K., Wang, Y. X., Barletta, B., Blake, D. R., Stanton, J. C., and Pilling, M. J.: Space-based formaldehyde measurements as constraints on volatile organic compound emissions in east and south Asia and implications for ozone, J. Geophys. Res., 112, D06312, doi:10.1029/2006JD007853, 2007.

Guenther, A., Karl, T., Harley, P., Wiedinmyer, C., Palmer, P. I., and Geron, C.: Estimates of global terrestrial isoprene emissions using MEGAN (Model of Emissions of Gases and Aerosols from Nature), Atmos. Chem. Phys., 6, 3181–3210, doi:10.5194/acp-6-3181-2006, 2006.

Hopkins, J. R., Evans, M. J., Lee, J. D., Lewis, A. C., Marsham, J. H., McQuaid, J. B., Parker, D. J., Stewart, D. J., Reeves, C. E., and Purvis, R. M.: Direct estimates of emissions from the megacity of Lagos, Atmos. Chem. Phys., 9, 8471–8477, doi:10.5194/acp-9-8471-2009, 2009.

Houweling, S., Dentener, F., and Lelieveld, J.: The impact of nonmethane hydrocarbon compounds on tropospheric photochemistry, J. Geophys. Res., 103, D9, doi:10.1029/97JD03582, 1998.

Meyer-Arnek, J., Ladstätter-Weißenmayer, A., Richter, A., Wittrock, F., and Burrows, J. P.: A study of the trace gas columns of O_3, NO_2 and HCHO over Africa in September 1997, Faraday Discuss., 130, 387–405, 2005.

Millet, D. B., Jacob, D. J., Boersma, K. F., Fu, T.-M., Kurosu, T. P., Chance, K., Heald, C. L., and Guenther, A.: Spatial distribution of isoprene emissions from North America derived from formaldehyde column measurements by the OMI satellite sensor, J. Geophys. Res., 113, D02307, doi:10.1029/2007JD008950, 2008.

PwC (Pricewaterhouse Coopers), http://www.pwc.com/en_GX/gx/world-2050/assets/pwc-world-in-2050-report-january-2013.pdf, World in 2050. The BRICs and beyond: prospects, challenges and opportunities, [Accessed: 26 April 2013].

Palmer, P. I., Jacob, D. J., Chance, K., Martin, R. V., Spurr, R. J. D., Kurosu, T. P., Bey, I., Yantosca, R., Fiore, A., and Li, Q.: Air mass factor formulation for spectroscopic measurements from satellites: Application to formaldehyde retrievals from the Global Ozone Monitoring Experiment, J. Geophys. Res., 106, 14539–14550, doi:10.1029/2000JD900772, 2001.

Palmer, P. I., Jacob, D. J., Fiore, A. M., Martin, R. V., Chance, K., and Kurosu, T. P.: Mapping isoprene emissions over North America using formaldehyde column observations from space, J. Geophys. Res., 108, 4180, doi:10.1029/2002JD002153, 2003.

Palmer, P. I., Abbot, D. S., Fu, T.-M., Jacob, D. J., Chance, K., Kurosu, T. P., Guenther, A., Wiedinmyer, C., Stanton, J. C., Pilling, M. J., Pressley, S. N., Lamb, B., and Sumner, A. L.: Quantifying the seasonal and interannual variability of North American isoprene emissions using satellite observations of the formaldehyde column, J. Geophys. Res., 111, D12315, doi:10.1029/2005JD006689, 2006.

Paulot, F., Crounse, J. D., Kjaergaard, H. G., Kroll, J. H., Seinfeld, J. H., and Wennberg, P. O.: Isoprene photooxidation: new insights into the production of acids and organic nitrates, Atmos. Chem. Phys., 9, 1479–1501, doi:10.5194/acp-9-1479-2009, 2009a.

Paulot, F., Crounse, J. D., Kjaergaard, H. G., K¨urten, A., St Clair, J. M., Seinfeld, J. H., and Wennberg, P. O.: Unexpected epoxide formation in the gas-phase photooxidation of isoprene, Science, 325, 730–733, 2009b.

Paulot, F., Henze, D. K., and Wennberg, P. O.: Impact of the isoprene photochemical cascade on tropical ozone, Atmos. Chem. Phys., 12, 1307-1325, 2012.

Pfister, G. G., Emmons, L. K., Hess, P. G., Larmaque, J.-F., Orlando, J. J., Walters, S., Guenther, A., Palmer, P. I., and Lawrence, P. J.: Contribution of isoprene to chemical budgets: A model tracer study with the NCAR CTM MOZART-4, J. Geophys. Res., 113, D05308, doi:10.1029/2007JD008948, 2008.

Sharkey, T. D., and Yeh, S.: Isoprene emission from plants, Annu. Rev. Plant Physiol. Plant Mol. Biol., 52, 407-436, 2001.

Shim, C., Wang, Y., Choi, Y., Palmer, P. I., Abbot, D. S., and Chance, K.: Constraining global isoprene emissions with Global Ozone Monitoring Experiment (GOME) formaldehyde column measurements, J. Geophys. Res., 110, D24301, doi:10.1029/2004JD005629, 2005.

Stavrakou, T., Müller, J.-F., De Smedt, I., Van Roozendael, M., van der Werf, G. R., Giglio, L., and Guenther, A.: Evaluating the performance of pyrogenic and biogenic emission inventories against one decade of space-based formaldehyde columns, Atmos. Chem. Phys., 9, 1037–1060, doi:10.5194/acp-9-1037-2009, 2009a.

Stavrakou, T., Müller, J.-F., De Smedt, I., Van Roozendael, M., van der Werf, G. R., Giglio, L., and Guenther, A.: Global emissions of non-methane hydrocarbons deduced from SCIAMACHY formaldehyde columns through 2003-2006, Atmos. Chem. Phys., 9, 3663-3679, doi:10.5194/acp-9-3663-2009, 2009b.

Trainer, M., Williams, E. J., Parrish, D. D., Buhr, M. P., Allwine, E. J., Westberg, H. H., Fehsenfeld, F. C., and Liu, S. C.: Models and observations of the impact of natural hydrocarbons on rural ozone, Nature, 329, 705–707, 1987.

Chapter 2.   Isoprene emissions in Africa inferred from OMI observations of formaldehyde columns

[E. A. Marais, Jacob, D. J., Kurosu, T. P., Chance, K., Murphy, J. G., Reeves, C., Mills, G., Casadio, S., Millet, D. B., Barkley, M. P., Paulot, F., Mao, J., 2012. Isoprene emissions in Africa inferred from OMI observations of formaldehyde columns. Atmospheric Chemistry and Physics, 12, 6219-6235.

Abstract

We use 2005-2009 satellite observations of formaldehyde (HCHO) columns from the OMI instrument to infer biogenic isoprene emissions at monthly $1\times1°$ resolution over the African continent. Our work includes new approaches to remove biomass burning influences using OMI absorbing aerosol optical depth data (to account for transport of fire plumes) and anthropogenic influences using AATSR satellite data for persistent small-flame fires (gas flaring). The resulting biogenic HCHO columns (Ω_{HCHO}) from OMI follow closely the distribution of vegetation patterns in Africa. We infer isoprene emission (E_{ISOP}) from the local sensitivity $S = \Delta\Omega_{HCHO}/\Delta E_{ISOP}$ derived with the GEOS-Chem chemical transport model using two alternate isoprene oxidation mechanisms, and verify the validity of this approach using AMMA aircraft observations over West Africa and a longitudinal transect across central Africa. Displacement error (smearing) is diagnosed by anomalously high values of S and the corresponding data are removed. We find significant sensitivity of S to NO_x under low-NO_x conditions that we fit to a linear function of tropospheric column NO_2. We estimate a 40 % error in our inferred isoprene

emissions under high-NO_x conditions and 40-90 % under low-NO_x conditions. Our results suggest that isoprene emission from the central African rainforest is much lower than estimated by the state-of-the-science MEGAN inventory.

2.1 Introduction

Isoprene ($CH_2 = C(CH_3)CH = CH_2$) is the dominant non-methane volatile organic compound (NMVOC) emitted by vegetation, accounting for about 50 % of global NMVOC emissions according to current inventories (Guenther et al., 1995; Olivier et al., 1996; Arneth et al., 2008). It is a major precursor of organic aerosol (Claeys et al., 2004; Henze and Seinfeld, 2006; Kroll et al., 2006) and of tropospheric ozone (Trainer et al., 1987; Tao et al., 2003; Fiore et al., 2011), thus impacting air quality, climate, and human health. Isoprene also affects the abundance of OH, the main atmospheric oxidant (Lelieveld et al., 2008; Ren et al., 2008). Satellite observations of formaldehyde (HCHO), a high-yield product of isoprene oxidation, can provide useful constraints on isoprene emissions (Palmer et al., 2003). Here we use HCHO satellite observations from the Ozone Monitoring Instrument (OMI) to better quantify isoprene emissions from the African continent. Africa appears as a major isoprene source region in global HCHO satellite data (Meyer-Arnek et al., 2005; De Smedt et al., 2008), yet it has thus far received little attention.

Isoprene emission inventories in atmospheric chemistry models generally follow the Guenther et al. (1995) framework, which uses base emissions for different ecosystem types modulated by local environmental factors. These inventories are constructed by extrapolation of limited ecosystem data and best understanding of processes, and are commonly called "bottom-up". Arneth et al. (2008) point out that there is considerable uncertainty in bottom-up isoprene emission inventories, more than is apparent from the spread of values in the literature, as all tend to rely on the same limited data and

algorithm framework. Direct isoprene emission measurements in Africa are particularly limited, consisting of a few data for tropical rainforests (Klinger et al., 1998; Greenberg et al., 1999; Serça et al., 2001), woodlands (Greenberg et al., 1999, 2003; Otter et al., 2002), savannas (Guenther et al., 1996; Klinger et al., 1998; Otter et al., 2002; Harley et al., 2003; Saxton et al., 2007), and shrublands (Otter et al., 2002).

An alternate "top-down" approach for estimating above-canopy isoprene emissions is to use HCHO column measurements made by satellites from solar backscatter in the 330–360 nm absorption bands (Chance et al., 2000). Isoprene has an atmospheric lifetime of typically less than 1 h against oxidation by OH, producing HCHO which has a midday lifetime of 1–2 h against photolysis and oxidation by OH. This adds to the HCHO background originating from the oxidation of methane. Thus the HCHO columns measured from space can be related to the underlying isoprene emission (Palmer et al., 2003). Contributions from other biogenic or anthropogenic NMVOCs are generally much weaker because emissions are lower and/or HCHO production is slower (Palmer et al., 2003), although care is needed to screen biomass burning and large anthropogenic influences (Fu et al., 2007; Barkley et al., 2008). Inference of isoprene emissions from HCHO column measurements by the GOME (1995 launch), SCIAMACHY (2002), and OMI (2004) satellite instruments has been reported in a number of studies for North America (Abbot et al., 2003; Palmer et al., 2003, 2006; Millet et al., 2008), Asia (Fu et al., 2007), Europe (Dufour et al., 2009; Curci et al., 2010), South America (Barkley et al., 2008), and globally (Shim et al., 2005; Stavrakou et al., 2009a).

Relating HCHO columns to isoprene emission requires a quantitative relationship between the two obtained with a chemical transport model (CTM). Most of our current understanding of isoprene chemistry has been developed for high concentrations of nitrogen oxide radicals ($NO_x \equiv NO + NO_2$) that originate in the atmosphere from combustion sources and soil emissions. Under these high-NO_x

14

conditions (>1 ppbv NO_x) the organic peroxy radicals (RO_2) produced from isoprene oxidation react preferentially with NO. The resulting HCHO yield is relatively well quantified and is mostly realized in the first stage of isoprene oxidation (Palmer et al., 2003; Millet et al., 2006). Under low-NO_x conditions more typical of Africa, the RO_2 radicals may instead react with HO_2 or isomerize (Peeters et al., 2009), modifying and delaying HCHO yields (Palmer et al., 2003, 2006; Mao et al., 2010). Delay in HCHO production causes smearing in the local relationship between isoprene emission and the HCHO column (Palmer et al., 2003). This smearing can in principle be resolved in a formal inversion accounting for CTM transport (Shim et al., 2005; Stavrakou et al., 2009a) but there is large uncertainty in the coupling between chemical and transport timescales.

Here we use a 5-yr record of OMI HCHO data (2005–2009) to constrain isoprene emissions from the African continent. We convert HCHO columns to isoprene emissions by using the GEOS-Chem CTM with updated isoprene chemistry (Paulot et al., 2009a, 2009b). We introduce a new method to screen biomass burning influence based on OMI observations of aerosol absorption optical depth (AAOD) (Torres et al., 2007) and also screen urban and gas flaring influences. We use aircraft observations from the African Monsoon Multidisciplinary Analysis (AMMA) campaign in West Africa during July–August 2006 (Murphy et al., 2010; Reeves et al., 2010; Stone et al., 2010) to test the GEOS-Chem simulation of isoprene chemistry and estimate smearing in the isoprene-HCHO relationship. We also derive a new approach to account for the NO_x dependence of the isoprene-HCHO relationship using OMI NO_2 data.

2.2 Constructing a data set of OMI biogenic HCHO columns

2.2.1 Slant columns

The Ozone Monitoring Instrument (OMI) (Levelt et al., 2006) was launched onboard the Aura satellite in 2004. It has spatial resolution of 13×24 km^2 at nadir, an equator crossing time of 13:38 local time (LT), and achieves daily global coverage with a cross-track swath width of 2600 km. HCHO slant columns (Ω_s) are a standard product from the OMI instrument, obtained by spectral fitting of backscattered solar radiation in the 327.5–356.5 nm window (http://www.cfa.harvard.edu/atmosphere/Instruments/OMI/PGEReleases/READMEs/ OMHCHO_README.pdf). We use OMHCHO Version 2.0 (Collection 3) retrievals for 2005–2009 from the NASA Data and Information Services Center (http://disc.sci.gsfc.nasa.gov/Aura/ data-holdings/OMI/omhcho_v003.shtml). We exclude observations that (1) do not pass all fitting and statistical quality checks specified in the standard product (*MainDataQualityFlag* = 0), (2) have a cloud fraction >0.4 determined from the OMI O_2–O_2 cloud product (Stammes et al., 2008), or (3) are affected by the OMI row anomaly (http://www.knmi.nl/omi/research/ product/rowanomaly-background.php).

The OMI data feature a slow increase in the baseline Ω_s with time over 2005–2009 that likely reflects degradation of the instrument. We correct for this using observations over the remote Pacific (40–50° S, 150–160° W) where the OMI data are essentially noise. Following the methodology of Kim et al. (2011) we fit a 4th order polynomial function to the baseline slant column $\Omega_{s,b}$ over that region as a function of time t :

$$\Omega_{s,b} = -2.0\times10^3 t^4 + 9.6\times10^6 t^3 - 1.3\times10^{10} t^2 + 7.5\times10^{12} t + 2.5\times10^{15} \qquad (2.1)$$

where $\Omega_{s,b}$ is in molecules cm^{-2} and t is in days ($t = 1$ on 1 January 2005). We remove $\Omega_{s,b}$ calculated

with Eq. (2.1) from the OMI measurement of Ω_s and refer to the residual as Ω_s in what follows.

We thus compile 8-day average values for Ω_s on a 1×1° (lat × lon) grid for 2005–2009 (**Figure**

2.1). The slant column fitting uncertainty for a single observation is $8×10^{15}$ molecules cm^{-2} on average.

8-day and 1×1° averaging reduces the uncertainty to $1–2×10^{15}$ molecules cm^{-2}.

2.2.2   Removing biomass burning and anthropogenic influences

We remove biomass burning and anthropogenic influences from the Ω_s data in order to isolate

the biogenic component. The standard procedure for removing biomass burning is to use space-based

observations of fire counts (Jaeglé et al., 2005; Barkley et al., 2008). We begin with this approach by

using MODIS day and night fire counts from the Terra satellite. The data are provided daily at a

resolution of $1×1$ km^2 (Giglio et al., 2003) and we average them for 8 days on the same 1×1° grid as

Ω_s. We exclude persistent fires associated with large industrial and urban areas of Cairo (Egypt), the

Mpumalanga Highveld region (South Africa), and the Niger Delta (Nigeria). We then remove as

contaminated by biomass burning all gridsquares with non-zero fire counts for the concurrent and

preceding 8-day periods.

Screening only on the basis of fire counts is insufficient as it does not account for the long-

range transport of HCHO in biomass burning plumes. Plume influences on HCHO far downwind of

fires in Africa are evident from Lagrangian analyses of satellite data (Meyer- Arnek et al., 2005) and

AMMA aircraft data (Janicot et al., 2008; Mari et al., 2008; Murphy et al., 2010; Reeves et al., 2010).

Solar backscatter satellite instruments retrieve both HCHO and NO_2, and Barkley et al. (2008)

previously used NO_2 as an additional filter to screen against biomass burning in tropical South

America. However, we find that this filter is insufficient because the atmospheric lifetime of NO_x
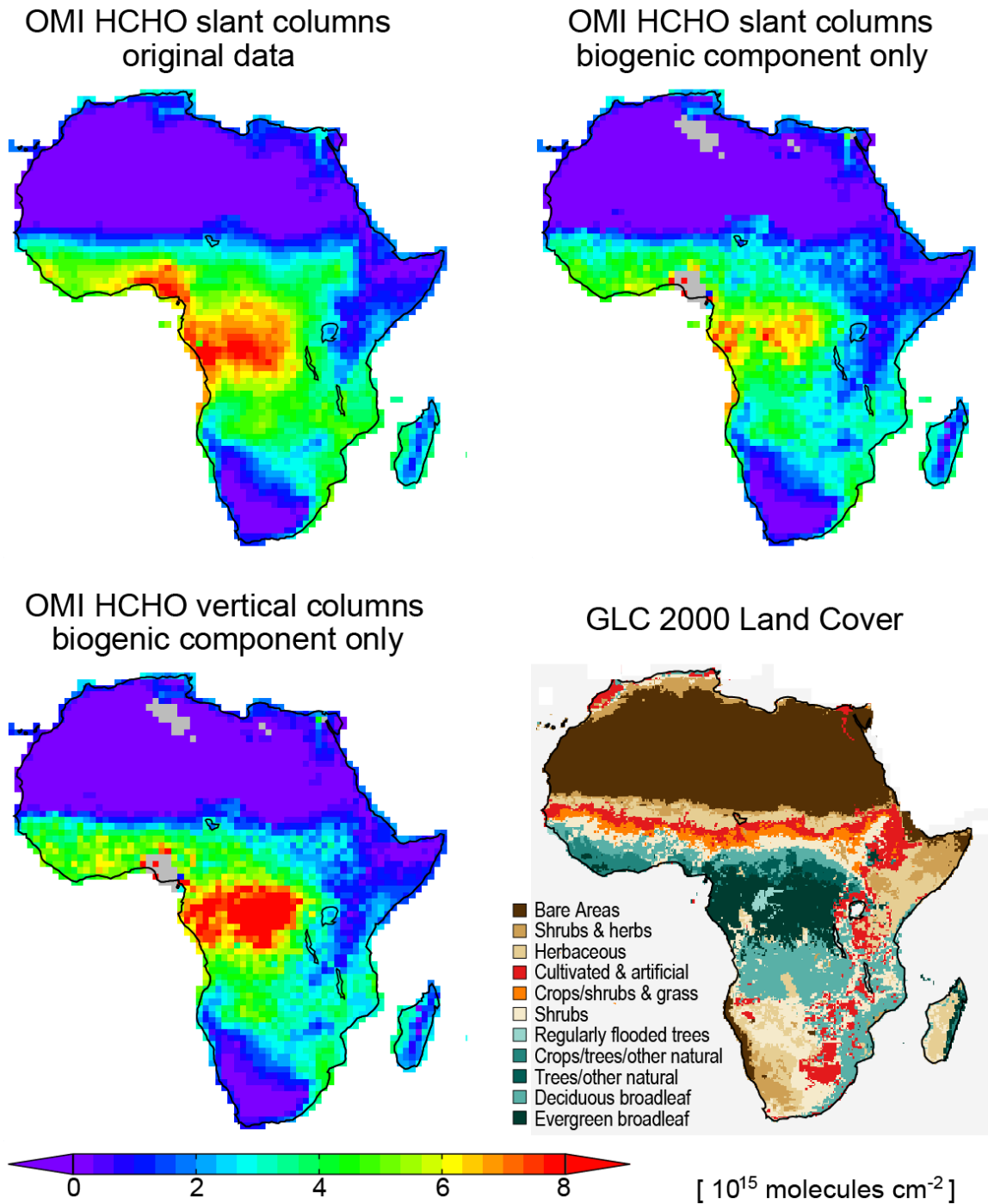
Figure 2.1: HCHO columns and land cover types over Africa. The first three panels are annual mean HCHO columns for 2005–2009 at 1×1° resolution: original slant columns (top left), biogenic slant columns after removing biomass burning, dust, and anthropogenic influences (top right), vertical columns obtained by applying air mass factors (AMFs) to the slant columns (bottom left). The bottom right panel shows the Global Land Cover (GLC) map for 2000 (Bartholomé and Belward, 2005).

emitted from biomass burning is only a few hours, whereas the influence of fires on HCHO is sustained downwind by oxidation of emitted NMVOCs (Hobbs et al., 1996; Trentmann et al., 2003; Alvarado et al., 2010).

Our method to diagnose biomass burning plumes is to use the AAOD product from OMI for the same scenes as HCHO (Torres et al., 2007). Absorbing aerosol is conserved in the plume in the absence of precipitation. We use the level 2 version 3 gridded OMI AAOD product (http://disc.sci.gsfc.nasa.gov/Aura/data-holdings/OMI/omaeruvg_v003.shtml), provided at 0.25×0.25° horizontal resolution, and average it over 8-day periods on the same 1×1° grid as Ω_s. The product includes separate contributions from dust and smoke aerosol but separation between the two can be difficult (Ahn et al., 2008) and we find that smoke AAOD is elevated in dusty regions. To address this problem, we subdivide the continent latitudinally into the Mediterranean strip (north of 20° N), northern Africa (4–19° N), equatorial Africa (5° S–4° N), and southern Africa (south of 5° S). For each region we plot the 5-yr frequency distribution of OMI smoke AAOD, as shown in **Figure 2.2** for southern Africa. This separates biomass burning and non-biomass burning scenes into two populations, and we remove the biomass burning scenes. The smoke AAOD thresholds are 0.02, 0.07, 0.05, and 0.04 for the Mediterranean strip, northern Africa, equatorial Africa, and southern Africa, respectively.

Large dust influence is also problematic in the interpretation of HCHO slant columns because of scattering and absorption by dust. Northern and equatorial Africa can be very dusty. We filter out high dust scenes with the OMI dust AAOD product previously described using a threshold value of 0.1, above which the radiative interference would be of concern. The OMI HCHO data show high values over Nigeria (**Figure 2.1**) that may reflect urban NMVOC emissions in Lagos (Oketola and Osibanjo, 2007; Hopkins et al., 2009; Reeves et al., 2010), biofuel use that is particularly intense in rural Nigeria (Yevich and Logan, 2003), and gas flaring in the Niger Delta (Casadio et al., 2012). Other African
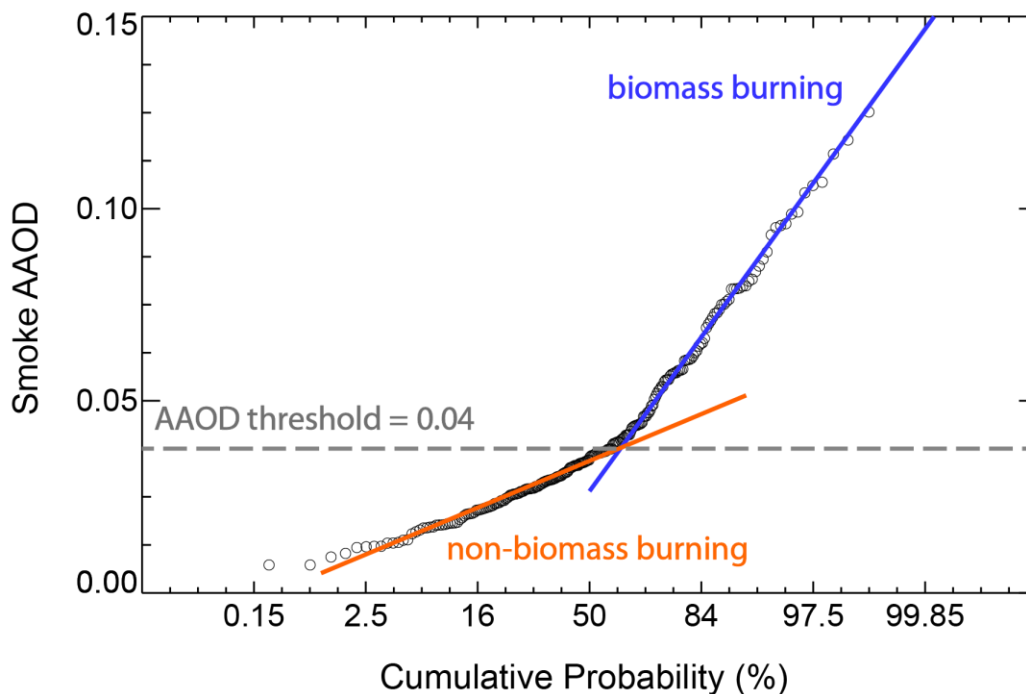
Figure 2.2: Cumulative probability distribution of OMI smoke AAOD 8-day average values at 1×1° resolution over southern Africa (south of 5° S) for 2005–2009. The *x*-axis is a probability scale such that a normal distribution would plot as a straight line. This allows us to separate biomass burning from non-biomass burning conditions by plotting separate regression lines fitted to the bottom and top quantiles of the data. Intersection of these regression lines defines a smoke AAOD threshold for diagnosing biomass burning conditions and we remove the corresponding scenes from the OMI data set. Different AAOD thresholds are used for different regions of Africa as discussed in the text.

countries that practice gas flaring related to the oil and gas industry include Libya, Algeria, Angola, Egypt, Gabon, Sudan, Congo and Tunisia (Casadio et al., 2012). We remove HCHO associated with gas flaring by using gas flare hotspots retrieved in the 1.6 μm band (Algorithm3 or ALGO3) from the Advanced Along Track Scanning Radiometer (AATSR) satellite instrument (Casadio et al., 2012). We average the AATSR fire counts over the same 1×1° grid and 8-day averaging period as OMI and remove gridsquares with non-zero gas flares. Over Nigeria the enhancements in HCHO occur beyond the region of flaring, which may reflect pollution transport as well as Lagos emissions and biofuel use. We therefore remove a more extensive 3×3° area around the gridsquares affected by flaring in Nigeria. The AATSR data do not extend over South Africa due to noise from the South Atlantic Anomaly

(Casadio et al., 2012), but we find that the six oil refineries in South Africa (SAPIA, 2008) are not associated with elevated HCHO in the OMI data of **Figure 2.1**.We therefore see no need for additional screening.

Our filtering scheme to remove biomass burning, dust, and anthropogenic contributions from the OMI Ω_s observations is summarized in **Figure 2.3**. It removes 40 % of observations over Africa on average and 70–80 % in the southern hemisphere during the dry season. These excluded areas account for 27 % of African isoprene emissions in the MEGAN inventory (**Section 2.3.3**). **Figure 2.1** shows the mean OMI Ω_s observations for 2005–2009 before (top left) and after (top right) application of the filtering scheme. The filtered observations are taken to represent biogenic HCHO in what follows.

2.2.3 Conversion to vertical columns

The slant column Ω_s obtained by spectral fitting is related to the true vertical column Ω_{HCHO} by an air mass factor (AMF = Ω_s / Ω_{HCHO}) obtained with a radiative transfer model. We use the formulation of Palmer et al. (2001), which calculates the AMF as the vertical integral of the relative vertical distribution of HCHO (shape factor) weighted by altitude-dependent coefficients (scattering weights). The scattering weights are functions of viewing geometry, surface albedo, and atmospheric scattering by air molecules, aerosols, and clouds. Cloud fraction and cloud top pressure are from the OMI O_2–O_2 cloud product (Stammes et al., 2008). The LIDORT radiative transfer model (Spurr et al., 2001) is used to calculate scattering weights for individual scenes. Clouds are represented by Lambertian surfaces with an albedo of 0.8, as recommended by Koelemeijer and Stammes (1999), and consistent with the O_2–O_2 cloud algorithm. Surface albedo for the African continent is from the OMI reflectance climatology at 345 nm (Kleipool et al., 2008). HCHO and aerosol vertical distributions are monthly mean values from the GEOS-Chem CTM, described in **Section 2.3.1**.
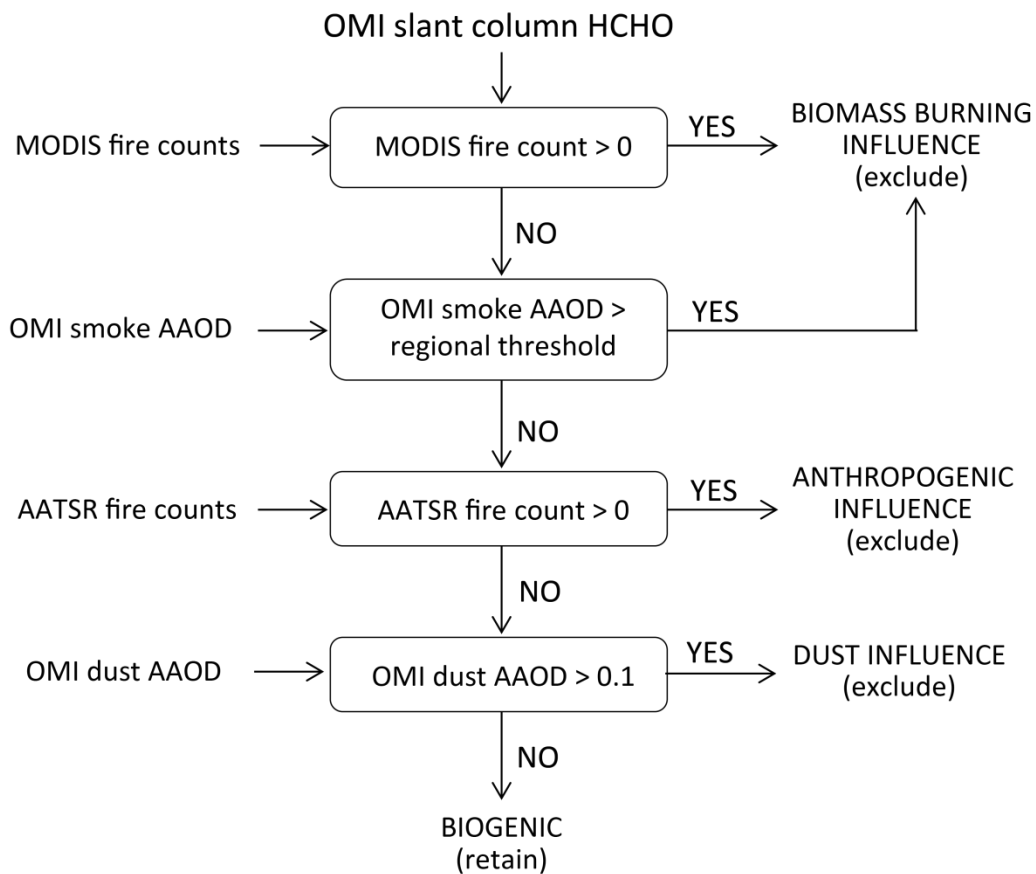
Figure 2.3: Flow chart of the filtering algorithm used to remove biomass burning, dust, and anthropogenic influences in OMI slant HCHO columns (Ω_s). All data are 8-day averages on the same 1×1° grid. The MODIS fire counts filter uses MODIS data for the 8-day periods preceding and concurrent with the OMI HCHO observation.

We find that 62 % of the spatial variability in the annual average AMFs over Africa is driven by OMI surface albedo. The AMF is close to unity for much of the continent (average 1.2), with larger values over the Sahara and Namib Deserts (high albedo) and lower values over central Africa (low albedo). **Figure 2.1** shows the resulting annual mean distribution of HCHO vertical columns Ω_{HCHO}. We see that most of the variability in Ω_{HCHO} is present in the slant column data and thus is not driven by the AMF. The Ω_{HCHO} patterns match closely the distribution of major land types in Africa (**Figure 2.1**), supporting the interpretation of HCHO as a proxy for isoprene emission. Maximum values are found

over evergreen broadleaf forests in the tropics. Low values occur over barren, shrub, herbaceous, and cultivated vegetation. Small-scale biogenic features are apparent such as the forested belt along the east coast of South Africa, crops along the Nile River, and the coastal vegetated Mediterranean strip.

2.3 GEOS-Chem model

2.3.1 General description

We use the GEOS-Chem global 3-D CTM (version 8-03-01, http://geos-chem.org) to (1) estimate the vertical distribution of HCHO for use in the AMF calculation and (2) quantify the relationship between isoprene emissions and HCHO column abundance. GEOS-Chem is driven by Goddard Earth Observing System (GEOS-5) assimilated meteorological data from the NASA Global Modeling and Assimilation Office (GMAO). The GEOS-5 meteorological data have a native horizontal resolution of $0.5 \times 0.67°$ with 72 vertical pressure levels and 6-h temporal frequency (3-h for surface variables and mixing depths). We use data for year 2006 and degrade the horizontal resolution to $2 \times 2.5°$ for input to GEOS-Chem. The model results presented here are from one year of simulation (2006) following one year of spinup for chemical initialization.

Biogenic emission of isoprene is calculated locally in GEOS-Chem using the MEGAN v2.1 inventory (Guenther et al., 2006), with modifications described below. Anthropogenic emissions of NO_x in Africa are from the EDGAR v2.0 inventory (Olivier et al., 1996). Biomass burning NMVOC and NO_x emissions are from the Global Fire Emissions Database v2 (van der Werf et al., 2006). NO_x emissions from soils and fertilizer use are from the algorithm of Yienger and Levy (1995) as implemented by Wang et al. (1998).

Dry deposition in GEOS-Chem follows the standard resistance-in-series scheme of Wesely (1989). In that scheme, gases are deposited as determined by their Henry's law solubility and their

surface reactivity (referenced to ozone). Here we have updated the dry deposition of HCHO and other oxygenated products of isoprene oxidation including methyl vinyl ketone (MVK), methacrolein (MACR), glycolaldehyde, and dicarbonyls to have the same surface reactivity as ozone, based on observational evidence of rapid deposition (Sumner et al., 2001; Karl et al., 2004, 2009) and following the recommendation of Karl et al. (2010). We also include in the model wet and dry deposition of isoprene hydroperoxides and epoxydiols using respective Henry's law constants of 1.7×10^6 M atm^{-1} (US EPA, 2011) and 1.3×10^8 M atm^{-1} (Eddingsaas et al., 2010). We account for the grid-scale transport of isoprene hydroperoxides, which have a sufficiently long lifetime against oxidation by OH (3–5 h; Paulot et al., 2009b) to contribute to spatial displacement (smearing) between isoprene emission and the resulting HCHO columns. Previous inversions of HCHO using GEOS-Chem did not include this transport and would therefore underestimate the smearing under low-NO_x conditions.

2.3.2 Improved treatment of isoprene chemistry

GEOS-Chem includes detailed ozone-NO_x-VOC-aerosol coupled chemistry originally described by Bey et al. (2001) and Park et al. (2004), with recent updates described by Mao et al. (2010).We have updated the rate coefficients for the reactions of HO_2 with $>C_2$ peroxy radicals to Eq. (iv) of Saunders et al. (2003). At 298 K the rate coefficient doubles from 0.8 to 1.6×10^{-11} cm^3 molecule^{-1} s^{-1} relative to previous versions of GEOS-Chem, increasing the relative importance of the low-NO_x isoprene oxidation pathway.

The standard isoprene oxidation scheme used in GEOS-Chem is largely based on Horowitz et al. (1998). As with all conventional schemes, it leads to OH titration by isoprene under low-NO_x conditions when the isoprene peroxy radicals (ISOPOO) produced from the isoprene + OH reaction react with HO_2 rather than NO to form isoprene hydroperoxides (ISOPOOH). This titration is not seen

in observations (Lelieveld et al., 2008; Ren et al., 2008). We implement as an alternate isoprene

oxidation scheme in GEOS-Chem the Paulot et al. (2009b) mechanism, where regeneration of OH

under low-NO_x conditions takes place via oxidation of epoxydiol species produced from oxidation of

ISOPOOH. Isomerization of ISOPOO leading to formation of hydroperoxyaldehydes is another

pathway for OH regeneration (Peeters et al., 2009; Peeters and Müller, 2010), but the kinetics are

highly uncertain (Crounse et al., 2011; Taraborrelli et al., 2012).We compare below results from the

"standard" and "Paulot" schemes to assess the degree of uncertainty in simulating HCHO yields. The

"standard" chemistry scheme is that in version 8-03-01 of GEOS-Chem with updated $RO_2 + HO_2$

kinetics as described above.

Figure 2.4 shows the time-dependent yields of HCHO from isoprene oxidation calculated in

the DSMACC box model (Emmerson and Evans, 2009) for the standard and Paulot schemes, as

implemented in GEOS-Chem with different NO_x levels. Each simulation uses fixed concentrations of

O_3 (28 ppbv), CO (150 ppbv), and NO_x (0.01, 0.1, and 1 ppbv). Isoprene is initially 1 ppbv and allowed

to decay. The temperature is 298 K. Diurnally varying photolysis frequencies are calculated for clear

sky conditions at the Equator with surface albedo of 0.1 and an ozone column of 260 Dobson units.

Under high-NO_x conditions (1 ppbv), we find that the ultimate HCHO yield is approached within a few

hours and is similar for both schemes. Under low-NO_x conditions (0.1 ppbv), the ultimate yield is 10–

20 % lower and takes 1–2 days to achieve, again with similar values for both schemes. The largest

difference is under very low NO_x conditions (0.01 ppbv) where the ultimate yield is 30–40 % lower

than under high-NO_x conditions and the timescale for reaching that yield is 5–6 days. The Paulot

scheme does not show a shorter timescale for reaching the ultimate yield than the standard scheme,

despite higher OH, because it generates more HCHO from later-generation isoprene oxidation

products. The implications of these results for the isoprene-HCHO relationship will be discussed
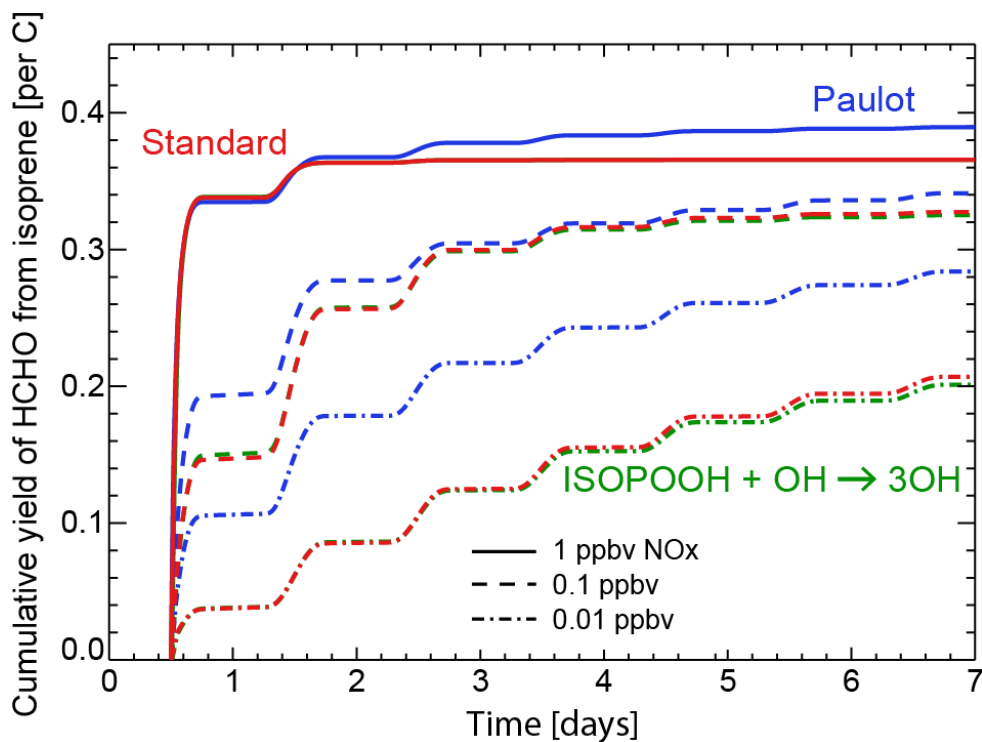
Figure 2.4: Cumulative yields of HCHO per unit carbon from isoprene oxidation as a function of time in the DSMACC chemistry box model using the standard GEOS-Chem chemistry scheme (red), the Paulot scheme (blue), and the standard scheme with artificial generation of OH from isoprene hydroperoxide (ISOPOOH) oxidation (green) for different NO_x levels initialized at local noon. Details on the box model simulation are given in the text.

further in **Section 2.4** in the context of GEOS-Chem results and using OMI NO_2 columns to identify NO_x regimes.

Also shown in **Figure 2.4** are box model results for the standard scheme including artificial OH generation from oxidation of ISOPOOH to prevent OH titration (Lelieveld et al., 2008). We find that this has almost no effect on the HCHO time-dependent yield. The reason is that HCHO formation by the low-NO_x channel involving ISOPOOH is limited in the standard scheme by the slow rate of ISOPOOH photolysis (lifetime of 8 days during daylight hours under box model conditions). Attack of ISOPOOH by OH in the standard scheme is assumed to take place mainly at the peroxide H and thus regenerate the peroxy radical ISOPOO. In the Paulot scheme, this attack results instead in the formation

26

of epoxydiols, with a different HCHO yield as shown in **Figure 2.4**.

2.3.3   MEGAN bottom-up isoprene emission inventory

We use the MEGAN algorithm of Guenther et al. (2006) as our best prior emission estimate for isoprene to which the constraints from the OMI HCHO data can be compared. This inventory is widely used in global CTMs. Isoprene accounts for 80 % of biogenic NMVOC emissions on a per-carbon basis in Africa according to MEGAN. The canopy-scale isoprene emission flux, E_{ISOP}, per unit area of Earth surface (atoms C cm^{-2} s^{-1}) is computed as:

$$E_{ISOP} = E_o \gamma_T \gamma_{AGE} \gamma_{SM} \gamma_{CE} \tag{2.2}$$

Here E_o is the emission at baseline conditions of air temperature (303 K), leaf age (80 % mature, 10 % growing, and 10 % old), volumetric soil moisture (0.3 m^3 m^{-3}), light (1500 µmol photons m^{-2} s^{-1}), and leaf area index (LAI = 5). The dimensionless environmental scaling factors (γ) describe the effects of temperature (T), leaf age (AGE), soil moisture (SM), and canopy radiative environment (CE) on E_o. CE includes the effects of both LAI and light. Values of E_o are specified for five plant functional types (PFTs): broadleaf trees, needleleaf trees, grasses, crops, and shrubs. The global distribution of PFTs is taken from the biome database of Olson et al. (2001), and the distribution of trees in Africa south of the Equator is overwritten by the regional database of Otter et al. (2003).

We apply the environmental scaling factors as given by Guenther et al. (2006) to the local GEOS-5 environment, except for soil moisture. Stavrakou et al. (2009b) found in their analysis of GOME and SCIAMACHY HCHO satellite data that water stress has a major effect on isoprene emissions over southern Africa and is not well represented in MEGAN. We use here the soil moisture

parameterization from Guenther et al. (2006) modified by Müller et al. (2008) and found by Ferreira et al. (2010) to achieve a good simulation of isoprene emission over West Africa during AMMA:

$$\gamma_{SM} = \sum_{i=1}^{n}\left[f_i \times \max\left(0, \min\left(1, \frac{\left(\theta_i - \theta_{i,w}\right)}{0.06} \right) \right) \right] \qquad (2.3)$$

where the summation is over n vertical soil layers, f_i is the root fraction within soil layer i such that

$\sum_{i=1}^{n} f_i = 1$, θ_i is the degree of saturation or volumetric ratio of soil moisture to the porosity of soil (m^3 water m^{-3} air), and $\theta_{i,w}$ is the degree of saturation at the wilting point. The GEOS-5 meteorological data provide θ_i for two layers ($n = 2$): a top soil layer (2 cm) and a root zone layer (1 m). Müller et al. (2008) used a fixed wilting point value of 0.171, but here we use gridded monthly average wilting points, ranging from 0.05 to 0.6 in Africa, from the GEOS-5 catchment land surface model (Koster et al., 2000). We determine f_i within each layer using the parameterization of Zeng (2001) applied to MODIS IGBP landcover (Friedl et al., 2002).

Our resulting global emission of isoprene in GEOS-Chem for 2006 is 470 Tg C a^{-1}, within the 440–660 Tg C a^{-1} range given by Guenther et al. (2006). Africa accounts for 20 % of global isoprene emissions. Implementation of the soil moisture scaling factor γ_{SM} as described above reduces annual isoprene emissions by about 10 % globally and 15 % over Africa. The global reduction in isoprene emissions is less than the 20 % reduction obtained by Müller et al. (2008), likely due to the spatially variable wilting points used here.

2.4 HCHO-isoprene relationship

Previous interpretation of the HCHO column Ω_{HCHO} in terms of above-canopy isoprene emission using GEOS-Chem has relied on a local linear regression between the two quantities in the model (Palmer et al., 2003):

$$\Omega_{HCHO} = S\,E_{ISOP} + B \qquad\qquad\qquad (2.4)$$

where S is the slope of the reduced-major-axis regression line and B is the intercept representing the background HCHO column. The value of S is determined by the HCHO yield from isoprene oxidation and by the HCHO lifetime. Millet et al. (2008) presented estimates of S for North America in summer by performing either a single regression for the ensemble of GEOS-Chem gridsquares covering North America or local regressions for individual 2×2.5° gridsquares. The first method yielded $S = 2.4 \times 10^3$ s with high correlation ($R^2 = 0.82$), while the second yielded variable slopes with an interquartile range of 2.0–3.0×10^3 s. These values were consistent with observation-based estimates for the PROPHET forest site in Michigan (2.1×10^3 s) and INTEX-A aircraft observations over the eastern US (2.3×10^3 s) (Palmer et al., 2003; Millet et al., 2006). Over tropical South America where NO_x levels are much lower, Barkley et al. (2008) found a strong spatial correlation ($R^2 > 0.7$) between E_{ISOP} and Ω_{HCHO} in GEOS-Chem but with large seasonal variability in S – ranging from 1.2×10^3 s in January–March to 2.2×10^3 s in May–July.

Here we use our updated version of GEOS-Chem, together with observational constraints from AMMA and OMI, to examine the local E_{ISOP}–Ω_{HCHO} relationships over Africa and their suitability for inferring isoprene emissions from the HCHO column data. We quantify smearing of the relationship caused by delay in HCHO production from isoprene, develop a parameterization for the dependence of

the E_{ISOP}–Ω_{HCHO} relationship on NO_x, and estimate errors in the resulting isoprene emission estimates.

2.4.1   Smearing

We first examine the extent of smearing in the HCHO-isoprene relationship over Africa using aircraft measurements of isoprene, the sum of MVK and MACR (MVK+MACR), and HCHO concentrations obtained during AMMA in West Africa in July–August 2006 (Murphy et al., 2010; Reeves et al., 2010). The AMMA wet season aircraft campaign (Redelsperger et al., 2006), based in Niamey, Niger, made latitudinal transects across sharp vegetation gradients from ocean to dense woodland to desert (**Figure 2.5**). 19 flights were conducted, mainly during daytime hours. Boundary layer winds were prevailingly from the south (West African Monsoon) (Janicot et al., 2008). We exclude biomass burning plumes as diagnosed by >250 pptv acetonitrile (Commane et al., 2010; Murphy et al., 2010) as well as the flights of 8 August (Lagos urban plume) and 15 August (mesoscale convective system).

      Figure 2.5 shows the AMMA flight tracks superimposed on a map of MODIS LAI for July–August 2006 (Yang et al., 2006), together with latitudinal mean profiles of observed and simulated isoprene, MVK+MACR, and HCHO concentrations below 1 km altitude. The model is sampled along the flight tracks and at the flight times. Also included in **Figure 2.5** is the HCHO concentration below 1 km inferred from OMI observations for July–August 2005–2009 averaged over the AMMA longitudinal domain (1–4° E) into 1° latitude bins (multi-year temporal averaging is needed to reduce measurement noise). The HCHO concentration below 1 km is inferred from OMI HCHO columns by using the mean HCHO vertical profile measured during AMMA (340 pptv above 2 km and linear increase from 2 km down to the surface). The break in the OMI data at 5–7° N reflects the exclusion of anthropogenic influence from Nigeria (**Section 2.2.2**). Boundary layer (<1 km) NO_x concentrations in the region of isoprene emission (7–13° N) averaged 360 pptv in the observations and 310 pptv in the
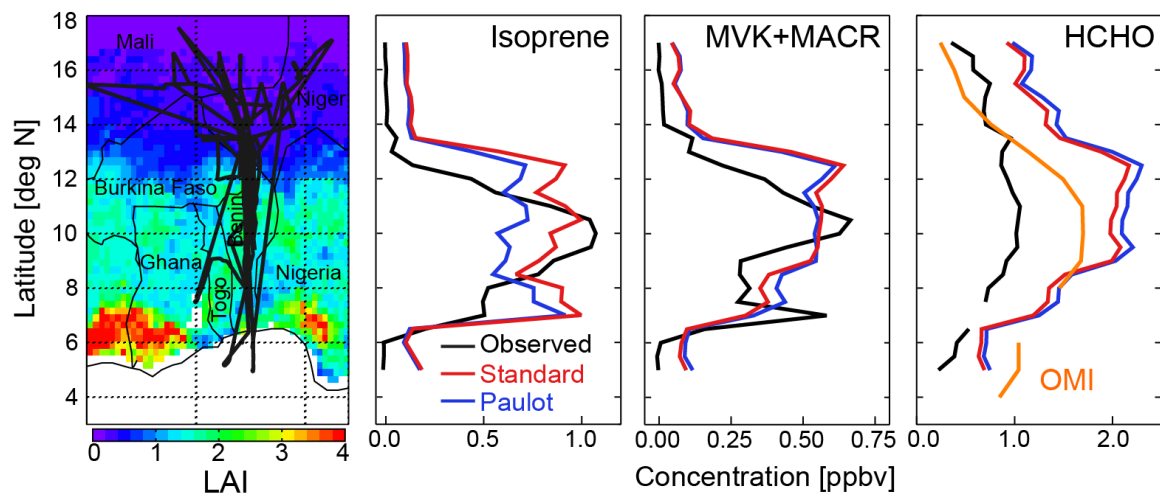
Figure 2.5: Mean latitudinal gradients of boundary layer (<1 km) isoprene, MVK+MACR, and HCHO concentrations during the AMMA aircraft campaign in July–August 2006. The left panel shows the AMMA flight tracks superimposed on a map of MODIS leaf area index (LAI) (Yang et al., 2006) for the AMMA period. Observations averaged over 0.5° latitudinal bins are shown in black. Model results sampled along the flight tracks and at the flight times are shown in red (standard GEOS-Chem isoprene oxidation scheme) and in blue (Paulot scheme). Mean OMI HCHO averaged over 1° latitude bins for July–August 2005–2009 is shown in orange (see text).

model, reflecting a mix of influences from soil, anthropogenic, and distant biomass burning sources (Stewart et al., 2008; Hopkins et al., 2009; Reeves et al., 2010).

The sharp vegetation gradients sampled in AMMA along the direction of the prevailing southerly monsoon winds make the data of great value for understanding smearing in the HCHO-isoprene relationship. We see from **Figure 2.5** that observed isoprene and MVK+MACR tightly follow the vegetation gradients and this is well captured by the model. Model values are much higher than observed at 11–13° N and 7– 8° N, reflecting a local overestimate of E_{ISOP} in MEGAN (Ferreira et al., 2010; Murphy et al., 2010). MVK and MACR are first-stage C_4 isoprene oxidation products, with HCHO produced from the additional carbon atom (Paulson et al., 1992). The tightness of the isoprene–(MVK+MACR) relationship in **Figure 2.5**, both in the observations and the model, demonstrates that there is no significant smearing of these species and provides an important test of the isoprene

oxidation scheme. Model isoprene concentrations are lower in the Paulot scheme because of OH

regeneration from the ISOPOO + HO$_2$ reaction pathway, as described in **Section 2.3.2**, but this has

negligible impact on the simulation of (MVK+MACR).

The far right panel of **Figure 2.5** shows that observed and simulated HCHO are also strongly

correlated with the vegetation gradients. The AMMA observations for HCHO are much lower than the

model or inferred from OMI, and we do not have an explanation for this beyond the possibility of large

bias in the Hantzsch-fluorometric instrument used on the aircraft (Hak et al., 2005, and references

therein). Because HCHO is produced together with MVK+MACR and this first-stage production

accounts for 80–90 % of the ultimate HCHO yield under the AMMA conditions (see below), it would

be difficult to account for a model bias in HCHO but not in MVK+MACR. Tests with the model

indicate little sensitivity to the assumed deposition velocities. In any case, comparison of the HCHO

and isoprene latitudinal gradients shows no significant northward smearing either in the observations or

the model. Correlation between observed isoprene and HCHO is strongest ($R^2 = 0.86$) for a 0.5°

northward shift of HCHO relative to isoprene. Smearing of ~ 0.5°, combined with a mean observed

southerly wind speed of 17 km h^{-1} south of 12° N, implies a timescale of less than a day for production

of HCHO from isoprene.

The negligible smearing in the AMMA observations may reflect the relatively high NO$_x$

conditions and low levels of isoprene, promoting loss of the ISOPOO radicals by reaction with NO

which results in fast HCHO production (high-NO$_x$ pathway). **Figure 2.6** shows the simulated fraction

of ISOPOO radicals reacting with NO across Africa in July 2006 (Paulot scheme). For the AMMA

region that fraction is ~ 50 %. Stone et al. (2010) previously found a 70 % mean fraction during

AMMA using the DSMACC box model constrained by the NO observations.
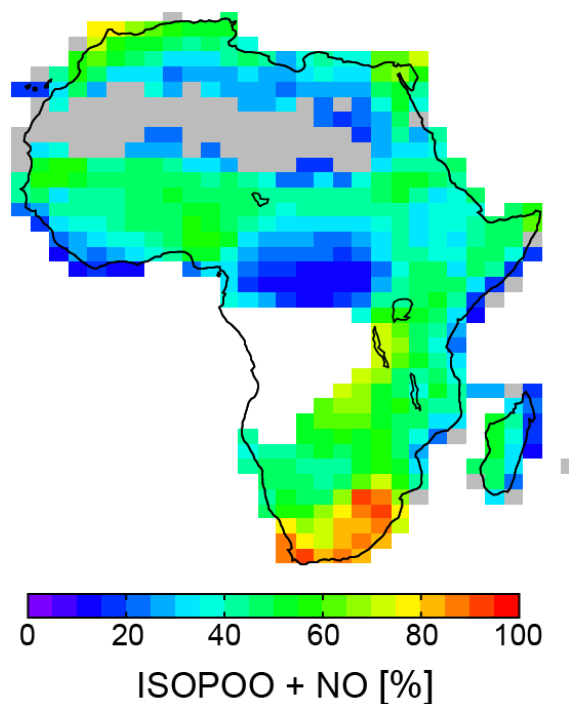
Figure 2.6: Percentage of isoprene peroxy radicals (ISOPOO) reacting with NO in the GEOS-Chem simulation for July 2006 using the Paulot scheme for isoprene chemistry. Values are computed from monthly mean reaction rates. Grey gridsquares have zero isoprene emissions in GEOS-Chem and white gridsquares are screened because of biomass burning influence.

The OMI NO_2 data offer a broad perspective on NO_x regimes across Africa. **Figure 2.7** shows

annual average tropospheric columns of NO_2 (Ω_{NO_2}) from OMI (Boersma et al., 2007) for 2005–2009

and compares to the GEOS-Chem simulation for 2006. Biomass burning influence has been removed

in the observations using MODIS fire counts and OMI AAOD (**Section 2.2.2**) and in GEOS-Chem

with black carbon AOD from the model, for consistency with the removal of biomass burning

influence in the OMI HCHO column product. Assuming a linear decrease of NO_2 mixing ratio from the

surface to 3 km with negligible NO_2 above, based on the AMMA observations (Stewart et al., 2008),

we can make a rough estimate of the boundary layer (<1 km) NO_x concentration from the OMI NO_2

data and this is also shown in **Figure 2.7**. Thus 1 ppbv of boundary layer NO_x corresponds roughly to a

tropospheric NO_2 column of 2×10^{15} molecules cm^{-2}. The fitting precision of 7–8×10^{14} molecules
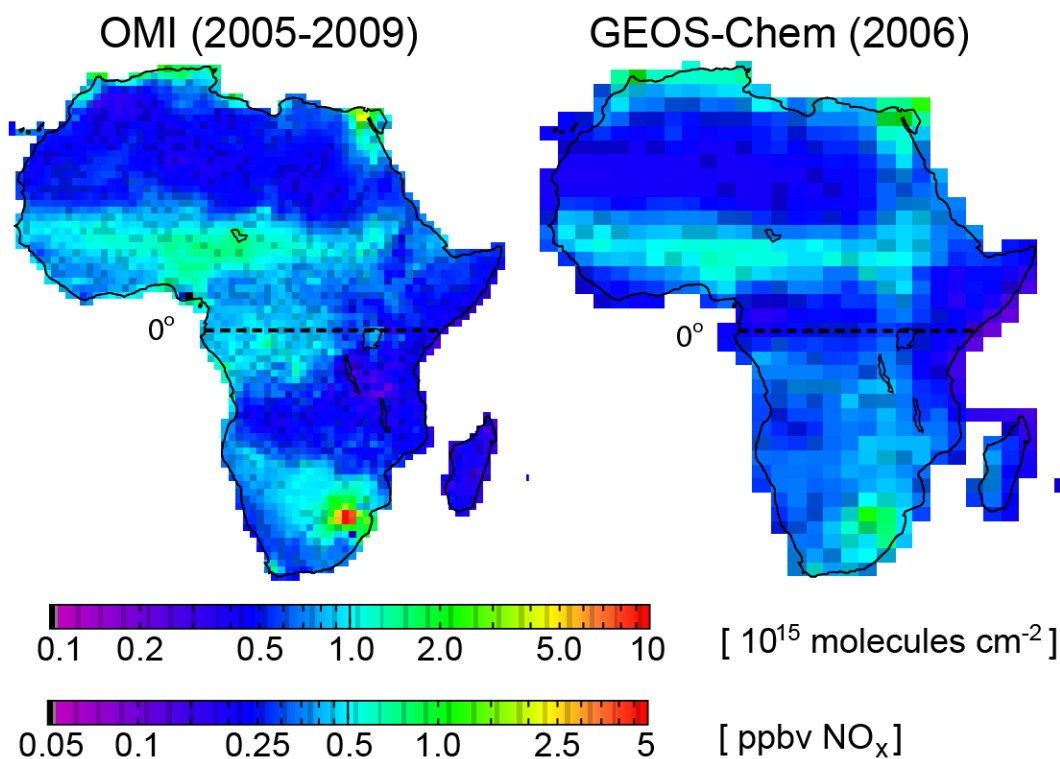
Figure 2.7: Annual mean tropospheric NO_2 columns over Africa at 12:00–15:00 LT. The left panel shows OMI 2005–2009 data at $1\times1°$ resolution (Boersma et al., 2007). The right panel shows GEOS-Chem model values for 2006. The colorbar includes boundary layer (<1 km) NO_x estimated from column NO_2 (see text for details). Biomass burning influence was removed using MODIS fire counts and OMI smoke AAOD in the observations, and black carbon AOD in GEOS-Chem. The Equator is indicated.

cm^{-2} for individual OMI NO_2 pixels (Boersma et al., 2007) is reduced to 3–4×10^{13} molecules cm^{-2} for monthly mean data at $1\times1°$ resolution, so that levels as low as ~ 0.02 ppbv NO_x are detectable. We see in **Figure 2.7** that much of Africa is in an intermediate NO_x regime (0.1–1 ppbv). Even in the absence of continental biomass burning influences, significant boundary layer NO_x levels are maintained in Africa by soil emissions (Jaeglé et al., 2005) and by decomposition of peroxyacetylnitrate (PAN) originating from outside the continent (Singh and Hanst, 1981; Moore and Remedios, 2010).

Inspection of **Figure 2.6** suggests that the equatorial rainforest, where isoprene emissions are very high, could be particularly sensitive to the expected smearing of the HCHO-isoprene relationship.

There the model fraction of ISOPOO radicals reacting with NO is only 15 %, even though boundary

layer NO_x is not particularly low (~ 300 pptv; **Figure 2.7**). That region is ventilated by a steady easterly

wind so that a longitudinal transect can reveal smearing. **Figure 2.8** shows the longitudinal gradients of

MEGAN E_{ISOP}, OMI Ω_{HCHO}, and model column HCHO (standard and Paulot schemes) across the

region at 0–3° N for gridsquares not influenced by biomass burning. Immediately downwind (to the

west) of the rainforest is a shadow region where elevated HCHO does not correspond to collocated

isoprene emission. The shadow region is well reproduced by the model using either the standard or

Paulot scheme. Assuming that MEGAN correctly represents the location of isoprene emission (mainly

determined by the location of the equatorial rainforest), enhancements in OMI Ω_{HCHO} are sustained ~

2–3° west of that location. Combined with a mean easterly wind speed of 5 km h^{-1} this implies a

timescale of ~ 2–3 days for production of HCHO from isoprene, consistent with **Figure 2.4**. We will

see below how we can screen such shadow regions when inferring isoprene emissions from the OMI

HCHO data.

2.4.2 NO_x dependence

We now examine the variability of the Ω_{HCHO}–E_{ISOP} relationship over Africa in GEOS-Chem

measured by the local slope S in equation (2.4). This variability reflects differences in the chemical

environment as well as the effect of smearing in an inhomogeneous isoprene emission field. Millet et

al. (2008) previously examined the spatial variability of S over North America by constructing local

Ω_{HCHO}–E_{ISOP} regressions at the 2×2.5° grid resolution of GEOS-Chem, relying on the temperature-

driven day-to-day variation of E_{ISOP} in a given gridsquare to define a dynamic range for the regression.

We find that this is not an effective approach in Africa as day-to-day variability in isoprene emission is

often small. We derive instead the Ω_{HCHO}–E_{ISOP} relationship in GEOS-Chem by conducting a
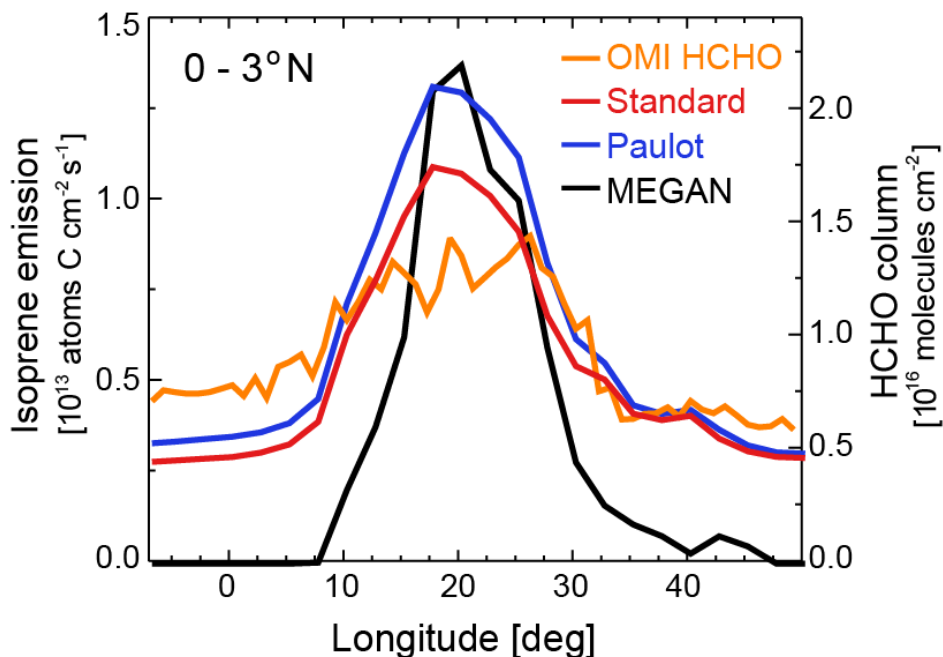
Figure 2.8: Mean longitudinal gradients of isoprene emission (black) and HCHO columns (color) across central Africa (0–3° N) at 12:00–15:00 LT in July. HCHO columns are shown for the OMI observations in 2005–2009 (orange) and from the GEOS-Chem simulations using the standard isoprene oxidation scheme (red) and the Paulot scheme (blue) in 2006. Isoprene emissions are from MEGAN. The HCHO columns have been filtered against biomass burning as described in the text.

sensitivity simulation with isoprene emissions reduced by a factor of 2 from the MEGAN values. We then infer $S = \Delta\Omega_{HCHO} / \Delta E_{ISOP}$ for individual gridsquares and months (gridsquare-months) where Δ is the monthly mean 12:00–15:00 LT change relative to the standard simulation, excluding periods of biomass burning influence (diagnosed with black carbon AOD in the model). Values of S over the southeast US (75–100° W, 27–40° N) for June–August 2006 using this approach are 1.9 and 2.0×10^3 s for the standard and Paulot schemes, respectively, similar to values reported by Millet et al. (2006, 2008) and Palmer et al. (2006).

We find that 41 % of gridsquare–months in GEOS-Chem over Africa have $S > 4 \times 10^3$ s, which is higher than HCHO yields from isoprene emission would allow. This reflects smearing as diagnosed in the model and mainly affects regions where isoprene emissions are very low (such as the vast desert

expanses as well as coastal gridsquares). We exclude this population from further analysis; although

this may seem like a large population to exclude, the corresponding area accounts for only 2 % of

isoprene emission over Africa in MEGAN and thus is largely irrelevant for our purpose.

For the remainder of the data we find a significant dependence of S on the local NO_x

concentration, as would be expected from our box model results in **Figure 2.4**. We choose to define this

relationship in the model in terms of S vs. Ω_{NO_2} so that the OMI Ω_{NO_2} data can be applied to remove

the effects of model errors in NO_x. **Figure 2.9** shows the S values calculated for individual $2\times2.5°$

gridsquare-months over the African continent in 2006 as a function of local model Ω_{NO_2}. The data are

averaged into 1×10^{14} molecules NO_2 cm^{-2} bins. For $\Omega_{NO_2} < 1 \times 10^{15}$ molecules cm^{-2} (roughly 0.5

ppbv boundary layer NO_x using our conversion factor) we find a linear relationship between S and

Ω_{NO_2} ($R^2 > 0.9$) reflecting the increasing importance of the $RO_2 + NO$ pathway with increasing NO_x.

For $\Omega_{NO_2} > 1 \times 10^{15}$ molecules cm^{-2} we find that S levels off as the $RO_2 + NO$ pathway becomes

dominant. 10–20 % higher HCHO yields in the Paulot scheme compared with the standard scheme are

consistent with the box model results of **Figure 2.4**.

2.4.3 Error analysis

Inference of isoprene emission from OMI column HCHO involves a number of steps, all of

which are prone to error. Here we estimate these different error terms and their contributions to the

overall error.

The spectral fitting uncertainty for Ω_s observations averaged over $1\times1°$ gridsquares and 8-day

periods is $1–2 \times 10^{15}$ molecules cm^{-2} (**Section 2.2.1**). We find (not shown) that the model can

reproduce the shape of the mean HCHO vertical profile observed in AMMA (linear decrease from the
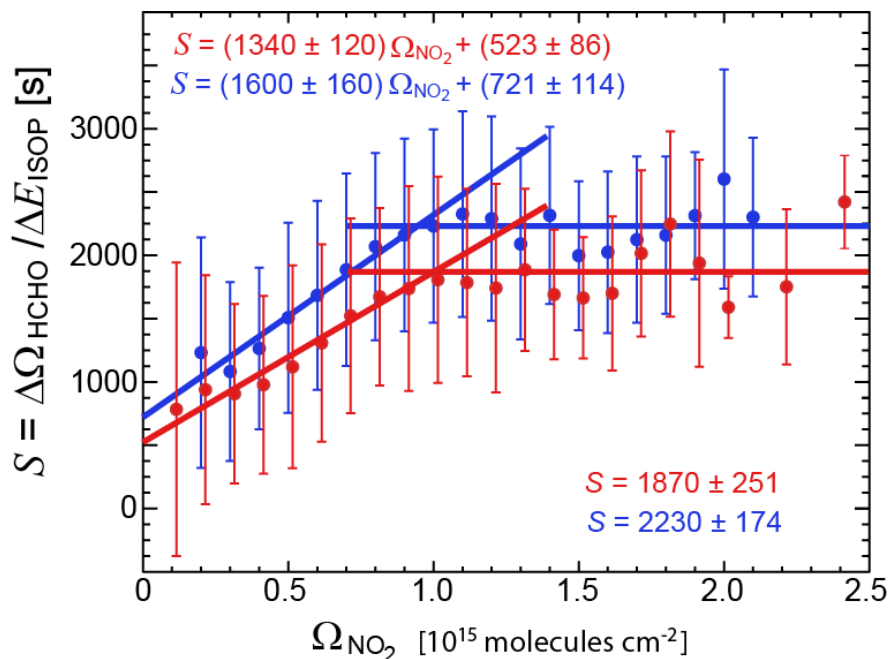
Figure 2.9: Dependence of the HCHO-isoprene relationship on the local tropospheric NO_2 column Ω_{NO_2} over Africa in GEOS-Chem. The figure shows statistics of $S = \Delta\Omega_{HCHO}/\Delta E_{ISOP}$ computed as described in the text for individual $2\times2.5°$ gridsquares and months in 2006 at 12:00–15:00 LT. Values of S have been sorted by the local value of Ω_{NO_2} in 1×10^{14} molecules cm^{-2} bins, and means and standard deviations are shown in each bin for GEOS-Chem using the standard isoprene oxidation scheme (red) and the Paulot scheme (blue). The data for $\Omega_{NO_2} \leq 1 \times 10^{15}$ molecules cm^{-2} show a linear relationship between S and Ω_{NO_2}, and reduced-major-axis regression parameters are shown inset with standard deviations determined using jackknife resampling (Manly, 1997). The data for $\Omega_{NO_2} > 1 \times 10^{15}$ molecules cm^{-2} show no significant dependence between S and Ω_{NO_2}, and the corresponding mean values and standard deviations of S are shown inset.

surface to 2 km, low values above 2 km), consistent with previous results for North America (Palmer et al., 2003; Millet et al., 2006), and suggesting that there is no particular problem in simulating the HCHO vertical shape factor under African conditions. We adopt the AMF error estimate of Millet et al. (2006) derived from aircraft observations in North America: 15 % for clear sky increasing to 24 % for 50 % cloud cover (Millet et al., 2006). Taking a fitting error of 2×10^{15} molecules cm^{-2} and an AMF error of 20 % (since we exclude scenes with >40 % cloud cover), and applying these errors in

quadrature to a vertical HCHO column of 1×10^{16} molecules cm^{-2} with AMF of 1.2, we estimate an

overall error on the OMI HCHO retrieval of 2×10^{15} molecules cm^{-2} or 20 %.

Conversion of HCHO columns to isoprene emission using equation (2.4) involves errors in the

slope S due both to the chemical mechanism and to smearing. **Figure 2.9** shows that the standard and

Paulot mechanisms differ by only 15% in their calculations of S, which is similar to the error estimates

from Palmer et al. (2006) and Millet et al. (2008) in comparing S values from GEOS-Chem to aircraft

and surface observations over the US. The error is certainly larger under low-NO$_x$ conditions where

better understanding of low-NO$_x$ yields of HCHO is needed. The error bars on S shown in **Figure 2.9**

(which we attribute mainly to smearing) are larger than errors induced by the chemical mechanism.

From these error bars we derive a smearing uncertainty in S of 750 s for the low-NO$_x$ regime ($\Omega_{NO_2} =$

0.2–1×10^{15} molecules cm^{-2}) and 690 s for the high-NO$_x$ regime ($\Omega_{NO_2} > 1 \times 10^{15}$ molecules cm^{-2}).

Error in the OMI tropospheric NO$_2$ column also propagates to error in the linear regression

equation $S = (1600 \pm 160 \times 10^{-15}) \times \Omega_{NO_2} + (721 \pm 114)$ for the low-NO$_x$ regime (Paulot scheme in

Figure 2.9). We use the expression from Boersma et al. (2008) to estimate the error standard deviation

σ_{NO_2} (molecules cm^{-2}) for 8-day average Ω_{NO_2} observations:

$$\sigma_{NO_2} = \frac{1.0 \times 10^{15} + 0.3 \times \Omega_{NO_2}}{\sqrt{8} \times \sqrt{3.5}} \qquad\qquad (2.5)$$

and propagate this with the linear regression errors in the slope m ($\sigma_m = 160 \times 10^{-15}$ s cm^2 molecule^{-1})

and intercept c ($\sigma_c = 114$ s). The resulting error standard deviation σ_S in S is

$\sigma_S = \sqrt{\left(m \times \sigma_{NO_2}\right)^2 + \left(\Omega_{NO_2} \times \sigma_m\right)^2 + \sigma_c^2}$ and is in the range 340–440 s for Ω_{NO_2} of 0.2–1.0×10^{15}

molecules cm^{-2}; smaller than the estimated smearing error of 750 s. The error in S at low NO$_x$, adding in quadrature the contributions from smearing and from the linear regression, is 823–870 s (35–84 %).

The overall error in inferring isoprene emission from OMI HCHO columns, adding in quadrature the errors in the OMI retrieval of HCHO columns and the conversion of HCHO columns to isoprene emission, is 40 % in the high-NO$_x$ regime and 40–90 % in the low-NO$_x$ regime. These errors apply to 8-day average 1×1° OMI HCHO data and could be reduced by further temporal averaging to the extent that they are random, which is difficult to assess given the uncertainties associated with the isoprene oxidation mechanism at low levels of NO$_x$.

2.5   Implications for OMI-derived isoprene emissions in Africa

We have presented here a new methodology for inferring isoprene emissions from HCHO satellite data and applied it to the African continent using OMI. Detailed discussion of the implications for African isoprene emissions and their dependence on environmental variables is left to a separate paper. We present here some preliminary results. For this purpose we use the 2005–2009 monthly mean OMI HCHO vertical columns at 1×1° horizontal resolution derived in **Section 2.2**, monthly mean S values computed from GEOS-Chem with the Paulot scheme, and 2005–2009 monthly mean NO$_2$ tropospheric column observations from OMI (Boersma et al., 2007).

Figure 2.10 shows the resulting spatial distribution of annual above-canopy isoprene emissions at 12:00–15:00 LT and compares with the corresponding values from the MEGAN inventory. Values are means for all 1×1° gridsquare-months that are not excluded from our analysis because of biomass burning, anthropogenic, dust, or smearing influences. Fully excluded areas are shown in grey. The right panel shows the difference between the OMI-derived emissions and values from MEGAN.

From the data in **Figure 2.10** we find that the annual mean isoprene emissions in Africa
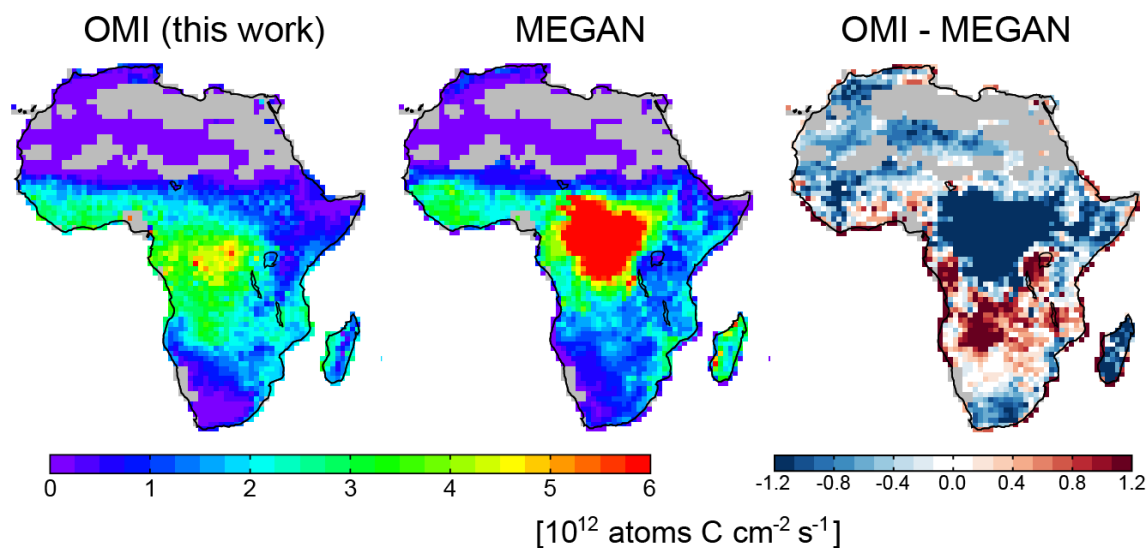
Figure 2.10: Annual average isoprene emissions from Africa at $1\times1°$ horizontal resolution at 12:00–15:00 LT. Values inferred from the OMI HCHO 2005–2009 data (left) are compared to values from the MEGAN bottom-up inventory (center). The right panel shows the difference between the two. Results are for the ensemble of $1\times1°$ gridsquare-months that are not excluded from our analysis due to biomass burning, anthropogenic, dust, or smearing influences (see text). Completely excluded areas are shown in grey.

inferred from OMI (60 Tg C a^{-1}) are on average 22 % lower than the MEGAN values (77 Tg C a^{-1}). Some larger regional discrepancies are apparent. Maximum isoprene emissions in central Africa are displaced north in MEGAN relative to OMI, and OMI is on average 43 % lower than MEGAN over the central African rainforest, and 21 % higher over the southern deciduous broadleaf forests. The discrepancy in central Africa increases to 53 % if scenes with >40 % cloud cover are excluded from the MEGAN emission inventory for consistency with the OMI screening threshold.

2.6 Summary

We presented a new method for inferring biogenic isoprene emissions from satellite observations of HCHO columns under the particularly challenging conditions of the tropics, and applied this method to 2005–2009 OMI HCHO observations over the African continent.

41

Removing biomass burning influence is critical for isolating the biogenic component of HCHO in the tropics. Previous procedures using satellite fire counts or NO_2 columns are insufficient because they do not account for long-range transport of fire plumes. Here we used OMI observations of absorbing aerosol optical depth (AAOD) as an additional screening tool. We also identified a significant anthropogenic component over Africa associated with gas flaring, particularly in Nigeria, and removed it using small-flame satellite fire data. Our resulting biogenic HCHO product shows close correspondence with the distribution of vegetation in Africa.

Inferring isoprene emission from HCHO column data requires knowledge of the time-dependent HCHO yield from isoprene oxidation. This is a challenge in the tropics because of the prevailing low-NO_x conditions under which the isoprene oxidation mechanism is not well understood and HCHO production may be delayed. Here we used two alternate mechanisms to quantify HCHO-isoprene relationships in GEOS-Chem. The two mechanisms show a similar positive NO_x dependence of the HCHO yield under low-NO_x conditions, and a delay between isoprene emission and HCHO production ranging from less than a day under high-NO_x conditions to several days under low-NO_x conditions. This delay smears the local relationship between isoprene emission (E_{ISOP}) and HCHO columns (Ω_{HCHO}).

We evaluated the GEOS-Chem simulation of the HCHO–isoprene relationship using aircraft observations from the AMMA campaign along a latitudinal transect of vegetation types in West Africa. Both observations and model show strong spatial correlation between isoprene, MVK+MACR (first-stage products of isoprene oxidation associated with HCHO formation), and HCHO. This implies insignificant (< 100 km) smearing in the HCHO-isoprene relationship. The conditions for isoprene oxidation in AMMA are intermediate between the low-NO_x and high-NO_x regimes, with 50% of isoprene peroxy radicals (ISOPOO) reacting with NO. Inspection of longitudinal gradients across the

equatorial forest of central Africa, which is more strongly in the low-NO_x regime (15 % of ISOPOO reacting with NO), indicates a smearing of ~ 200–300 km. This means that large isoprene source regions under low-NO_x conditions produce a shadow effect downwind that affects interpretation of the local HCHO-isoprene relationship.

We computed local relationships between HCHO columns and isoprene emission at the 2×2.5° GEOS-Chem grid resolution and on a monthly basis by conducting a sensitivity simulation with uniformly perturbed isoprene emission and inferring the relationship $S = \Delta\Omega_{HCHO} / \Delta E_{ISOP}$. Smearing was diagnosed by anomalously high S values and the corresponding scenes were excluded from further analysis. We found that S is sensitive to NO_x at levels below 500 pptv (tropospheric NO_2 column $\leq 1 \times 10^{15}$ molecules cm^{-2}). From there we used the OMI NO_2 column observations to diagnose S for the corresponding OMI HCHO data. The estimated error in OMI-derived isoprene emissions is 40 % at high NO_x and 40–90 % at low NO_x for 8-day averages with 1×1° resolution. Smearing makes the largest contribution to the estimated error for both NO_x regimes.

We presented a preliminary comparison of the OMI-derived annual mean isoprene emissions over Africa to the values computed from the bottom-up MEGAN inventory. The total OMI-derived isoprene emission for the African continent is 22 % lower than MEGAN. Large regional discrepancies are apparent for the high-emitting evergreen broadleaf trees of central Africa and the southern hemisphere deciduous broadleaf trees. In a follow-up paper we will exploit the OMI HCHO data to develop improved understanding of the environmental, seasonal, and interannual variations in isoprene emission over Africa using the OMI HCHO observations.

The two main uncertainties in using space-based HCHO column data to infer isoprene emission are (1) the isoprene oxidation mechanism as it relates to HCHO production under low-NO_x conditions, (2) the coupling between transport and chemistry determining the displacement between

observed HCHO columns and precursor isoprene emissions. The latter could be addressed by using a CTM adjoint inversion (Stavrakou et al., 2009a). This will eventually be necessary if we are to exploit the fine resolution of the satellite observations (13×24 km^2 in nadir for OMI) to obtain correspondingly fine constraints on isoprene emission. However, the value of such an approach is hampered at present by inadequate knowledge of the time-dependent HCHO yields from isoprene oxidation under low-NO_x conditions, and by the difficulty of representing the coupling between transport and chemistry over timescales relevant to boundary layer mixing and mesoscale motions. Future progress most critically requires an improved understanding of isoprene oxidation chemistry through laboratory and field measurements.

References:

Abbot, D. S., Palmer, P. I., Martin, R. V., Chance, K. V., Jacob, D. J., and Guenther, A.: Seasonal and interannual variability of North American isoprene emissions as determined by formaldehyde column measurements from space, Geophys. Res. Lett., 30, 1886, doi:10.1029/2003GL017336, 2003.

Ahn, C., Torres, O., and Bhartia, P. K.: Comparison of Ozone Monitoring Instrument UV Aerosol Products with Aqua/Moderate Resolution Imaging Spectroradiometer and Multiangle Imaging Spectroradiometer observations in 2006, J. Geophys. Res., 113, D16S27, doi:10.1029/2007JD008832, 2008.

Alvarado, M. J., Logan, J. A., Mao, J., Apel, E., Riemer, D., Blake, D., Cohen, R. C., Min, K.-E., Perring, A. E., Browne, E. C., Wooldridge, P. J., Diskin, G. S., Sachse, G. W., Fuelberg, H., Sessions,W. R., Harrigan, D. L., Huey, G., Liao, J., Case-Hanks, A., Jimenez, J. L., Cubison, M. J., Vay, S. A., Weinheimer, A. J., Knapp, D. J., Montzka, D. D., Flocke, F. M., Pollack, I. B., Wennberg, P. O., Kurten, A., Crounse, J., St. Clair, J. M., Wisthaler, A., Mikoviny, T., Yantosca, R. M., Carouge, C. C., and Le Sager, P.: Nitrogen oxides and PAN in plumes from boreal fires during ARCTAS-B and their impact on ozone: an integrated analysis of aircraft and satellite observations, Atmos. Chem. Phys., 10, 9739–9760, doi:10.5194/acp-10-9739-2010, 2010.

Arneth, A., Monson, R. K., Schurgers, G., Niinemets, Ü., and Palmer, P. I.: Why are estimates of global terrestrial isoprene emissions so similar (and why is this not so for monoterpenes)?, Atmos. Chem. Phys., 8, 4605–4620, doi:10.5194/acp-8-4605-2008, 2008.

Barkley, M. P., Palmer, P. I., Kuhn, U., Kesselmeier, J., Chance, K., Kurosu, T. P., Martin, R. V., Helmig, D., and Guenther, A.: Net ecosystem fluxes of isoprene over tropical South America inferred from Global Ozone Monitoring Experiment (GOME) observations of HCHO columns, J. Geophys. Res., 113, D20304, doi:10.1029/2008JD009863, 2008.

Bartholomé, E. and Belward, A. S.: GLC2000: a new approach to global land cover mapping from Earth observation data, Int. J. Remote Sens., 26, 1959–1977, 2005.

Bey, I., Jacob, D. J., Yantosca, R. M., Logan, J. A., Field, B. D., Fiore, A. M., Li, Q., Liu, H. Y., Mickley, L. J., and Schultz, M. G.: Global modeling of tropospheric chemistry with assimilated meteorology: Model description and evaluation, J. Geophys. Res., 106, 23073–23095, doi:10.1029/2001JD000807, 2001.

Boersma, K. F., Eskes, H. J., Veefkind, J. P., Brinksma, E. J., van der A, R. J., Sneep, M., van den Oord, G. H. J., Levelt, P. F., Stammes, P., Gleason, J. F., and Bucsela, E. J.: Near-real time retrieval of tropospheric NO_2 from OMI, Atmos. Chem. Phys., 7, 2103–2118, doi:10.5194/acp-7-2103-2007, 2007.

Boersma, K. F., Jacob, D. J., Eskes, H. J., Pinder, R. W., Wang, J., and van der A, R. J.: Intercomparison of SCIAMACHY and OMI tropospheric NO_2 columns: Observing the diurnal evolution of chemistry and emissions from space, J. Geophys. Res., 113, D16S26,

doi:10.1029/2007JD008816, 2008.

Casadio, S., Arino, O., and Serpe, D.: Gas flaring monitoring from space using the ATSR instrument series, Remote Sens. Environ., 116, 239–249, doi:10.1016/j.rse.2010.11.022, 2012.

Chance, K., Palmer, P. I., Spurr, R. J. D., Martin, R. V., Kurosu, T. P., and Jacob, D. J.: Satellite observations of formaldehyde over North America from GOME, Geophys. Res. Lett., 27, 3461–3464, doi:10.1029/2000GL011857, 2000.

Claeys, M., Graham, B., Vas, G.,Wang,W., Vermeylen, R., Pashynska, V., Cafmeyer, J., Guyon, P., Andreae, M. O., Artaxo, P., and Maenhaut, W.: Formation of secondary organic aerosols through photooxidation of isoprene, Science, 303, 1173–1176, 2004.

Commane, R., Floquet, C. F. A., Ingham, T., Stone, D., Evans, M. J., and Heard, D. E.: Observations of OH and HO$_2$ radicals over West Africa, Atmos. Chem. Phys., 10, 8783–8801, doi:10.5194/acp-10-8783-2010, 2010.

Crounse, J. D., Paulot, F., Kjaergaard, H. G., and Wennberg, P. O.: Peroxy radical isomerization in the oxidation of isoprene, Phys. Chem. Chem. Phys., 13, 13607–13613, 2011.

Curci, G., Palmer, P. I., Kurosu, T. P., Chance, K., and Visconti, G.: Estimating European volatile organic compound emissions using satellite observations of formaldehyde from the Ozone Monitoring Instrument, Atmos. Chem. Phys., 10, 11501–11517, doi:10.5194/acp-10-11501-2010, 2010.

De Smedt, I., Müller, J.-F., Stavrakou, T., van der A, R., Eskes, H., and Van Roozendael, M.: Twelve years of global observations of formaldehyde in the troposphere using GOME and SCIAMACHY sensors, Atmos. Chem. Phys., 8, 4947–4963, doi:10.5194/acp-8-4947-2008, 2008.

Dufour, G., Wittrock, F., Camredon, M., Beekmann, M., Richter, A., Aumont, B., and Burrows, J. P.: SCIAMACHY formaldehyde observations: constraint for isoprene emission estimates over Europe?, Atmos. Chem. Phys., 9, 1647–1664, doi:10.5194/acp-9-1647-2009, 2009.

Eddingsaas, N. C., VanderVelde, D. G., and Wennberg, P. O.: Kinetics and products of the acid-catalyzed ring-opening of atmospherically relevant butyl epoxy alcohols, J. Phys. Chem. A, 114, 8106–8113, 2010.

Emmerson, K. M. and Evans, M. J.: Comparison of tropospheric gas-phase chemistry schemes for use within global models, Atmos. Chem. Phys., 9, 1831–1845, doi:10.5194/acp-9-1831-2009, 2009.

Ferreira, J., Reeves, C. E., Murphy, J. G., Garcia-Carreras, L., Parker, D. J., and Oram, D. E.: Isoprene emissions modelling for West Africa: MEGAN model evaluation and sensitivity analysis, Atmos. Chem. Phys., 10, 8453–8467, doi:10.5194/acp-10-8453-2010, 2010.

46

Fiore, A. M., Levy II, H., and Jaffe, D. A.: North American isoprene influence on intercontinental ozone pollution, Atmos. Chem. Phys., 11, 1697–1710, doi:10.5194/acp-11-1697-2011, 2011.

Friedl, M. A., McIver, D. K., Hodges, J. C. F., Zhang, X. Y., Muchoney, D., Strahler, A. H., Woodcock, C. E., Gopal, S., Schneider, A., Cooper, A., Baccini, A., Gao, F., and Schaaf, C.: Global land cover mapping from MODIS: algorithms and early results, Remote Sens. Environ., 83, 287–302, 2002.

Fu, T.-M., Jacob, D. J., Palmer, P. I., Chance, K., Wang, Y. X., Barletta, B., Blake, D. R., Stanton, J. C., and Pilling, M. J.: Space-based formaldehyde measurements as constraints on volatile organic compound emissions in east and south Asia and implications for ozone, J. Geophys. Res., 112, D06312, doi:10.1029/2006JD007853, 2007.

Giglio, L., Descloitres, J., Justice, C. O., and Kaufman, Y. J.: An enhanced contextual fire detection algorithm for MODIS, Remote Sens. Environ., 87, 273–282, 2003.

Greenberg, J. P., Guenther, A. B., Madronich, S., Baugh, W., Ginoux, P., Druilhet, A., Delmas, R., and Delon, C.: Biogenic volatile organic compound emissions in central Africa during the Experiment for the Regional Sources and Sinks of Oxidants (EXPRESSO) biomass burning season, J. Geophys. Res., 104, 30659–30671, doi:10.1029/1999JD900475, 1999.

Greenberg, J. P., Guenther, A., Harley, P., Otter, L., Veenendaal, E. M., Hewitt, C. N., James, A. E., and Owen, S. M.: Eddy flux and leaf-level measurements of biogenic VOC emissions from mopane woodland of Botswana, J. Geophys. Res., 108, 8466, doi:10.1029/2002JD002317, 2003.

Guenther, A., Hewitt, C. N., Erickson, D., Fall, R., Geron, C., Graedel, T., Harley, P., Klinger, L., Lerdau, M., McKay, W. A., Pierce, T., Scholes, B., Steinbrecher, R., Tallamraju, R., Taylor, J., and Zimmerman, P.: A global model of natural volatile organic compound emissions, J. Geophys. Res., 100, 8873–8892, doi:10.1029/94JD02950, 1995.

Guenther, A., Otter, L., Zimmerman, P., Greenberg, J., Scholes, R., and Scholes, M.: Biogenic hydrocarbon emissions from southern African savannas, J. Geophys. Res., 101, 25859–25865, doi:10.1029/96JD02597, 1996.

Guenther, A., Karl, T., Harley, P., Wiedinmyer, C., Palmer, P. I., and Geron, C.: Estimates of global terrestrial isoprene emissions using MEGAN (Model of Emissions of Gases and Aerosols from Nature), Atmos. Chem. Phys., 6, 3181–3210, doi:10.5194/acp-6-3181-2006, 2006.

Hak, C., Pundt, I., Trick, S., Kern, C., Platt, U., Dommen, J., Ordóñez, C., Prévôt, A. S. H., Junkermann,W., Astorga-Lloréns, C., Larsen, B. R., Mellqvist, J., Strandberg, A., Yu, Y., Galle, B., Kleffmann, J., Lörzer, J. C., Braathen, G. O., and Volkamer, R.: Intercomparison of four different in-situ techniques for ambient formaldehyde measurements in urban air, Atmos. Chem. Phys., 5, 2881–2900, doi:10.5194/acp-5-2881-2005, 2005.

Harley, P., Otter, L., Guenther, A., and Greenberg, J.: Micrometeorological and leaf-level measurements of isoprene emissions from a southern African savanna, J. Geophys. Res., 108, 8468, doi:10.1029/2002JD002592, 2003.

Henze, D. K. and Seinfeld, J. H.: Global secondary organic aerosol from isoprene oxidation, Geophys. Res. Lett., 33, L09812, doi:10.1029/2006GL025976, 2006.

Hobbs, P. V., Reid, J. S., Herring, J. A., Nance, J. D., Weiss, R. E., Ross, J. L., Hegg, D. A., Ottmar, R. D., and Liousse, C.: Particle and trace gas measurements in the smoke from prescribed burns of forest products in the Pacific Northwest, in: Biomass Burning and Global Change, edited by: Levine, J. S., MIT Press, Cambridge, MA, 697–715, 1996.

Hopkins, J. R., Evans, M. J., Lee, J. D., Lewis, A. C., Marsham, J. H., McQuaid, J. B., Parker, D. J., Stewart, D. J., Reeves, C. E., and Purvis, R. M.: Direct estimates of emissions from the megacity of Lagos, Atmos. Chem. Phys., 9, 8471–8477, doi:10.5194/acp-9-8471-2009, 2009.

Horowitz, L. W., Liang, J., Gardner, G. M., and Jacob, D. J.: Export of reactive nitrogen from North America during summertime: Sensitivity to hydrocarbon chemistry, J. Geophys. Res., 103, 13451–13476, doi:10.1029/97JD03142, 1998.

Jaeglé, L., Steinberger, L., Martin, R. V., and Chance, K.: Global partitioning of NO_x sources using satellite observations: Relative roles of fossil fuel combustion, biomass burning and soil emissions, Faraday Discuss., 130, 407–423, 2005.

Janicot, S., Thorncroft, C. D., Ali, A., Asencio, N., Berry, G., Bock, O., Bourles, B., Caniaux, G., Chauvin, F., Deme, A., Kergoat, L., Lafore, J.-P., Lavaysse, C., Lebel, T., Marticorena, B., Mounier, F., Nedelec, P., Redelsperger, J.-L., Ravegnani, F., Reeves, C. E., Roca, R., de Rosnay, P., Schlager, H., Sultan, B., Tomasini, M., Ulanovsky, A., and ACMAD forecasters team: Large-scale overview of the summer monsoon over West Africa during the AMMA field experiment in 2006, Ann. Geophys., 26, 2569–2595, doi:10.5194/angeo-26-2569-2008, 2008.

Karl, T., Potosnak, M., Guenther, A., Clark, D., Walker, J., Herrick, J. D., and Geron, C.: Exchange processes of volatile organic compounds above a tropical rain forest: Implications for modeling tropospheric chemistry above dense vegetation, J. Geophys. Res., 109, D18306, doi:10.1029/2004JD004738, 2004.

Karl, T., Guenther, A., Turnipseed, A., Tyndall, G., Artaxo, P., and Martin, S.: Rapid formation of isoprene photo-oxidation products observed in Amazonia, Atmos. Chem. Phys., 9, 7753–7767, doi:10.5194/acp-9-7753-2009, 2009.

Karl, T., Harley, P., Emmons, L., Thornton, B., Guenther, A., Basu, C., Turnipseed, A., and Jardine, K.: Efficient atmospheric cleansing of oxidized organic trace gases by vegetation, Science, 330, 816–819, 2010.

Kim, J. H., Kim, S. M., Baek, K. H., Wang, L., Kurosu, T., De Smedt, I., Chance, K., and Newchurch, M. J.: Evaluation of satellite-derived HCHO using statistical methods,

Atmos. Chem. Phys. Discuss., 11, 8003–8025, doi:10.5194/acpd-11-8003-2011, 2011.

Kleipool, Q. L., Dobber, M. R., de Haan, J. F., and Levelt, P. F.: Earth surface reflectance climatology from 3 years of OMI data, J. Geophys. Res., 113, D18308, doi:10.1029/2008JD010290, 2008.

Klinger, L. F., Greenberg, J., Guenther, A., Tyndall, G., Zimmerman, P., M'Bangui, M., Moutsamboté, J.-M., and Kenfack, D.: Patterns in volatile organic compound emissions along a savanna-rainforest gradient in central Africa, J. Geophys. Res., 103, 1443–1454, doi:10.1029/97JD02928, 1998.

Koelemeijer, R. B. A. and Stammes, P.: Validation of Global Ozone Monitoring Experiment cloud fractions relevant for accurate ozone column retrieval, J. Geophys. Res., 104, 18801–18814, doi:10.1029/1999JD900279, 1999.

Koster, R. D., Suarez, M. J., Ducharne, A., Stieglitz, M., and Kumar, P.: A catchment-based approach to modeling land surface processes in a general circulation model 1, Model structure, J. Geophys. Res., 105, 24809–24822, doi:10.1029/2000JD900327, 2000.

Kroll, J. H., Ng, N. L., Murphy, S. M., Flagan, R. C., and Seinfeld, J. H.: Secondary organic aerosol formation from isoprene photooxidation, Environ. Sci. Technol., 40, 1869–1877, 2006.

Lelieveld, J., Butler, T. M., Crowley, J. N., Dillon, T. J., Fischer, H., Ganzeveld, L., Harder, H., Lawrence, M. G., Martinez, M., Taraborrelli, D., and Williams, J.: Atmospheric oxidation capacity sustained by a tropical forest, Nature, 452, 737–740, 2008.

Levelt, P. F., van den Oord, G. H. J., Dobber, M. R., Mälkki, A., Visser, H., de Fries, J., Stammes, P., Lundell, J. O. V., and Saari, H.: The Ozone Monitoring Instrument, IEEE T. Geosci. Remote Sens., 44, 1093–1101, 2006.

Manly, B. F. J.: Randomization, bootstrap and Monte Carlo methods in biology, Chapman and Hall, New York., 1997.

Mao, J., Jacob, D. J., Evans, M. J., Olson, J. R., Ren, X., Brune, W. H., St. Clair, J. M., Crounse, J. D., Spencer, K. M., Beaver, M. R., Wennberg, P. O., Cubison, M. J., Jimenez, J. L., Fried, A., Weibring, P., Walega, J. G., Hall, S. R., Weinheimer, A. J., Cohen, R. C., Chen, G., Crawford, J. H., McNaughton, C., Clarke, A. D., Jaeglé, L., Fisher, J. A., Yantosca, R. M., Le Sager, P., and Carouge, C.: Chemistry of hydrogen oxide radicals (HO$_x$) in the Arctic troposphere in spring, Atmos. Chem. Phys., 10, 5823–5838, doi:10.5194/acp-10-5823-2010, 2010.

Mari, C. H., Cailley, G., Corre, L., Saunois, M., Attié, J. L., Thouret, V., and Stohl, A.: Tracing biomass burning plumes from the Southern Hemisphere during the AMMA 2006 wet season experiment, Atmos. Chem. Phys., 8, 3951–3961, doi:10.5194/acp-8-3951-2008, 2008.

Meyer-Arnek, J., Ladstätter-Weißenmayer, A., Richter, A., Wittrock, F., and Burrows, J. P.: A

study of the trace gas columns of O_3, NO_2 and HCHO over Africa in September 1997, Faraday Discuss., 130, 387–405, 2005.

Millet, D. B., Jacob, D. J., Turquety, S., Hudman, R. C., Wu, S., Fried, A., Walega, J., Heikes, B. G., Blake, D. R., Singh, H. B., Anderson, B. E., and Clarke, A. D.: Formaldehyde distribution over North America: Implications for satellite retrievals of formaldehyde columns and isoprene emission, J. Geophys. Res., 111, D24S02, doi:10.1029/2005JD006853, 2006.

Millet, D. B., Jacob, D. J., Boersma, K. F., Fu, T.-M., Kurosu, T. P., Chance, K., Heald, C. L., and Guenther, A.: Spatial distribution of isoprene emissions from North America derived from formaldehyde column measurements by the OMI satellite sensor, J. Geophys. Res., 113, D02307, doi:10.1029/2007JD008950, 2008.

Moore, D. P. and Remedios, J. J.: Seasonality of Peroxyacetyl nitrate (PAN) in the upper troposphere and lower stratosphere using the MIPAS-E instrument, Atmos. Chem. Phys., 10, 6117–6128, doi:10.5194/acp-10-6117-2010, 2010.

Müller, J.-F., Stavrakou, T., Wallens, S., De Smedt, I., Van Roozendael, M., Potosnak, M. J., Rinne, J., Munger, B., Goldstein, A., and Guenther, A. B.: Global isoprene emissions estimated using MEGAN, ECMWF analyses and a detailed canopy environment model, Atmos. Chem. Phys., 8, 1329–1341, doi:10.5194/acp-8-1329-2008, 2008.

Murphy, J. G., Oram, D. E., and Reeves, C. E.: Measurements of volatile organic compounds over West Africa, Atmos. Chem. Phys., 10, 5281–5294, doi:10.5194/acp-10-5281-2010, 2010.

Oketola, A. A. and Osibanjo, O.: Estimating sectoral pollution load in Lagos by Industrial Pollution Projection System (IPPS), Sci. Total Environ., 377, 125–141, 2007.

Olivier, J. G. J., Bouwman, A. F., van der Maas, C. W. M., Berdowski, J. J. M., Veldt, C., Bloos, J. P. J., Visschedijk, A. J. H., Zandveld, P. Y. J., and Haverlag, J. L.: Description of EDGAR Version 2.0: A set of global emission inventories of greenhouse gases and ozone-depleting substances for all anthropogenic and most natural sources on a per country basis and on 1×1° grid, Bilthoven, The Netherlands., 1996.

Olson, D. M., Dinerstein, E., Wikramanayake, E. D., Burgess, N. D., Powell, G. V. N., Underwood, E. C., D'amico, J. A., Itoua, I., Strand, H. E., Morrison, J. C., Loucks, C. J., Allnutt, T. F., Rickets, T. H., Kura, Y., Lamoreux, J. F., Wettengel, W. W., Hedao, P., and Kassem, K. R.: Terrestrial ecoregions of the world: a new map of life on earth, BioScience, 51, 933–938, 2001.

Otter, L. B., Guenther, A., and Greenberg, J.: Seasonal and spatial variations in biogenic hydrocarbon emissions from southern African savannas and woodlands, Atmos. Environ., 36, 4265–4275, 2002.

Otter, L., Guenther, A., Wiedinmyer, C., Fleming, G., Harley, P., and Greenberg, J.: Spatial and temporal variations in biogenic volatile organic compound emissions for Africa south of

the equator, J. Geophys. Res., 108, 8505, doi:10.1029/2002JD002609, 2003.

Palmer, P. I., Jacob, D. J., Chance, K., Martin, R. V., Spurr, R. J. D., Kurosu, T. P., Bey, I., Yantosca, R., Fiore, A., and Li, Q.: Air mass factor formulation for spectroscopic measurements from satellites: Application to formaldehyde retrievals from the Global Ozone Monitoring Experiment, J. Geophys. Res., 106, 14539–14550, doi:10.1029/2000JD900772, 2001.

Palmer, P. I., Jacob, D. J., Fiore, A. M., Martin, R. V., Chance, K., and Kurosu, T. P.: Mapping isoprene emissions over North America using formaldehyde column observations from space, J. Geophys. Res., 108, 4180, doi:10.1029/2002JD002153, 2003.

Palmer, P. I., Abbot, D. S., Fu, T.-M., Jacob, D. J., Chance, K., Kurosu, T. P., Guenther, A., Wiedinmyer, C., Stanton, J. C., Pilling, M. J., Pressley, S. N., Lamb, B., and Sumner, A. L.: Quantifying the seasonal and interannual variability of North American isoprene emissions using satellite observations of the formaldehyde column, J. Geophys. Res., 111, D12315, doi:10.1029/2005JD006689, 2006.

Park, R. J., Jacob, D. J., Field, B. D., Yantosca, R. M., and Chin, M.: Natural and transboundary pollution influences on sulfate-nitrate-ammonium aerosols in the United States: Implications for policy, J. Geophys. Res., 109, D15204, doi:10.1029/2003JD004473, 2004.

Paulot, F., Crounse, J. D., Kjaergaard, H. G., Kroll, J. H., Seinfeld, J. H., and Wennberg, P. O.: Isoprene photooxidation: new insights into the production of acids and organic nitrates, Atmos. Chem. Phys., 9, 1479–1501, doi:10.5194/acp-9-1479-2009, 2009a.

Paulot, F., Crounse, J. D., Kjaergaard, H. G., K¨urten, A., St Clair, J. M., Seinfeld, J. H., and Wennberg, P. O.: Unexpected epoxide formation in the gas-phase photooxidation of isoprene, Science, 325, 730–733, 2009b.

Paulson, S. E., Flagan, R. C., and Seinfeld, J. H.: Atmospheric photooxidation of isoprene. I: The hydroxyl radical and ground state atomic oxygen reactions, Int. J. Chem. Kinet., 24, 79–101, 1992.

Peeters, J. and Müller, J.-F.: HO$_x$ radical regeneration in isoprene oxidation via peroxy radical isomerisations. II: experimental evidence and global impact, Phys. Chem. Chem. Phys., 12, 14227–14235, 2010.

Peeters, J., Nguyen, T. L., and Vereecken, L.: HO$_x$ radical regeneration in the oxidation of isoprene, Phys. Chem. Chem. Phys., 11, 5935–5939, 2009.

Redelsperger, J.-L., Thorncroft, C. D., Diedhiou, A., Lebel, T., Parker, D. J., and Polcher, J.: African Monsoon Multidisciplinary Analysis (AMMA): An international research project and field campaign, B. Am. Meteorol. Soc., 87, 1739–1746, 2006.

Reeves, C. E., Formenti, P., Afif, C., Ancellet, G., Attié, J.-L., Bechara, J., Borbon, A., Cairo, F., Coe, H., Crumeyrolle, S., Fierli, F., Flamant, C., Gomes, L., Hamburger, T., Jambert, C.,

Law, K. S., Mari, C., Jones, R. L., Matsuki, A., Mead, M. I., Methven, J., Mills, G. P., Minikin, A., Murphy, J. G., Nielsen, J. K., Oram, D. E., Parker, D. J., Richter, A., Schlager, H., Schwarzenboeck, A., and Thouret, V.: Chemical and aerosol characterisation of the troposphere over West Africa during the monsoon period as part of AMMA, Atmos. Chem. Phys., 10, 7575–7601, doi:10.5194/acp-10-7575-2010, 2010.

Ren, X., Olson, J. R., Crawford, J. H., Brune, W. H., Mao, J., Long, R. B., Chen, Z., Chen, G., Avery, M. A., Sachse, G. W., Barrick, J. D., Diskin, G. S., Huey, L. G., Fried, A., Cohen, R. C., Heikes, B., Wennberg, P. O., Singh, H. B., Blake, D. R., and Shetter, R. E.: HOx chemistry during INTEX-A 2004: Observation, model calculation, and comparison with previous studies, J. Geophys. Res., 113, D05310, doi:10.1029/2007JD009166, 2008.

Saunders, S. M., Jenkin, M. E., Derwent, R. G., and Pilling, M. J.: Protocol for the development of the Master Chemical Mechanism, MCM v3 (Part A): tropospheric degradation of non-aromatic volatile organic compounds, Atmos. Chem. Phys., 3, 161–180, doi:10.5194/acp-3-161-2003, 2003.

Saxton, J. E., Lewis, A. C., Kettlewell, J. H., Ozel, M. Z., Gogus, F., Boni, Y., Korogone, S. O. U., and Serça, D.: Isoprene and monoterpene measurements in a secondary forest in northern Benin, Atmos. Chem. Phys., 7, 4095–4106, doi:10.5194/acp-7-4095-2007, 2007.

Serça, D., Guenther, A., Klinger, L., Vierling, L., Harley, P., Druilhet, A., Greenberg, J., Baker, B., Baugh, W., Bouka-Biona, C., and Loemba-Ndembi, J.: EXPRESSO flux measurements at upland and lowland Congo tropical forest site, Tellus B, 53, 220–234, 2001.

Shim, C., Wang, Y., Choi, Y., Palmer, P. I., Abbot, D. S., and Chance, K.: Constraining global isoprene emissions with Global Ozone Monitoring Experiment (GOME) formaldehyde column measurements, J. Geophys. Res., 110, D24301, doi:10.1029/2004JD005629, 2005.

Singh, H. B. and Hanst, P. L.: Peroxyacetyl nitrate (PAN) in the unpolluted atmosphere: An important reservoir for nitrogen oxides, Geophys. Res. Lett., 8, 941–944, 1981.

South African Petroleum Industry Association (SAPIA): Annual Report., 2008.

Spurr, R. J. D., Kurosu, T. P., and Chance, K. V.: A linearized discrete ordinate radiative transfer model for atmospheric remote sensing retrieval, J. Quant. Spectrosc. Ra., 68, 689–735, 2001.

Stammes, P., Sneep, M., de Haan, J. F., Veefkind, J. P., Wang, P., and Levelt, P. F.: Effective cloud fractions from the Ozone Monitoring Instrument: Theoretical framework and validation, J. Geophys. Res., 113, D16S38, doi:10.1029/2007JD008820, 2008.

Stavrakou, T., Müller, J.-F., De Smedt, I., Van Roozendael, M., van der Werf, G. R., Giglio, L., and Guenther, A.: Global emissions of non-methane hydrocarbons deduced from SCIAMACHY formaldehyde columns through 2003–2006, Atmos. Chem. Phys., 9, 3663–3679, doi:10.5194/acp-9-3663-2009, 2009a.

Stavrakou, T., Müller, J.-F., De Smedt, I., Van Roozendael, M., van der Werf, G. R., Giglio, L., and Guenther, A.: Evaluating the performance of pyrogenic and biogenic emission inventories against one decade of space-based formaldehyde columns, Atmos. Chem. Phys., 9, 1037–1060, doi:10.5194/acp-9-1037-2009, 2009b.

Stewart, D. J., Taylor, C. M., Reeves, C. E., and McQuaid, J. B.: Biogenic nitrogen oxide emissions from soils: impact on NO_x and ozone over west Africa during AMMA (African Monsoon Multidisciplinary Analysis): observational study, Atmos. Chem. Phys., 8, 2285–2297, doi:10.5194/acp-8-2285-2008, 2008.

Stone, D., Evans, M. J., Commane, R., Ingham, T., Floquet, C. F. A., McQuaid, J. B., Brookes, D. M., Monks, P. S., Purvis, R., Hamilton, J. F., Hopkins, J., Lee, J., Lewis, A. C., Stewart, D., Murphy, J. G., Mills, G., Oram, D., Reeves, C. E., and Heard, D. E.: HO_x observations over West Africa during AMMA: impact of isoprene and NO_x, Atmos. Chem. Phys., 10, 9415–9429, doi:10.5194/acp-10-9415-2010, 2010.

Sumner, A. L., Shepson, P. B., Couch, T. L., Thornberry, T., Carroll, M. A., Sillman, S., Pippin, M., Bertman, S., Tan, D., Faloona, I., Brune, W., Young, V., Cooper, O., Moody, J., and Stockwell, W.: A study of formaldehyde chemistry above a forest canopy, J. Geophys. Res., 106, 24387–24405, doi:10.1029/2000JD900761, 2001.

Tao, Z., Larson, S. M., Wuebbles, D. J., Williams, A., and Caughey, M.: A summer simulation of biogenic contributions to ground-level ozone over the continental United States, J. Geophys. Res., 108, 4404, doi:10.1029/2002JD002945, 2003.

Taraborrelli, D., Lawrence, M. G., Crowley, J. N., Dillon, T. J., Gromov, S., Groß, C. B. M., Vereecken, L., and Lelieveld, J.: Hydroxyl radical buffered by isoprene oxidation over tropical forests, Nature Geoscience, 5, 190–193, doi:10.1038/NGEO1405, 2012.

Torres, O., Tanskanen, A., Veihelmann, B., Ahn, C., Braak, R., Bhartia, P. K., Veefkind, P., and Levelt, P.: Aerosols and surface UV products from Ozone Monitoring Instrument observations: An overview, J. Geophys. Res., 112, D24S47, doi:10.1029/2007JD008809, 2007.

Trainer, M., Williams, E. J., Parrish, D. D., Buhr, M. P., Allwine, E. J., Westberg, H. H., Fehsenfeld, F. C., and Liu, S. C.: Models and observations of the impact of natural hydrocarbons on rural ozone, Nature, 329, 705–707, 1987.

Trentmann, J., Andreae, M. O., and Graf, H.-F.: Chemical processes in a young biomass-burning plume, J. Geophys. Res., 108, 4705, doi:10.1029/2003JD003732, 2003.

US EPA: Estimation Programs Interface for Windows Vista v4.10, US EPA, 2011.

van der Werf, G. R., Randerson, J. T., Giglio, L., Collatz, G. J., Kasibhatla, P. S., and Arellano Jr., A. F.: Interannual variability in global biomass burning emissions from 1997 to 2004, Atmos. Chem. Phys., 6, 3423–3441, doi:10.5194/acp-6-3423-2006, 2006.

Wang, Y., Jacob, D. J., and Logan, J. A.: Global simulation of tropospheric O_3-NO_x-hydrocarbon

chemistry, 1. Model formulation, J. Geophys. Res., 103, 10713–10725, doi:10.1029/98JD00158, 1998.

Wesely, M. L.: Parameterization of surface resistances to gaseous dry deposition in regional-scale numerical models, Atmos. Environ., 23, 1293–1304, 1989.

Yang,W., Shabanov, N. V., Huang, D., Wang, W., Dickinson, R. E., Nemani, R. R., Knyazikhin, Y., and Myneni, R. B.: Analysis of leaf area index products from combination of MODIS Terra and Aqua data, Remote Sens. Environ., 104, 297–312, 2006.

Yevich, R. and Logan, J. A.: An assessment of biofuel use and burning of agricultural waste in the developing world, Global Biogeochem. Cy., 17, 1095, doi:10.1029/2002GB001952, 2003.

Yienger, J. J. and Levy II, H.: Empirical model of global soil biogenic NO_x emissions, J. Geophys. Res., 100, 11447–11464, doi:10.1029/95JD00370, 1995.

Zeng, X.: Global vegetation root distribution for land modeling, J. Hydrometeorol., 2, 525–530, 2001.

Chapter 3. Improved model of isoprene emissions in Africa using OMI satellite observations of formaldehyde: implications for oxidants and particulate matter

[Marais, E. A., Jacob, D.J., Guenther, A., Chance, K., Kurosu, T. P., Murphy, J., Reeves, C., Pye, H. O. T., submitted to Atmos. Chem. Phys.]

Abstract

We use a 2005-2009 record of isoprene emissions over Africa derived from OMI satellite observations of formaldehyde (HCHO) to better understand the factors controlling isoprene emission on the scale of the continent. OMI-derived isoprene emissions show large seasonality over savannas driven by temperature and leaf area index (LAI), and much weaker seasonality over equatorial forests driven by temperature. The commonly used MEGAN global isoprene emission inventory reproduces this seasonality but is too high, particularly for equatorial forests and including comparison with relaxed-eddy accumulation measurements. Isoprene emissions in MEGAN are computed as the product of a leaf-level emission factor E_o, LAI, and activity factors dependent on environmental variables. We use the OMI-derived emissions to provide improved estimates of E_o for different plant functional types and show that these are in good agreement with direct leaf measurements from field campaigns in different environments ($r = 0.55$, bias = -19%). The largest downward correction to MEGAN E_o values are for equatorial forests and semi-arid environments, and this is consistent with latitudinal transects of isoprene over West Africa from the AMMA aircraft campaign. The total African emission of isoprene derived by

OMI is 77 Tg C a^{-1}, as compared to 104 Tg C a^{-1} in MEGAN, with equatorial forests accounting for most of the difference. A GEOS-Chem chemical transport model simulation using OMI-derived African isoprene emissions indicates mean increases in surface ozone and particulate matter of up to 8 ppbv and 1.5 µg m^{-3}, respectively, relative to a simulation without African isoprene emissions.

3.1 Introduction

Isoprene is the dominant biogenic non-methane volatile organic compound (NMVOC) emitted by vegetation, accounting for 50% of global NMVOC emissions in current inventories (Olivier et al,. 1996; Guenther et al., 2006). Isoprene affects the oxidative capacity of the atmosphere through reaction with OH (Lelieveld et al., 2008; Ren et al., 2008) and as a precursor of O_3 (Trainer et al., 1987). It is also an important precursor for secondary organic aerosols (SOA) (Claeys et al., 2004) and a sink for nitrogen oxide radicals ($NO_x \equiv NO + NO_2$) by formation of organic nitrates (Paulot et al., 2012). Isoprene thus has a range of impacts on air quality and climate that need to be included in atmospheric composition models. The widely used MEGAN global emission inventory (Guenther et al., 2006, 2012) indicates that 80% of global isoprene emission takes place in the tropics and 25% in Africa, but there are large uncertainties in these estimates due to lack of data. In previous work we developed a method to estimate isoprene emissions from Africa on the basis of observations of formaldehyde (HCHO) from the OMI satellite instrument. Here we use our OMI-derived isoprene emissions evaluated with local data to better understand the factors controlling isoprene emissions in Africa, improve inventory estimates for different African plant functional types (PFTs), and assess the implications for atmospheric oxidants and aerosols.

Isoprene produced in the chloroplasts of plants is released to the atmosphere via the stomata of leaves (Sharkey and Yeh, 2001). Above-canopy emission rates E_{ISOP} (in atoms C cm^{-2} of Earth surface s^{-1}) depend on plant species, foliage density, leaf age, temperature, photosynthetically active radiation (PAR), and water stress (Guenther et al., 1995). This is commonly represented in isoprene emission inventories by multiplying an emission factor E_o (in mg C m^{-2} of leaf surface h^{-1}) defined for each PFT at standard conditions with an ensemble of coefficients describing the sensitivity to local environmental variables. In the MEGAN (version 2.1) inventory (Guenther et al., 2012) this is given as:

$$E_{\text{ISOP}} = E_o \times C_{\text{CE}} \times \text{LAI} \times \gamma_{\text{PAR}} \times \gamma_T \times \gamma_{\text{AGE}} \times \gamma_{\text{SM}}$$ (3.1),

where LAI is the leaf area index (m^2 leaf surface per m^2 of Earth surface) and the activity factors γ describe the sensitivity to above-canopy radiation (PAR), temperature (T), leaf age distribution (AGE), and soil moisture (SM). The coefficient C_{CE} enforces $E_{\text{ISOP}} = E_o$ under standard conditions, which for MEGAN are defined as leaf-level $T = 303$ K and PAR $= 1500$ µmol photons m^{-2} s^{-1}, and a canopy with LAI $= 5$ m^2 m^{-2}, leaf age distribution of 80% mature, 10% growing, and 10% senescing, and volumetric soil moisture of 0.3 m^3 m^{-3}. The value of C_{CE} depends on the radiative transfer model used to describe the attenuation of PAR by the canopy.

Isoprene emission data for African vegetation are very limited, and emission models require extrapolation with data from other continents and across plant species (Guenther et al., 2006; 2012). This can lead to substantial errors, as differences in isoprene fluxes within and across plant species are large. Uncertainty in the distribution of land cover (PFT) in the tropics

can further lead to a 5-fold discrepancy in isoprene emissions in Equatorial Africa (Pfister et al., 2008).

Space-based observations of HCHO, a high-yield oxidation product of isoprene, have been used in a number of studies to infer isoprene emissions and evaluate inventories globally (Shim et al., 2005; Stavrakou et al., 2009) and regionally in Southeast Asia (Fu et al., 2007), South America (Barkley et al., 2008), North America (Palmer et al., 2003; 2006; Millet et al., 2008), Europe (Dufour et al., 2009; Curci et al., 2010), and Africa (Marais et al., 2012). These studies have confirmed the dependence on temperature as the dominant factor of month-to-month variability of isoprene emissions across North America (Palmer et al., 2006; Millet et al., 2008) and Amazonia (Barkley et al., 2008). Leaf phenology and PAR were found to be important drivers of seasonality of isoprene emissions in Amazonia (Barkley et al., 2008; 2009). Stavrakou et al. (2009) found that water stress reduces isoprene emissions in southern Africa during the dry season. Here we use our previous work for Africa (Marais et al., 2012) to better understand the factors controlling isoprene emissions across the continent, evaluate and update the MEGANv2.1 emission inventory, and examine the impact on surface air quality.

3.2 OMI-derived isoprene emissions in Africa

The derivation of isoprene emissions in Africa using OMI HCHO data is described in detail in Marais et al. (2012) and summarized briefly here. OMI is a UV/VIS solar backscatter instrument on the Aura polar sun-synchronous satellite launched in 2004 (Levelt et al., 2006). It has a 13×24 km^2 nadir pixel resolution, daily global coverage through cross-track viewing, and 13:30 local time (LT) overpass. HCHO slant columns are obtained from Version 2.0 (Collection 3) retrievals for 2005–2009 (http://disc.sci.gsfc.nasa.gov/Aura/data-

holdings/OMI/omhcho_v003.shtml). They are corrected for instrument drift and converted to vertical columns using local air mass factors (AMF) for the scattering atmosphere (Palmer et al., 2001) with vertical HCHO profiles from the GEOS-Chem chemical transport model v9-01-03 (http://www.geos-chem.org) and scattering weights from the LIDORT radiative transfer model (Spurr et al., 2001).

HCHO enhancements over Africa originate from isoprene emission, biomass burning, and fuel combustion. Scenes affected by biomass burning were excluded on the basis of MODIS satellite observations of fire counts and OMI satellite observations of aerosol absorption optical depth (AAOD) (Torres et al., 2007). The latter enabled the tracking of fire plumes transported across the continent. Scenes affected by gas flaring were excluded on the basis of a specialized hotspot product from the AATSR satellite sensor (Casadio et al., 2012) and this led to the exclusion of much of Nigeria where that source is particularly large and urban and industrial sources may contribute as well (Marais et al., 2014).

Marais et al. (2012) thus obtained a 2005-2009 monthly data set of vertical HCHO columns with $1 \times 1°$ spatial resolution screened for biomass burning and anthropogenic influences and thus attributable to isoprene emissions (**Figure 3.1**, left panel). They derived using GEOS-Chem a local NO_x-dependent sensitivity, S, of the HCHO column Ω_{HCHO} to a perturbation Δ in isoprene emissions E_{ISOP} ($S = \Delta\Omega_{HCHO}/ \Delta E_{ISOP}$) and applied it to the Ω_{HCHO} data set using NO_x concentrations inferred from concurrent OMI observations of tropospheric NO_2. Locations affected by smearing (displacement between isoprene emission and HCHO production) were diagnosed from anomalous values of S and excluded from the data set.

Figure 3.1 (center panel) shows the resulting mean OMI-derived isoprene emissions for 2005-2009. The OMI overpass is at 13:30 LT and the corresponding isoprene emissions are for

12-15 LT. Also shown (right) is the MODIS IGBP land cover map (Friedl et al., 2002).

Dominant vegetation types in Africa are roughly defined by latitudinal bands, with evergreen (broadleaf) trees along the Equator successively transitioning to the north and south to woody savannas (30-60% tree coverage), savannas (10-30%), grasslands, and deserts. The HCHO column data follow this vegetation gradient and so too do the inferred isoprene emissions.
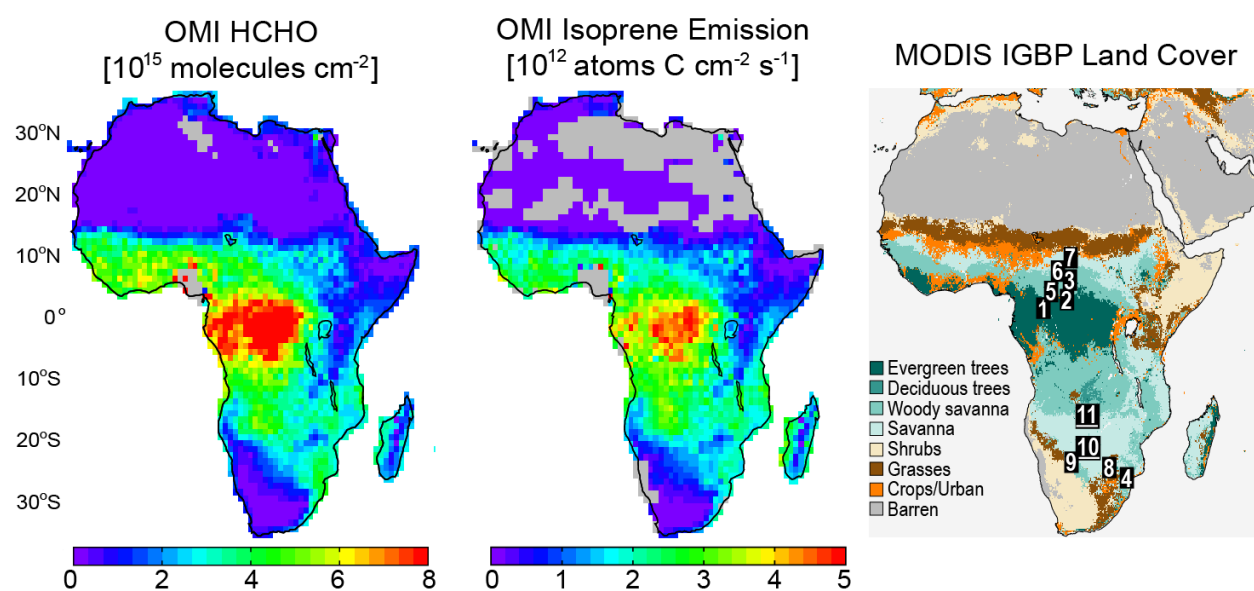
Figure 3.1: Annual mean (2005-2009) OMI HCHO vertical columns at 1×1° horizontal resolution screened for biomass burning and anthropogenic HCHO (left), and resulting OMI-derived isoprene emissions (center), as derived by Marais et al. (2012) and summarized in the text. The OMI observations are at 13:30 local time (LT) and the OMI-derived isoprene emissions are for 12-15 LT. The right panel is a MODIS IGBP land cover map (Friedl et al., 2002) with numbers showing the location of isoprene flux measurements used to evaluate the OMI-derived isoprene emissions. These include 1. Serça et al. (2001) for March and November 1996; 2. Greenberg et al. (1999) for November-December 1996 (**Figure 3.2**), and Klinger et al. (1998) for 1995-1996 (**Figure 3.5**) 3. Greenberg et al. (1999) for November-December 1996, 4. Guenther et al. (1996) for December 1992 (**Figure 3.5**) and Harley et al. (2003) for February 2001 (**Figure 3.2**), 5-7. Klinger et al. (1998) for 1995-1996, 8-11. Otter et al. (2002) for February-March 2001.

Marais et al. (2012) presented a detailed error characterization of their OMI-derived

isoprene emissions. Spectral fitting of the HCHO column has an error standard deviation of $8 \times$

10^{15} molecules cm^{-2} for individual observations, but this error is random and thus greatly reduced

by averaging (Boeke et al., 2011). Relating the fitted slant HCHO columns to isoprene emissions

incurs additional errors in the AMF estimate (20%), the isoprene oxidation mechanism (15%),

the use of OMI NO_2 to obtain S under low-NO_x conditions (20-30%), and smearing (30% for

high-NO_x conditions, 30-70% for low-NO_x). The resulting error in isoprene emission estimates

for individual scenes, adding in quadrature all error contributions, is 40% for high-NO_x

conditions and 40-90% for low-NO_x (Marais et al., 2012). Here we use monthly isoprene

emission data for 2005-2009 over a $1\times1°$ grid and this typically averages 3200 individual scenes.

Averaging is expected to greatly reduce the error though only to the extent that the error

components are random.

3.3 Evaluation with canopy flux measurements

Canopy-scale isoprene flux measurements by relaxed-eddy accumulation (REA) from a

few African field campaigns can be used to evaluate our OMI-derived emissions. **Figure 3.2**

compares OMI-derived isoprene emissions to REA measurements over equatorial evergreen

trees (Greenberg et al., 1999; Serça et al., 2001), woody savannas (Greenberg et al., 1999), and

savannas (Harley et al., 2003) in central and southern Africa (sites 1-4, **Figure 3.1**). Also shown

are the values calculated using equation (3.1) with MODIS LAI (Yang et al., 2006) and GEOS-5

assimilated meteorological data. The Serça et al. (2001) and Harley et al. (2003) measurements

(sites 1 and 4) are from walk-up towers with a flux footprint of about 600 m, while the

Greenberg et al. (1999) measurements (sites 2 and 4) are from aircraft with a flux footprint of

~100×100 km^2 at site 2 and 30×30 km^2 at site 3. All values in **Figure 3.2** are for 12-15 LT. REA

fluxes at sites 2-3, obtained in the morning (9:30-11:30), are increased by a factor of 1.4 as a

diurnal correction for temperature and PAR following MEGAN.
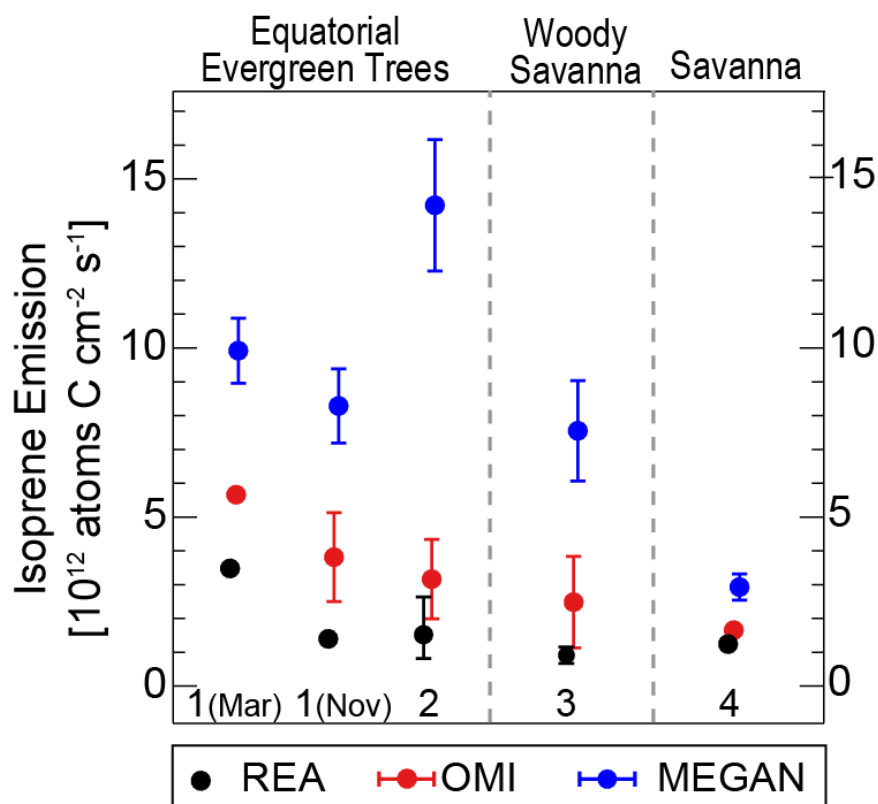
Figure 3.2: Mean canopy-scale isoprene emissions at African sites 1-4 (see **Figure 3.1**) measured by relaxed-eddy accumulation (REA), and comparison to OMI-derived and MEGAN values. All values are for 12-15 local time, with diurnal correction for REA measurements at sites 2 and 3 (see text). Vertical bars on the REA measurements for sites 2-3 are the interquartile ranges over the aircraft sampling domain. OMI-derived and MEGAN values are 2005-2009 monthly averages for the site locations and observation times, with interannual standard deviations shown as vertical bars for gridsquares where there are observations over multiple years. OMI at site 3 is for September-October as no OMI data are retained in November-December due to biomass burning interference.

OMI and MEGAN are sampled for the 1×1° gridsquare coincident with the observation site and for the corresponding months. Interannual variability is of similar magnitude in the OMI-derived and MEGAN data at sites 1 (November), 2 and, 3 where multi-year OMI data is available. The variability is driven in MEGAN predominantly by temperature. At site 3 there are no OMI data in the months of observation (November-December) because of biomass burning interference and we show instead OMI-derived emissions in September-October, which should be similar to November-December according to MEGAN.

For the equatorial evergreen tree sites in central Africa (sites 1 and 2) OMI-derived isoprene emissions are on average 2 times higher than the REA measurements and MEGAN is 5 times higher. Fluxes at site 2, where the sampling footprint is similar to OMI, have large spatial variability implying that differences in the sampling footprint may contribute to the discrepancies. Harley et al. (2003) applied a positive correction of ~20% to flux measurements at sites 2-3 to account for transport not accumulated in the two REA reservoirs. A similar negative bias may affect measurements at site 1. OMI and MEGAN reproduce the March-November decline at site 1 and this is driven in MEGAN by temperature. Errors in both land cover maps and emission factors may contribute to the large positive biases in MEGAN. At the woody savanna site OMI is 2.7 times higher than the REA measurement, while MEGAN is an order of magnitude higher. At the savanna site OMI agrees with the REA flux measurement while MEGAN is 2.5 times higher.

Overall the REA flux measurements indicate canopy-scale isoprene emissions that are somewhat lower than derived from OMI and much lower than derived from MEGAN. However, as we will show in **Section 3.5**, landscape-level isoprene emission factors measured during African field campaigns are more consistent with OMI.

3.4 Seasonality of isoprene emissions in Africa

We examine the seasonality of our OMI-derived isoprene emissions in relation to environmental variables, focusing on three seasonally and ecologically coherent regions in Africa where emissions are highest (**Figure 3.3**): (1) equatorial forests dominated by tropical broadleaf evergreen trees, (2) northern savannas (including woody), and (3) southern savannas (including woody). **Figure 3.4** shows the seasonality of OMI-derived isoprene emissions for these three regions together with MODIS LAI and the Goddard Earth Observing System (GEOS-5) assimilated 2-m air temperature. Isoprene emissions and 2-m temperature are for 12-15 LT and MODIS LAI is the combined Terra and Aqua product (Yang et al., 2006). Multi-year averages (2005-2009) are shown as the regionally averaged interannual variability is small, except over northern savannas in August as discussed below.
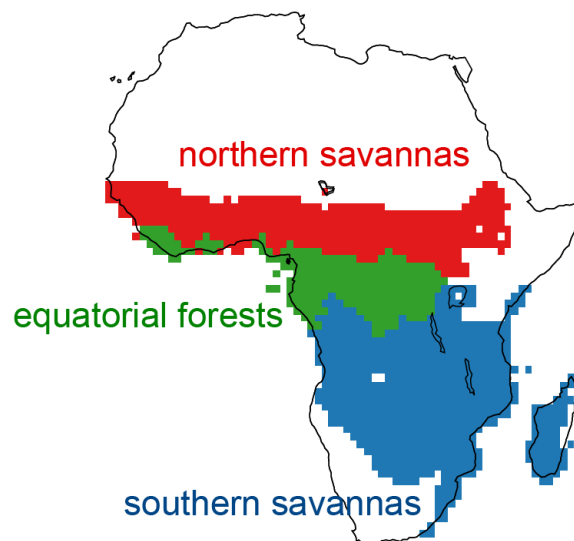
Figure 3.3: Coherent regions used for analysis of the factors controlling OMI-derived isoprene emissions: equatorial forests (green), northern savannas (red), and southern savannas (blue). Land cover definitions are from the MODIS IGBP map (**Figure 3.1**).
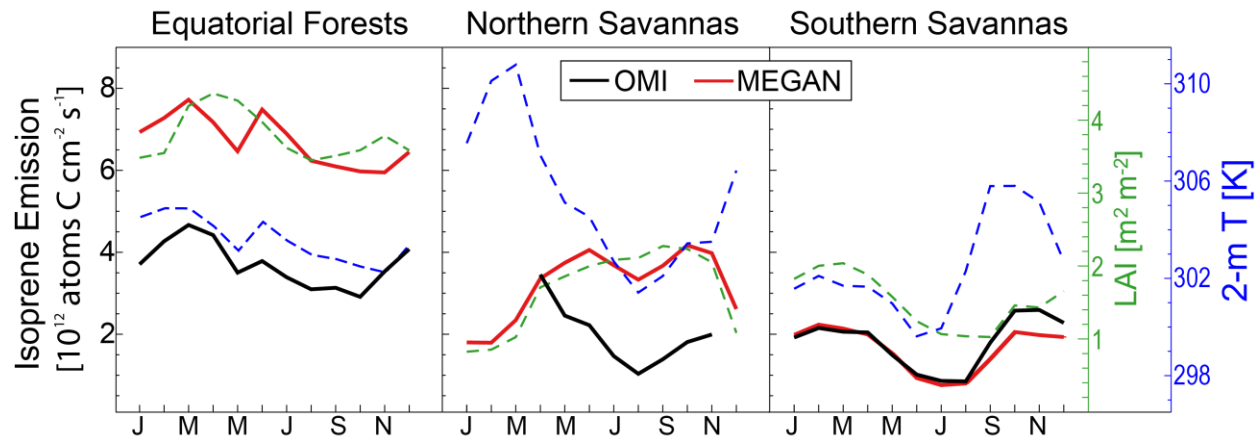
Figure 3.4: Seasonality of isoprene emissions and environmental variables averaged over the coherent African regions of **Figure 3.3**. Monthly mean OMI-derived (black) and MEGAN (red) isoprene emissions are shown together with GEOS-5 2-m temperature (blue) and MODIS LAI (green). OMI-derived isoprene emissions are not available for northern savannas in December-March because of biomass burning interference. Emissions and 2-m temperature are for 12-15 local time. LAI is the combined Terra and Aqua product (Yang et al., 2006). All data are means for 2005-2009.

OMI-derived isoprene emissions for equatorial forests are a factor of 2 lower than MEGAN and both show similar weak seasonality, with a decline from March to November that is consistent with the Serça et al. (2001) REA flux measurements (**Figure 3.2**) and is driven in MEGAN principally by temperature. Although LAI exhibits similar seasonality, it remains above 3.5 m^2 m^{-2} year-round and MEGAN finds that sensitivity to LAI saturates above 2-3 m^2 m^{-2} because of the shading of lower-canopy leaves (Guenther et al., 2006).

Availability of OMI-derived isoprene emission data for the northern savannas is limited to April-November because of pervasive biomass burning influence during the December-March dry season. Emissions are maximum in April, at the beginning of the wet season, and minimum in August when the West African Monsoon (WAM) is fully developed over the continent (Janicot et al., 2008) resulting in cooler temperatures. OMI-derived emissions largely follow temperature over the April-November period. Year-to-year variability in the WAM affects

temperature in August, leading to interannual variability in OMI isoprene emissions over the 2005-2009 period that is correlated with temperature ($r = 0.65$).

The complete seasonality simulated by MEGAN in northern savannas shows low isoprene emissions in the December-March dry season when LAI is less than 1, and a broad maximum in the April-November wet season as the August minimum in temperature is compensated by a corresponding maximum in LAI. MODIS LAI in the northern savannas is less than 2.5 m^2 m^{-2} year-round, sufficiently low that the MEGAN dependence on LAI does not saturate (Guenther et al., 2012). However, MODIS may underestimate LAI in West Africa during the wet season because of cloud contamination (Gessner et al., 2013).

OMI-derived emissions for southern savannas are in close agreement with MEGAN with a minimum in the winter dry season and a maximum in the summer wet season. The seasonal minimum of isoprene emission (July-August) follows that of temperature (June-July) with a 1-month lag that reflects the very dry conditions in July-September. We find that LAI and temperature are both important for driving the seasonality of isoprene emissions in southern savannas.

3.5 Satellite-derived isoprene emission factors for African vegetation types

The general ability of MEGAN to reproduce the seasonal variation of OMI-derived isoprene emissions suggests that the MEGAN activity factors (γ in equation (3.1)) are appropriate for conditions in Africa, with temperature and LAI as the principal drivers. The large MEGAN bias over equatorial forests and northern savannas can therefore be attributed to an overestimate of emission factors that results from uncertainties in PFT distribution and limited emission data for plant species in these regions (E_o in equation (3.1)). The emission factors are

leaf-level isoprene fluxes at standard conditions of air temperature (T = 303 K) and light (PAR = 1500 μmol photons m^{-2} s^{-1}) gridded to a detailed regional land cover map for Africa south of the Equator (Otter et al., 2003) and the Olson et al. (2001) global ecoregion data in the north (Guenther et al., 2006). We can infer them from the OMI-derived canopy-level isoprene emission data by using equation (3.1). In so doing we only consider individual activity factors γ within the range 0.5-1.5 to prevent unrealistically high emission factors over low LAI grasslands and coastlines. **Figure 3.5** shows the distribution of MEGAN and OMI emission factors E_o over Africa together with observations from field campaigns. The latter are at the landscape-level and were obtained by scaling measured leaf-level isoprene fluxes for representative plant species to the sampling domain with foliage density and species distribution data. Leaf-level measurements at standard conditions were obtained by using enclosure measurements with controlled temperature and PAR (Otter et al., 2002; Serça et al., 2001), or adjusting to standard conditions with MEGAN activity factors for temperature and PAR (Guenther et al., 1996). Leaf-level fluxes of Klinger et al. (1998) were determined to be at standard conditions with coincident measurements of temperature and PAR.

We find from **Figure 3.5** remarkable agreement between OMI-derived emission factors and the field observations (r = 0.55, OMI normalized mean bias = -19%). Woody savannas in Zambia and savannas in South Africa have large variability in E_o (0.5-4.5 mg C m^{-2} h^{-1}) that is reproduced by OMI. The two sites in Botswana have low OMI and field campaign emission factors, as these sites are dominated by shrubs with low emissions and the monoterpene emitting mopane vegetation (Otter et al., 2002).
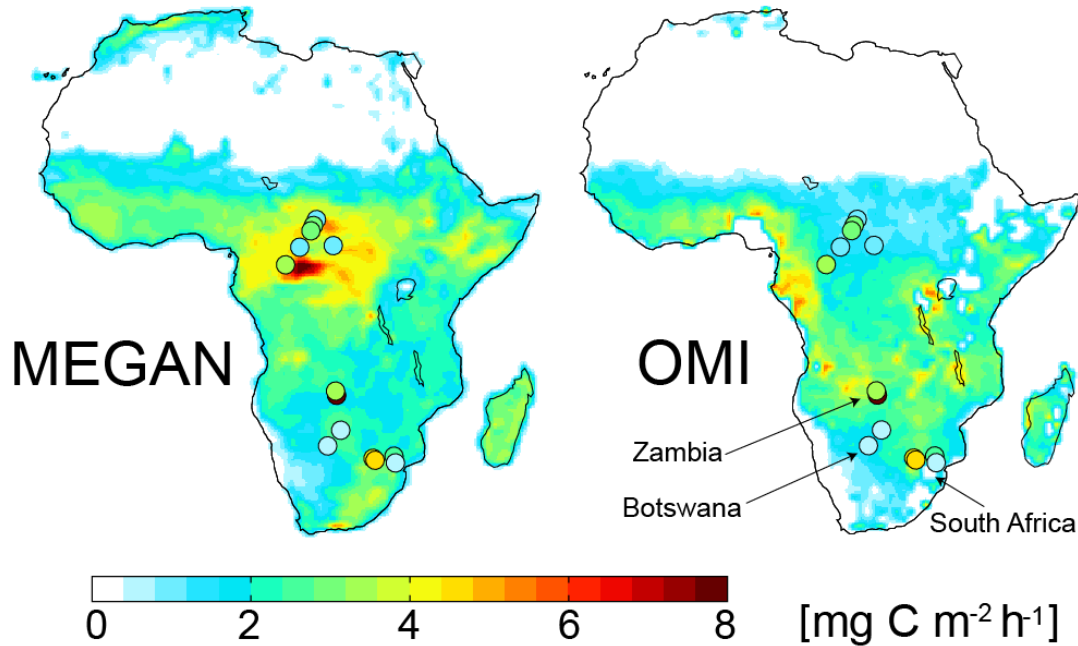
Figure 3.5: Isoprene emission factors (E_o in equation (3.1)) representing the emission flux under standard conditions. Measured landscape-level emission factors from field sites (circles; references given in **Figure 3.1**) are compared to those used in MEGAN (left) and obtained with OMI (right). OMI data missing in Nigeria are due to interference from anthropogenic HCHO, and in East Africa and Namibia/South Africa due to excessive departure from standard conditions (see text for details).

Differences between OMI and MEGAN emission factors are largest for equatorial forests, and field observations there are in good agreement with OMI and much lower than MEGAN. Emission factors in MEGAN are maximum in that region but the field observations do not support this, consistent with the large MEGAN overestimate of REA flux measurements (**Figure 3.2**). OMI emission factors for equatorial forests are larger in the west than east and this may result from differences in the proportion of isoprene emitting species. The west is dominated by dry tropical forests, while the east is dominated by permanently or seasonally flooded forests (White, 1983).

Table 3.1 shows mean isoprene emission factors for individual plant functional types as obtained by mapping the data from **Figure 3.5** onto the MODIS IGBP land map (Friedl et al.,

Table 3.1: Isoprene emission factors for African plant functional types[a]

Plant functional type	Emission factor [mg C m^{-2} h^{-1}]	
	MEGAN	OMI
MODIS IGBP classification[b]		
Evergreen broadleaf trees	4.3 ± 2.0	2.7 ± 1.0
Deciduous broadleaf trees	4.4 ± 1.7	2.9 ± 0.2
Woody savannas	3.2 ± 1.3	2.6 ± 1.0
Savannas	2.9 ± 1.2	2.3 ± 0.8
Shrubs	3.0 ± 1.3	1.6 ± 0.8
Grasses	1.8 ± 0.9	1.6 ± 0.9
Crops	1.4 ± 0.9	1.6 ± 0.6
Mosaic of crops and natural vegetation	2.3 ± 1.1	2.5 ± 1.0
GLC 2000 classification[c]		
Evergreen broadleaf trees	4.4 ± 1.9	2.5 ± 1.0
Deciduous broadleaf trees	3.0 ± 1.3	2.7 ± 0.9
Shrubs	3.1 ± 1.6	2.2 ± 1.0
Herbs	2.4 ± 1.3	1.9 ± 0.9
Sparse herbs or shrubs	2.4 ± 1.2	1.5 ± 0.7
Cultivated land	1.8 ± 1.1	2.2 ± 0.9
Mosaic of crops and natural vegetation	3.0 ± 1.3	2.7 ± 0.7
Mosaic of crops and shrubs or grasses	2.6 ± 1.0	1.9 ± 0.9

[a] Leaf-level isoprene emission E_o in equation (3.1) at standard conditions of temperature (303 K) and photosynthetically active radiation (1500 μmol photons m^{-2} s^{-1}). Values are means and standard deviations obtained by mapping the E_o data from **Figure 3.5** onto the MODIS IGBP and GLC 2000 land maps. Plant functional type classifications are as given by each land map.

[b] Friedl et al. (2002) and shown in **Figure 3.1**.

[c] Mayaux et al. (2006).

2002) and the independent Global Land Cover (GLC) 2000 land map (Mayaux et al., 2006). The distribution of MODIS IGBP woody savannas is spatially consistent with GLC 2000 broadleaf trees and MODIS IGBP savannas correspond to GLC 2000 shrubs interspersed with broadleaf trees and cultivated land. The GLC 2000 classification scheme is more consistent with the PFTs

of MEGANv2.1 (Guenther et al., 2012). OMI gives higher emission factors for forested vegetation than for grasslands but the difference is not as large as MEGAN and more consistent with the field observations. The largest differences between OMI and MEGAN emission factors are for broadleaf evergreen trees and semi-arid vegetation (shrubs and herbs).

The OMI-derived emission factors in **Figure 3.5** can be used to improve the MEGAN isoprene emission estimates as computed from equation (3.1). **Figure 3.6** compares the resulting isoprene concentrations simulated by GEOS-Chem with a latitudinal profile of isoprene concentration measurements below 1 km across West Africa during the AMMA wet season aircraft campaign in July-August 2006 (Murphy et al., 2010). There is a strong vegetation gradient along the AMMA flight track from the Gulf of Guinea to Benin woodlands to arid conditions in the north, and this is reflected in the isoprene data. Simulated isoprene in GEOS-Chem is almost a factor of 2 too low over Benin woodlands, which might reflect seasonal low bias of LAI over West Africa (Gessner et al., 2013). However, the OMI-derived emission factors are much better able to reproduce the latitudinal gradient than the original MEGAN emission factors, including in particular the decline to the north associated with increased aridity. Throughout Africa MEGAN emission factors are too high for semi-arid PFTs, as indicated by the overestimate in MEGAN for GLC 2000 sparse herb/shrub cover in **Table 3.1**.

3.6 Implications for oxidants and aerosols

Total isoprene emissions in Africa using OMI-derived emission factors are 77 Tg C a^{-1}, as compared to 104 Tg C a^{-1} in MEGAN v2.1. The difference is mainly for the equatorial evergreen forest PFT in central Africa, where OMI-derived isoprene emissions are 2-3 times lower than MEGAN. GEOS-Chem using OMI-derived isoprene emissions indicates a factor of 4
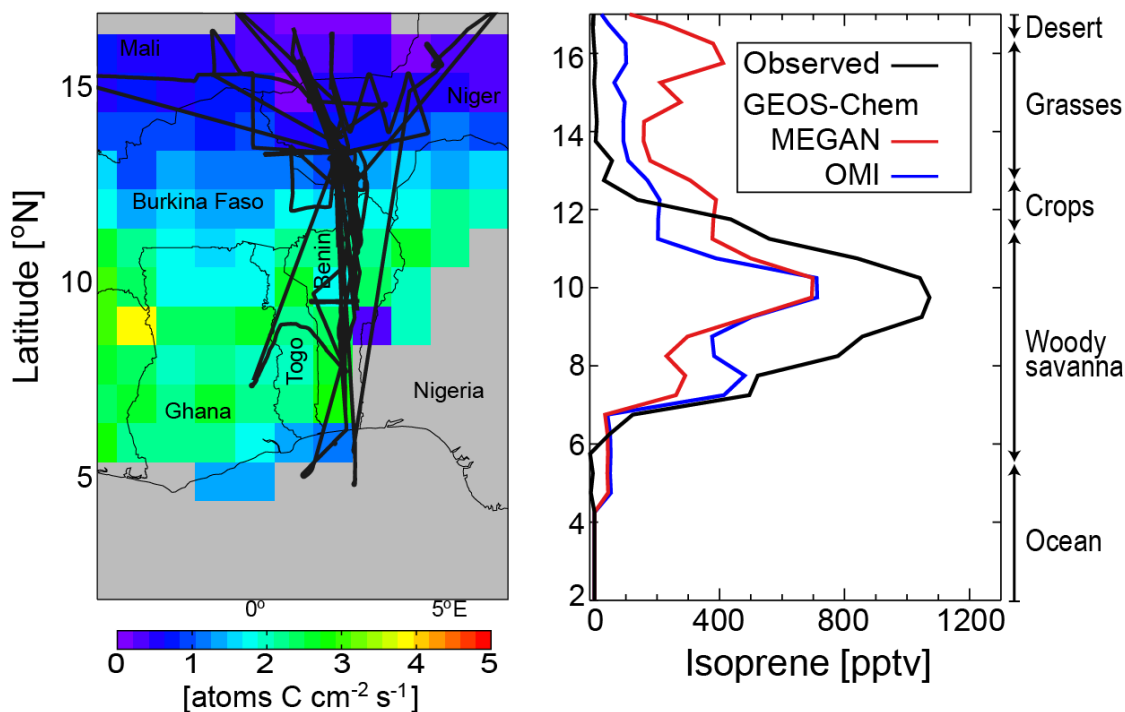
Figure 3.6: Latitudinal variability of isoprene in West Africa. Left panel shows the July-August 2006 AMMA flight tracks superimposed on July-August 2005-2009 OMI-derived isoprene emissions (Marais et al., 2012). Right panel shows boundary-layer (< 1 km) isoprene concentrations along the AMMA flight tracks; observations averaged over 0.5° latitude bands are compared to GEOS-Chem model results using either MEGAN or OMI-derived isoprene emission factors E_o. Dominant MODIS IGBP biomes along the flight tracks are indicated.

increase in boundary layer OH concentrations over central Africa, and a 4 ppbv increase in surface ozone, relative to a simulation using MEGAN emissions. The increase in ozone is mostly due to reduced loss by reaction with isoprene.

We conducted GEOS-Chem simulations with and without OMI-derived isoprene emissions in Africa (**Figure 3.5**) to quantify the regional impact of isoprene emissions on oxidants and aerosols. The simulations include the standard GEOS-Chem representation of oxidant-aerosol chemistry as described for example by Mao et al. (2010) with updates to the isoprene oxidation (Paulot et al., 2009a; 2009b) and secondary organic aerosol (Pye et al., 2013) mechanisms.

71
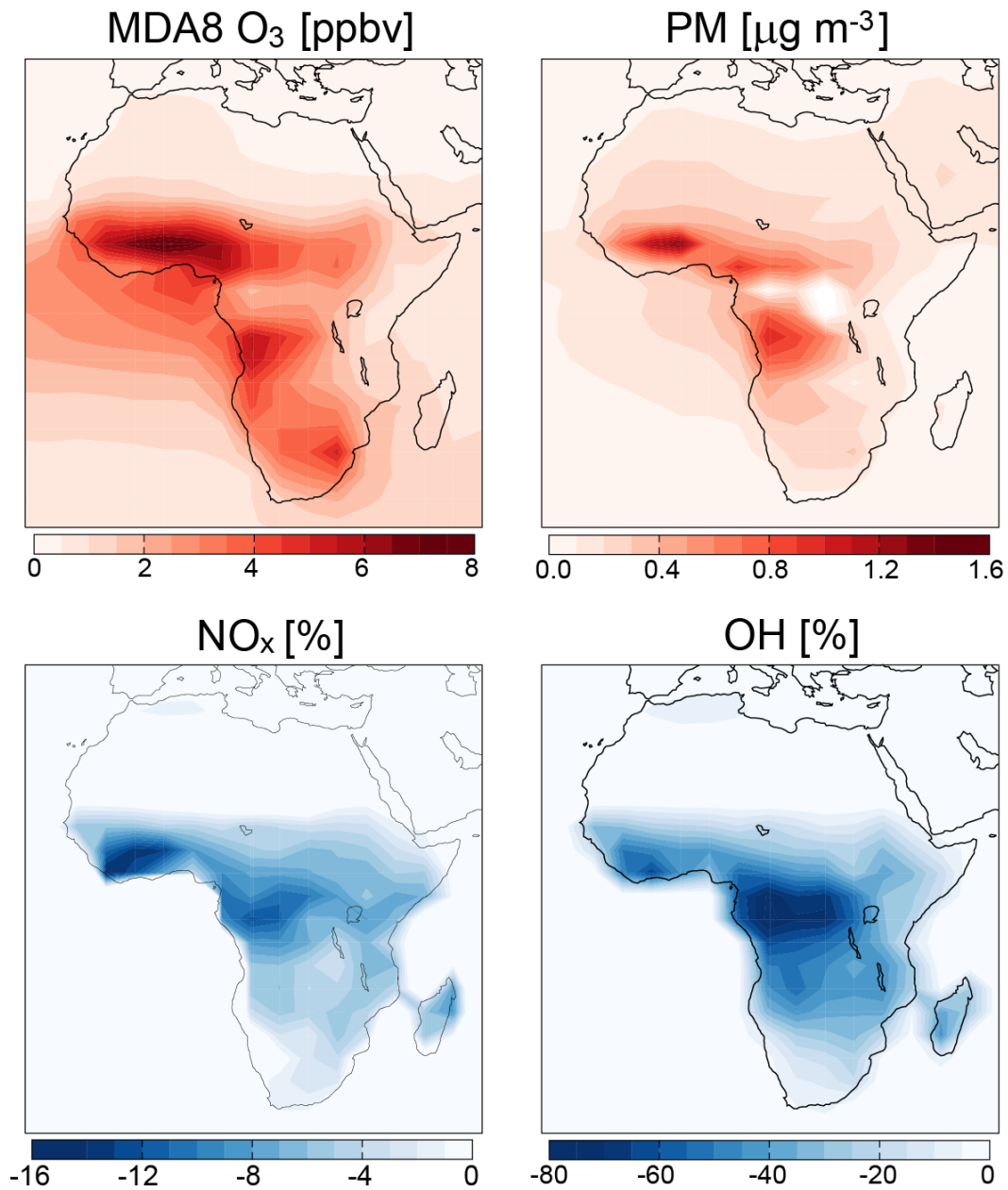
Figure 3.7: Contribution of African isoprene emissions to regional oxidants and particulate matter. Shown are the annual mean differences between GEOS-Chem simulations with and without African isoprene emissions for surface daily maximum 8-hour average (MDA8) O_3, particulate matter (PM), NO_x, and OH. MDA8 O_3 and PM are absolute differences and NO_x and OH are relative differences.

Figure 3.7 shows the impact of African isoprene emissions on surface concentrations of daily maximum 8-hour average (MDA8) O_3, particulate matter (PM), NO_x, and OH. The largest effect on O_3 is over West Africa because of high NO_x anthropogenic, soil, and biomass burning emissions (Marais et al., 2014). The largest effect on PM is also over West Africa and reflects the availability of high pre-existing primary PM from combustion (biomass burning and fuel) on which isoprene oxidation products can condense. South of the tropics NO_x emissions and primary PM are lower than in West Africa so the effect of isoprene emissions on O_3 and PM is smaller. NO_x declines in West Africa and the tropics due to formation of isoprene nitrates. Loss of OH from reaction with isoprene is highest in the tropics where low levels of NO_x reduce recycling efficiency of HO_x radicals.

3.7 Summary

We used a 2005-2009 data set of monthly isoprene emissions in Africa derived from OMI satellite observations of formaldehyde (HCHO) to study the factors controlling these emissions in different areas of the continent. Our goal was to achieve a better representation of isoprene emission in chemical transport models (CTMs), in part through evaluation and improvement of the commonly used MEGAN emission inventory, and to examine the implications for oxidants and aerosols over the continent.

We began by evaluating the OMI-derived isoprene emissions with relaxed-eddy accumulation (REA) flux measurements obtained from tall towers and aircraft during African field campaigns. OMI-derived isoprene emissions are on average 2 times higher than REA measurements over the equatorial forest and woody savannas, while MEGAN emissions are 5-10

times higher. The REA measurements may be biased low as air masses are not collected during calm periods.

We then subdivided Africa into 3 seasonally and ecologically coherent regions to examine the seasonality in OMI-derived isoprene emissions, and compare to the seasonality in MEGAN and in driving environmental variables. Equatorial forests exhibit weak seasonality that is driven predominantly by temperature, while seasonality in savannas is driven by both temperature and LAI, in a manner consistent with MEGAN.

Isoprene emissions in MEGAN are computed as the product of (1) a leaf-level emission factor characteristic of the plant functional type, (2) the LAI, and (3) activity factors dependent on local environmental variables. We applied the LAI and MEGAN activity factors to our OMI-derived isoprene emissions to obtain emission factors representative of different plant functional types. These agree well with the ensemble of leaf-level flux measurements in Africa and imply large downward corrections to MEGAN emission factors for equatorial forests and semi-arid vegetation. This is also consistent with the latitudinal gradient of isoprene across West Africa measured in the AMMA field campaign.

The OMI-derived emission factors can be incorporated into the MEGAN formalism (equation (3.1)) to improve modeling of isoprene emissions in Africa. The resulting isoprene emissions for the continent are 77 Tg C a^{-1}, as compared to 104 Tg C a^{-1} in the standard MEGAN inventory. Most of the difference is over equatorial Africa. We conducted GEOS-Chem simulations with and without African isoprene emissions (using OMI-derived emission factors) to examine the impact on regional particulate matter (PM) and oxidants. The largest effect of isoprene emissions on surface O_3 is over West Africa where NO_x from anthropogenic activity,

74

soils, and biomass burning is high, and the largest effect on PM is also over West Africa because of pre-existing high concentrations of primary PM from combustion.

References:

Barkley, M. P., Palmer, P. I., Kuhn, U., Kesselmeier, J., Chance, K., Kurosu, T. P., Martin, R. V., Helmig, D., and Guenther, A.: Net ecosystem fluxes of isoprene over tropical South America inferred from Global Ozone Monitoring Experiment (GOME) observations of HCHO columns, J. Geophys. Res., 113, D20304, doi:10.1029/2008JD009863, 2008.

Barkley, M. P., Palmer, P. I., De Smedt, I., Karl, T., Guenther, A., and Van Roozendael, M.: Regulated large-scale annual shutdown of Amazonian isoprene emissions?, Geophys. Res. Lett., 36, L04803, doi:10.1029/2008GL036843, 2009.

Boeke, N. L., Marshall, J. D., Alvarez, S., Chance, K. V., Fried, A., Kurosu, T. P., Rappenglück, B., Richter, D., Walega, J., Weibring, P., and Millet, D. B.: Formaldehyde columns from the Ozone Monitoring Instrument: Urban versus background levels and evaluation using aircraft data and a global model, J. Geophys. Res., 116, D05303, doi:10.1029/2010JD014870, 2011.

Casadio, S., Arino, O., and Serpe, D.: Gas flaring monitoring from space using the ATSR instrument series, Remote Sens. Environ., 116, 239–249, doi:10.1016/j.rse.2010.11.022, 2012.

Claeys, M., Graham, B., Vas, G., Wang, W., Vermeylen, R., Pashynska, V., Cafmeyer, J., Guyon, P., Andreae, M. O., Artaxo, P., and Maenhaut, W.: Formation of secondary organic aerosols through photooxidation of isoprene, Science, 303, 1173–1176, doi:10.1126/science.1092805, 2004.

Curci, G., Palmer, P. I., Kurosu, T. P., Chance, K., and Visconti, G.: Estimating European volatile organic compound emissions using satellite observations of formaldehyde from the Ozone Monitoring Instrument, Atmos. Chem. Phys., 10, 11501–11517, doi:10.5194/acp-10-11501-2010, 2010.

Dufour, G., Wittrock, F., Camredon, M., Beekmann, M., Richter, A., Aumont, B., and Burrows, J. P.: SCIAMACHY formaldehyde observations: constraint for isoprene emission estimates over Europe?, Atmos. Chem. Phys., 9, 1647–1664, doi:10.5194/acp-9-1647-2009, 2009.

Friedl, M. A., McIver, D. K., Hodges, J. C. F., Zhang, X. Y., Muchoney, D., Strahler, A. H., Woodcock, C. E., Gopal, S., Schneider, A., Cooper, A., Baccini, A., Gao, F., and Schaaf, C.: Global land cover mapping from MODIS: algorithms and early results, Remote Sens. Environ., 83, 287–302, 2002.

Fu, T.-M., Jacob, D. J., Palmer, P. I., Chance, K., Wang, Y. X., Barletta, B., Blake, D. R., Stanton, J. C., and Pilling, M. J.: Space-based formaldehyde measurements as constraints on volatile organic compound emissions in east and south Asia and implications for ozone, J. Geophys. Res., 112, D06312, doi:10.1029/2006JD007853, 2007.

Gessner, U., Niklaus, M., Kuenzer, C., and Dech, S.: Intercomparison of leaf area index products for a gradient of sub-humid to arid environments in West Africa, Remote Sens., 5, 1235-1257, doi:10.3390/rs5031235, 2013.

Greenberg, J. P., Guenther, A. B., Madronich, S., Baugh, W., Ginoux, P., Druilhet, A., Delmas, R., and Delon, C.: Biogenic volatile organic compound emissions in central Africa during the Experiment for the Regional Sources and Sinks of Oxidants (EXPRESSO) biomass burning season, J. Geophys. Res., 104, D23, 30659–30671, doi:10.1029/1999JD900475, 1999.

Guenther, A., Hewitt, C. N., Erickson, D., Fall, R., Geron, C., Graedel, T., Harley, P., Klinger, L., Lerdau, M., McKay, W. A., Pierce, T., Scholes, B., Steinbrecher, R., Tallamraju, R., Taylor, J., and Zimmerman, P.: A global model of natural volatile organic compound emissions, J. Geophys. Res., 100, D5, 8873–8892, doi:10.1029/94JD02950, 1995.

Guenther, A., Otter, L., Zimmerman, P., Greenberg, J., Scholes, R., and Scholes, M.: Biogenic hydrocarbon emissions from southern African savannas, J. Geophys. Res., 101, D20, 25859–25865, doi:10.1029/96JD02597, 1996.

Guenther, A., Karl, T., Harley, P., Wiedinmyer, C., Palmer, P. I., and Geron, C.: Estimates of global terrestrial isoprene emissions using MEGAN (Model of Emissions of Gases and Aerosols from Nature), Atmos. Chem. Phys., 6, 3181–3210, doi:10.5194/acp-6-3181-2006, 2006.

Guenther, A. B., Jiang, X., Heald, C. L., Sakulyanontvittaya, T., Duhl, T., Emmons, L. K., and Wang, X.: The Model of Emissions of Gases and Aerosols from Nature version 2.1 (MEGAN2.1): an extended and updated framework for modeling biogenic emissions, Geosci. Model Dev., 5, 1471-1492, doi:10.5194/gmd-5-1471-2012, 2012.

Harley, P., Otter, L., Guenther, A., and Greenberg, J.: Micrometeorological and leaf-level measurements of isoprene emissions from a southern African savanna, J. Geophys. Res., 108, D13, 8468, doi:10.1029/2002JD002592, 2003.

Janicot, S., Thorncroft, C. D., Ali, A., Asencio, N., Berry, G., Bock, O., Bourles, B., Caniaux, G., Chauvin, F., Deme, A., Kergoat, L., Lafore, J.-P., Lavaysse, C., Lebel, T., Marticorena, B., Mounier, F., Nedelec, P., Redelsperger, J.-L., Ravegnani, F., Reeves, C. E., Roca, R., de Rosnay, P., Schlager, H., Sultan, B., Tomasini, M., Ulanovsky, A., and ACMAD forecasters team: Large-scale overview of the summer monsoon over West Africa during the AMMA field experiment in 2006, Ann. Geophys., 26, 2569–2595, doi:10.5194/angeo-26-2569-2008, 2008.

Klinger, L. F., Greenberg, J., Guenther, A., Tyndall, G., Zimmerman, P., M'Bangui, M., Moutsamboté, J.-M., and Kenfack, D.: Patterns in volatile organic compound emissions along a savanna-rainforest gradient in central Africa, J. Geophys. Res., 103, D1, 1443–1454, doi:10.1029/97JD02928, 1998.

Lelieveld, J., Butler, T. M., Crowley, J. N., Dillon, T. J., Fischer, H., Ganzeveld, L., Harder, H., Lawrence, M. G., Martinez, M., Taraborrelli, D., and Williams, J.: Atmospheric

oxidation capacity sustained by a tropical forest, Nature, 452, 737–740, doi:10.1038/nature06870, 2008.

Levelt, P. F., van den Oord, G. H. J., Dobber, M. R., Mälkki, A., Visser, H., de Fries, J., Stammes, P., Lundell, J. O. V., and Saari, H.: The Ozone Monitoring Instrument, IEEE T. Geosci. Remote Sens., 44, 1093–1101, doi:10.1109/TGRS.2006.872333, 2006.

Mao, J., Jacob, D. J., Evans, M. J., Olson, J. R., Ren, X., Brune, W. H., St. Clair, J. M., Crounse, J. D., Spencer, K. M., Beaver, M. R., Wennberg, P. O., Cubison, M. J., Jimenez, J. L., Fried, A., Weibring, P., Walega, J. G., Hall, S. R., Weinheimer, A. J., Cohen, R. C., Chen, G., Crawford, J. H., McNaughton, C., Clarke, A. D., Jaeglé, L., Fisher, J. A., Yantosca, R. M., Le Sager, P., and Carouge, C.: Chemistry of hydrogen oxide radicals (HO_x) in the Arctic troposphere in spring, Atmos. Chem. Phys., 10, 5823–5838, doi:10.5194/acp-10-5823-2010, 2010.

Marais, E. A., Jacob, D. J., Kurosu, T. P., Chance, K., Murphy, J. G., Reeves, C., Mills, G., Casadio, S., Millet, D. B., Barkley, M. P., Paulot, F., and Mao, J.: Isoprene emissions in Africa inferred from OMI observations of formaldehyde columns, Atmos. Chem. Phys., 12, 6219-6235, doi:10.5194/acp-12-6219-2012, 2012.

Marais, E. A., Jacob, D. J., Wecht, K., Lerot, C., Kurosu, T. P., and Chance, K.: Anthropogenic emissions in Nigeria and air quality implications: a view from space, Submitted to Atmos. Environ. (*in review*), 2014.

Mayaux, P., Eva, H., Gallego, J., Strahler, A. H., Herold, M., Agrawal, S., Naumov, S., De Miranda, E. E., Di Bella, C. M., Ordoyne, C., Kopin, Y., and Roy, P. S.: Validation of the Global Land Cover 2000 map, IEEE T. Geosci. Remote Sens., 44, 1728-1739, doi: 10.1109/TGRS.2006.864370, 2006.

Millet, D. B., Jacob, D. J., Boersma, K. F., Fu, T.-M., Kurosu, T. P., Chance, K., Heald, C. L., and Guenther, A.: Spatial distribution of isoprene emissions from North America derived from formaldehyde column measurements by the OMI satellite sensor, J. Geophys. Res., 113, D02307, doi:10.1029/2007JD008950, 2008.

Murphy, J. G., Oram, D. E., and Reeves, C. E.: Measurements of volatile organic compounds over West Africa, Atmos. Chem. Phys., 10, 5281–5294, doi:10.5194/acp-10-5281-2010, 2010.

Olivier, J. G. J., Bouwman, A. F., van der Maas, C. W. M., Berdowski, J. J. M., Veldt, C., Bloos, J. P. J., Visschedijk, A. J. H., Zandveld, P. Y. J., and Haverlag, J. L.: Description of EDGAR Version 2.0: A set of global emission inventories of greenhouse gases and ozone-depleting substances for all anthropogenic and most natural sources on a per country basis and on 1×1° grid, Bilthoven, The Netherlands., 1996.

Olson, D. M., Dinerstein, E., Wikramanayake, E. D., Burgess, N. D., Powell, G. V. N., Underwood, E. C., D'Amico, J. A., Itoua, I., Strand, H. E., Morrison, J. C., Loucks, C. J., Allnutt, T. F., Rickets, T. H., Kura, Y., Lamoreux, J. F., Wettengel, W. W., Hedao, P.,

and Kassem, K. R.: Terrestrial ecoregions of the world: a new map of life on earth, BioScience, 51, 933–938, 2001.

Otter, L. B., Guenther, A., and Greenberg, J.: Seasonal and spatial variations in biogenic hydrocarbon emissions from southern African savannas and woodlands, Atmos. Environ., 36, 4265–4275, 2002.

Otter, L., Guenther, A., Wiedinmyer, C., Fleming, G., Harley, P., and Greenberg, J.: Spatial and temporal variations in biogenic volatile organic compound emissions for Africa south of the equator, J. Geophys. Res., 108, D13, 8505, doi:10.1029/2002JD002609, 2003.

Palmer, P. I., Jacob, D. J., Chance, K., Martin, R. V., Spurr, R. J. D., Kurosu, T. P., Bey, I., Yantosca, R., Fiore, A., and Li, Q.: Air mass factor formulation for spectroscopic measurements from satellites: Application to formaldehyde retrievals from the Global Ozone Monitoring Experiment, J. Geophys. Res., 106, D13, 14539–14550, doi:10.1029/2000JD900772, 2001.

Palmer, P. I., Jacob, D. J., Fiore, A. M., Martin, R. V., Chance, K., and Kurosu, T. P.: Mapping isoprene emissions over North America using formaldehyde column observations from space, J. Geophys. Res., 108, D6, 4180, doi:10.1029/2002JD002153, 2003.

Palmer, P. I., Abbot, D. S., Fu, T.-M., Jacob, D. J., Chance, K., Kurosu, T. P., Guenther, A., Wiedinmyer, C., Stanton, J. C., Pilling, M. J., Pressley, S. N., Lamb, B., and Sumner, A. L.: Quantifying the seasonal and interannual variability of North American isoprene emissions using satellite observations of the formaldehyde column, J. Geophys. Res., 111, D12315, doi:10.1029/2005JD006689, 2006.

Paulot, F., Crounse, J. D., Kjaergaard, H. G., Kroll, J. H., Seinfeld, J. H., and Wennberg, P. O.: Isoprene photooxidation: new insights into the production of acids and organic nitrates, Atmos. Chem. Phys., 9, 1479–1501, doi:10.5194/acp-9-1479-2009, 2009a.

Paulot, F., Crounse, J. D., Kjaergaard, H. G., Kürten, A., St Clair, J. M., Seinfeld, J. H., and Wennberg, P. O.: Unexpected epoxide formation in the gas-phase photooxidation of isoprene, Science, 325, 730–733, doi:10.1126/science.1172910, 2009b.

Paulot, F., Henze, D. K., and Wennberg, P. O.: Impact of the isoprene photochemical cascade on tropical ozone, Atmos. Chem. Phys., 12, 1307-1325, doi:10.5194/acp-12-1307-2012, 2012.

Pfister, G. G., Emmons, L. K., Hess, P. G., Lamarque, J.-F., Orlando, J. J., Walters, S., Guenther, A., Palmer, P. I., and Lawrence, P. J.: Contribution of isoprene to chemical budgets: A model tracer study with the NCAR CTM MOZART-4, J. Geophys. Res., 113, D05308, doi:10.1029/2007JD008948, 2008.

Pye, H. O. T., Pinder, R. W., Piletic, I. R., Xie, Y., Capps, S. L., Lin, Y.-H., Surratt, J. D., Zhang, Z., Gold, A., Luecken, D. J., Hutzell, W. T., Jaoui, M., Offenberg, J. H., Kleindienst, T. E., Lewandowski, M., and Edney, E. O.: Epoxide pathways improve model predictions of

isoprene markers and reveal key role of acidity in aerosol formation, Environ. Sci. Technol., doi:10.1021/es402106h, 2013.

Ren, X., Olson, J. R., Crawford, J. H., Brune, W. H., Mao, J., Long, R. B., Chen, Z., Chen, G., Avery, M. A., Sachse, G. W., Barrick, J. D., Diskin, G. S., Huey, L. G., Fried, A., Cohen, R. C., Heikes, B., Wennberg, P. O., Singh, H. B., Blake, D. R., and Shetter, R. E.: HO_x chemistry during INTEX-A 2004: Observation, model calculation, and comparison with previous studies, J. Geophys. Res., 113, D05310, doi:10.1029/2007JD009166, 2008.

Serça, D., Guenther, A., Klinger, L., Vierling, L., Harley, P., Druilhet, A., Greenberg, J., Baker, B., Baugh, W., Bouka-Biona, C., and Loemba-Ndembi, J.: EXPRESSO flux measurements at upland and lowland Congo tropical forest site, Tellus B, 53, 220–234, 2001.

Sharkey, T. D., and Yeh, S.: Isoprene emission from plants, Annu. Rev. Plant Physiol. Plant Mol. Biol., 52, 407-436, 2001.

Shim, C., Wang, Y., Choi, Y., Palmer, P. I., Abbot, D. S., and Chance, K.: Constraining global isoprene emissions with Global Ozone Monitoring Experiment (GOME) formaldehyde column measurements, J. Geophys. Res., 110, D24301, doi:10.1029/2004JD005629, 2005.

Spurr, R. J. D., Kurosu, T. P., and Chance, K. V.: A linearized discrete ordinate radiative transfer model for atmospheric remote-sensing retrieval, J. Quant. Spectrosc. Ra., 68, 689–735, 2001.

Stavrakou, T., Müller, J.-F., De Smedt, I., Van Roozendael, M., van der Werf, G. R., Giglio, L., and Guenther, A.: Evaluating the performance of pyrogenic and biogenic emission inventories against one decade of space-based formaldehyde columns, Atmos. Chem. Phys., 9, 1037–1060, doi:10.5194/acp-9-1037-2009, 2009.

Torres, O., Tanskanen, A., Veihelmann, B., Ahn, C., Braak, R., Bhartia, P. K., Veefkind, P., and Levelt, P.: Aerosols and surface UV products from Ozone Monitoring Instrument observations: An overview, J. Geophys. Res., 112, D24S47, doi:10.1029/2007JD008809, 2007.

Trainer, M., Williams, E. J., Parrish, D. D., Buhr, M. P., Allwine, E. J., Westberg, H. H., Fehsenfeld, F. C., and Liu, S. C.: Models and observations of the impact of natural hydrocarbons on rural ozone, Nature, 329, 705–707, 1987.

White, F.: The Vegetation of Africa - a descriptive memoir to accompany the UNESCO/AETFAT/UNSO vegetation map of Africa; Natural Resources Research Report XX; U. N. Educational, Scientific and Cultural Organization, 356 pp., Paris, 1983.

Yang, W., Shabanov, N. V., Huang, D., Wang, W., Dickinson, R. E., Nemani, R. R., Knyazikhin, Y., and Myneni, R. B.: Analysis of leaf area index products from combination of MODIS Terra and Aqua data, Remote Sens. Environ., 104, 297-312, doi:10.1016/j.rse.2006.04.016, 2006.

Chapter 4. Anthropogenic emissions in Nigeria and air quality implications: a view from space

Abstract

Satellite observations of formaldehyde (HCHO) and glyoxal (CHOCHO) over Nigeria reveal very large sources of anthropogenic non-methane volatile organic compounds (NMVOCs) from the Lagos megacity and oil/gas operations in the Niger Delta. This is supported by aircraft observations over Lagos. Satellite observations of methane also show very high values in the Niger Delta. Satellite observations of carbon monoxide (CO), nitrogen dioxide (NO_2), and aerosol show much weaker anthropogenic enhancements. This ensemble of satellite data reflects a very poorly managed energy system in a country with high population density and large fossil fuel resources. We estimate Nigerian anthropogenic emissions of 5.7 Tg C a^{-1} NMVOCs and 0.21 Tg N a^{-1} nitrogen oxides ($NO_x \equiv NO + NO_2$), leading to seasonal concentrations of surface ozone in excess of 80 ppbv during the dry season (December-February). Ozone pollution in Nigeria could greatly increase in the future with economic development and continued fast population growth. We project a 15-fold future increase in anthropogenic NO_x emissions if per capita power use increases to the current level of BRICS nations without emission controls. This would lead to severe ozone pollution and also to significant radiative forcing through convective pumping of Nigerian pollution to the upper troposphere.

4.1 Introduction

Nigeria is Africa's most populous country (170 million people as of 2012). Its population grew 60% between 1990 and 2008 and this growth is projected to continue, with population estimates for 2100 of 0.5-1 billion people (UN, 2013). Nigeria's 2012 GDP growth rate of 7% per year, forecast to continue (PwC, 2013), is amongst the highest in the world. The coastal megacity Lagos has higher emissions of non-methane volatile organic compounds (NMVOCs) than megacities in China and India (Hopkins et al., 2009). The oil and gas sector is a large source of pollution due to flaring (Ologunorisa, 2001; Osuji and Avwiri, 2005), illegal oil refining (EIA, 2012), gas leakage and venting (Hopkins et al., 2009), and frequent pipeline explosions (Minga et al., 2010; Fadeyibi et al., 2011). In the densely populated Niger Delta, where oil and gas extraction is concentrated, carcinogenic polycyclic aromatic hydrocarbon (PAH) concentrations are amongst the highest in the world (Ana et al., 2012). Pollution from mobile sources in Nigerian cities is exacerbated by inefficient vehicles, disorganized road networks, and traffic congestion (Assamoi et al., 2010; Hopkins et al., 2009). Inadequate electricity distribution results in dependence of industries and households on diesel-powered backup generators (BUGs), kerosene, and fuelwood (Ikeme and Ebohon, 2005; Akinlo, 2009).

Satellites provide a unique resource for observing atmospheric composition in a region such as Nigeria where ground-based information is sparse. In recent work we used formaldehyde (HCHO) observations from the space-based Ozone Monitoring Instrument (OMI) to map African emissions of isoprene, a volatile organic compound (VOC) emitted by vegetation that is in general the principal contributor to elevated HCHO in absence of open fires (Marais et al., 2012). However, we found that we could not retrieve isoprene emissions over Nigeria because of

extremely high HCHO of apparently anthropogenic origin, comparable to levels observed over China (Fu et al., 2007).

Here we conduct a comprehensive analysis of satellite observations of atmospheric composition over Nigeria, including not only HCHO but also carbon monoxide (CO), nitrogen dioxide (NO_2), glyoxal (CHOCHO), methane (CH_4), and aerosol optical depth (AOD). We also use limited aircraft measurements obtained during the African Monsoon Multidisciplinary Analysis (AMMA) campaign in 2006 (Hopkins et al., 2009; Redelspeger et al., 2006) and the Measurement of Ozone and Water Vapor aboard Airbus In-service Aircraft (MOZAIC) program in 2003 (Marenco et al., 1998). We interpret these data with the GEOS-Chem chemical transport model (CTM) in terms of the information they provide for Nigerian emissions, air quality, and climate implications.

4.2 Pollution sources and transport in Nigeria

Nigeria's geography ranges from humid landscapes along the Gulf of Guinea to the semi-arid Sahelian zone in the north. **Figure 4.1** shows the major population centers and industrial point sources. Highest population densities are in the northern state Kano, the southwestern state Lagos, and the Niger Delta states in the southeast. Metropolitan Lagos has a population of 21 million people and is growing at a rate of 670 000 people per year (Cocks, 2013). Baumbach et al. (1995) measured average benzene concentrations in Lagos of 80 ppbv, 8 times more than the highest concentrations found by Barletta et al. (2005) in Chinese cities. The majority of Nigeria's industry is concentrated in 5 cities – Kano and Kaduna in the north, Lagos in the southwest, and Warri and Port Harcourt in the Niger Delta.

Oil and gas extraction, including 2.1 million bbl/d (barrels per day) crude oil (3% of global production) and 28 billion m^3 associated gas (0.9%) in 2011, is concentrated in the Niger Delta. Up to
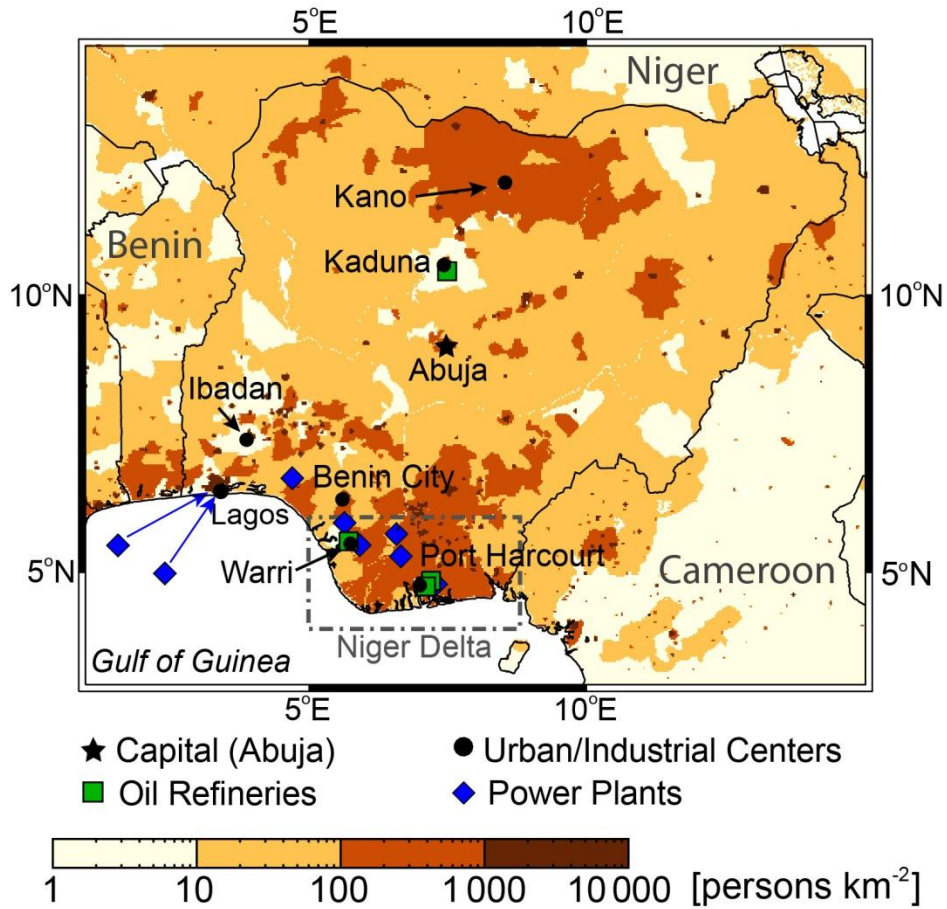
Figure 4.1: Map of Nigeria highlighting major emission centers. The population density map is for 2000 (CIESN, 2005).

70% of natural gas is lost by venting, leakage, or flaring (Ashton-Jones et al., 1998), as the oil extraction infrastructure was commissioned when natural gas had no marketability. Extensive pipeline networks transport crude oil from wells to export terminals and also link wells to refineries, but the latter only operate at 20% capacity due to mismanagement, poor maintenance, and pipeline vandalism (EIA, 2012). Low refining capacity has forced Nigeria to import more than 80 % of its refined products, while more than 80 % of extracted crude oil is exported (EIA, 2012). Theft of crude oil at

pipelines is between 100 000 and 400 000 bbl/d and much of this is refined illegally in the Niger Delta for local and international sale of kerosene, diesel, and bitumen (EIA, 2012).

Electricity generation in Nigeria includes oil- and gas-fueled thermal power plants and hydropower. Hydroelectric plants are concentrated in central Nigeria, while thermal power plants are close to industry in Lagos and oil extraction facilities in the Delta (**Figure 4.1**). Although coal fueled the industrialization of Nigeria in the early 20th century, most coal mines were abandoned following the Nigerian-Biafran civil war (1967-1970) (Oguejiofor, 2010). Inadequate supply of electricity and regular power outages have led to dependence on diesel for BUGs and kerosene for lighting. BUGs are used by 97 % of businesses and in 1990 accounted for 30 % of the nation's grid capacity (Ikeme and Ebohon, 2005). Fuelwood and waste burning, a source of energy for illegal oil refining in the Niger Delta and domestic use by rural populations, accounts for > 80 % of the country's energy consumption (Hyman et al., 1994; Maconachie et al., 2009; EIA, 2012).

Pollution emitted from this array of sources has different transport patterns depending on season. **Figure 4.2** shows 2006 surface winds and 500 hPa convective mass fluxes for the dry season (December-February – DJF) and wet season (June-August – JJA). The West African Monsoon (WAM) is a prominent feature in JJA over Nigeria. Deep convection is present year-round and shifts seasonally from the coast in January to central Nigeria in July. Coastal Nigeria is ventilated with oceanic air year-round. South-central Nigeria is highly susceptible to pollution events in DJF because of open fires, transport of urban/industrial effluent from the south, low winds, and temperature inversions associated with northeasterly (Harmattan) winds between 900-750 hPa (Sauvage et al., 2005).
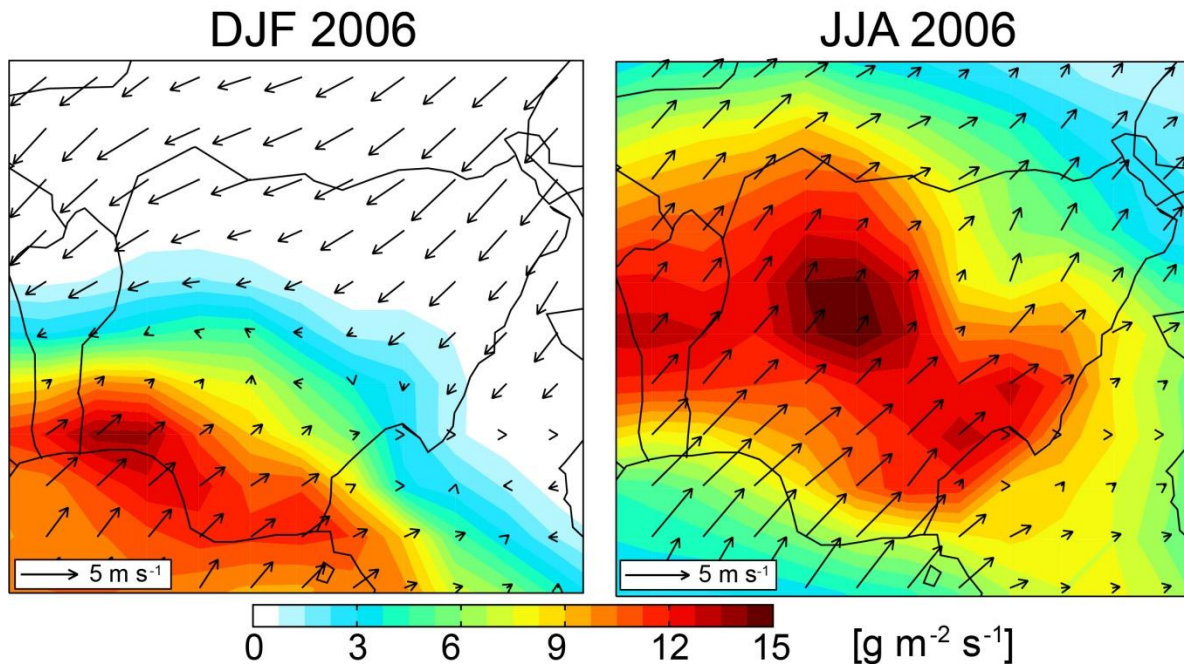
Figure 4.2: Surface winds and deep convection over Nigeria. Mean 0-1 km wind vectors (arrows) and 500 hPa convective mass fluxes (contours) are shown for winter (December-February) and summer (June-August) of 2006. Data are from NASA MERRA (Rienecker et al., 2011).

4.3 Atmospheric composition over Nigeria observed from space

Figure 4.3 shows annual mean satellite observations of atmospheric composition over Nigeria mapped on a 0.5×0.5° grid: CO from AIRS, tropospheric NO_2 and HCHO from OMI, CH_4 from SCIAMACHY, CHOCHO from GOME-2, and AOD (550 nm) from MISR. Sources of data are given in **Table 4.1**. Observations are averaged over 2005-2007, except for CHOCHO which is 2007 only as GOME-2 was launched in October 2006. MODIS Terra fire counts at 1×1 km^2 resolution, superimposed on AIRS CO, indicate the location of seasonal open fires. Gas flaring leads to enhanced levels of sulfur dioxide (SO_2) near oil fields (Obanijesu et al., 2009), but OMI SO_2 observations are close to the instrument detection limit and not included here.
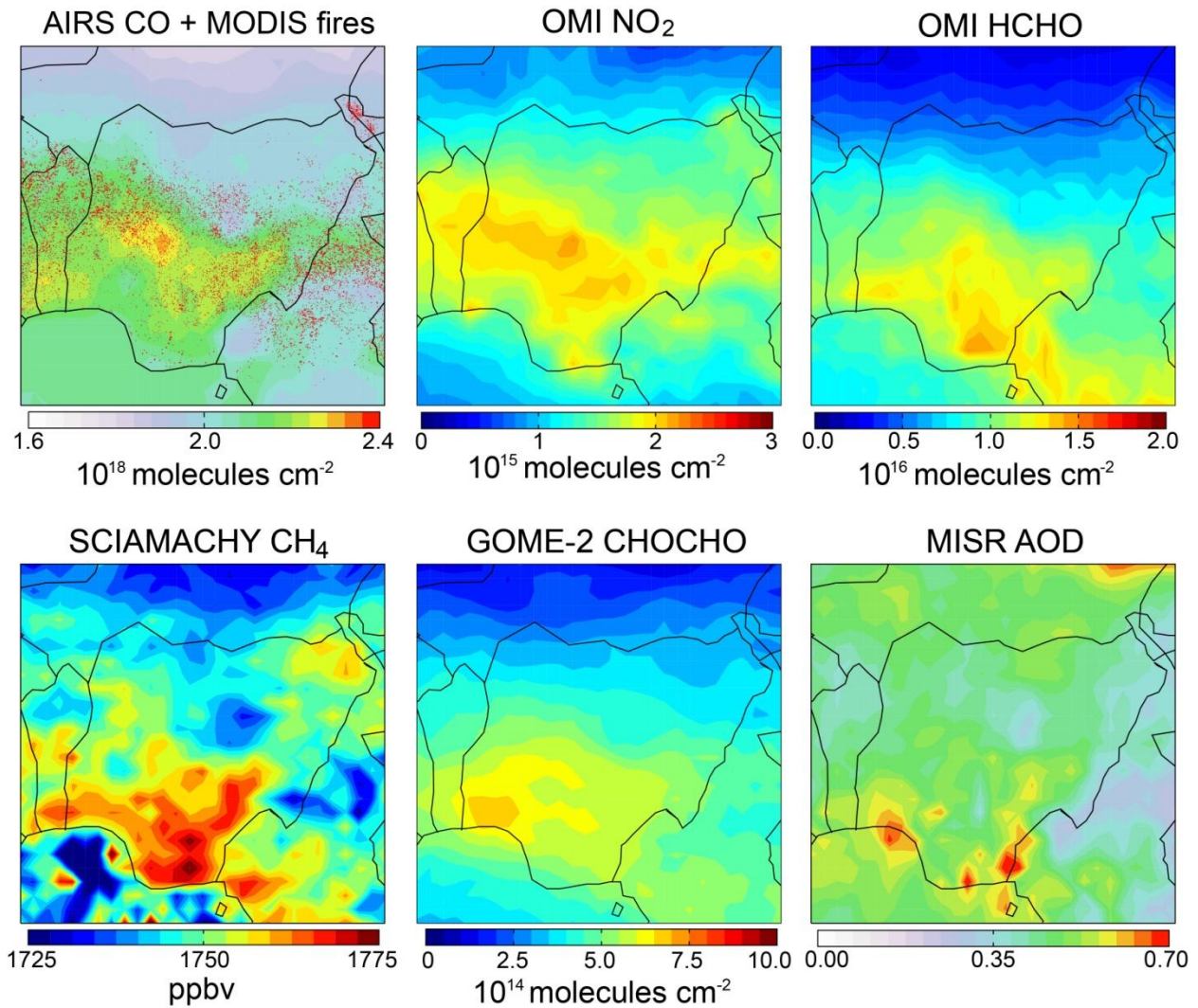
Figure 4.3: Satellite observations of atmospheric composition over Nigeria. Values are annual means for 2005-2007 (2007 only for CHOCHO) averaged on a $0.5 \times 0.5^{\circ}$ grid. They are atmospheric columns except for NO_2 (tropospheric column) and CH_4 (column-averaged mixing ratio). Individual fire counts at 1×1 km^2 are also shown. See **Table 4.1** for sources of data.

CO and NO_2 show dominant enhancements from seasonal open fires (October-March).

Urban and industrial activity in Lagos and the Niger Delta is also apparent in the NO_2

observations. AIRS CO has little sensitivity in the boundary layer (McMillan et al., 2011), which

may explain the lack of enhancement in urban regions.

Table 4.1: Satellite data used in this work

Species	Instrument	Product[a]	Reference
CO	AIRS[b]	NASA v5 L2	McMillan et al. (2011)
NO_2	OMI	ESA TEMIS v2 L2	Boersma et al. (2007)
CH_4	SCIAMACHY[c]	SRON/JPL v5.5	Frankenberg et al. (2011)
HCHO	OMI	NASA v2 L3	Kurosu (2008)
CHOCHO	GOME-2	Research Product	Lerot et al. (2010)
AOD[d]	MISR	NASA v4 L3	Martonchik et al. (2002)
Fire Counts	MODIS	NASA v5 L3	Giglio et al. (2003)

[a] v = version; L = level.
[b] Only daytime data are used as these have higher quality than nighttime data (Kopacz et al., 2010). A 10% downward correction is applied to correct for positive bias (Yurganov et al., 2008, 2010; Warner et al., 2010; McMillan et al., 2011).
[c] Includes empirical correction for a water-dependent bias in the SCIAMACHY CH_4 observations (Wecht et al., Estimate of North American methane emissions with high spatial resolution by adjoint inversion of SCIAMACHY satellite data, manuscript in preparation, 2013). Water vapor is obtained from the GEOS-5 meteorology.
[d] Aerosol optical depth

Satellite observations of HCHO over Africa generally show a dominant source from open fires and vegetation (Stavrakou et al., 2009; Marais et al., 2012). However, we find that HCHO in Nigeria is highest in the Delta and to a lesser extent over Lagos, indicating a dominant source from anthropogenic NMVOCs. CH_4 follows a similar pattern as HCHO, indicative of the oil/gas source. By contrast, CHOCHO is higher over Lagos than over the Delta. CHOCHO is not produced from oxidation of alkanes (a large fraction of oil/gas emissions; Gilman et al. (2013)) but has a high yield from oxidation of aromatics associated with vehicle emissions (Fu et al., 2008; Liu et al., 2012).

The satellite data indicate HCHO:NO_2 molar ratios of 6-8 over Lagos, whereas values for megacities in China and the US tend to be less than unity (Martin et al., 2004; Duncan et al., 2010; Witte et al., 2011). This reflects an unusually high NMVOC/NO_x emission ratio in Lagos,

as would be expected from the very inefficient energy infrastructure and lack of pollution control.

Aerosol optical depth (AOD) is highest over Lagos and the Delta, and is relatively localized. MISR distinguishes fine (<0.35 μm) and coarse (>0.7 μm) aerosols in its AOD retrieval. Fine aerosol (associated with combustion) generally dominates in Nigeria except in Lagos and the Sahel where coarse aerosol (dust) dominates.

The satellite data show large seasonality with generally much higher values in DJF than JJA, reflecting open fires in DJF and the efficient WAM ventilation in JJA. Data in JJA tend to be very noisy because of cloud cover. The seasonality is illustrated in **Figure 4.4** for NO_2. NO_2 is elevated over northern Nigeria (Sahel) in JJA and this may reflect stimulation of soil NO_x emission by precipitation following the dry season (Yienger and Levy, 1995; Jaegle et al., 2004). NO_2 is particularly high in the northeast corner, southwest of Lake Chad, which may be due to year-round crop cultivation together with mineral input from river systems and receding shorelines (Batello et al., 2004).

4.4 Constraints on Nigerian emissions

We use the GEOS-Chem global 3-D CTM (see **Appendix**) to simulate atmospheric composition over Nigeria and compare with aircraft and satellite observations. **Table 4.2** shows Nigerian emissions in the model, including corrections on the basis of observations as discussed below.

Some information on emissions from Lagos is offered by the AMMA aircraft campaign (Redelsperger et al., 2006). The BAe-146 aircraft flew over Lagos on Thursday 8 August 2006 in the late afternoon (1530-1700 local time). **Figure 4.5** compares observed and simulated
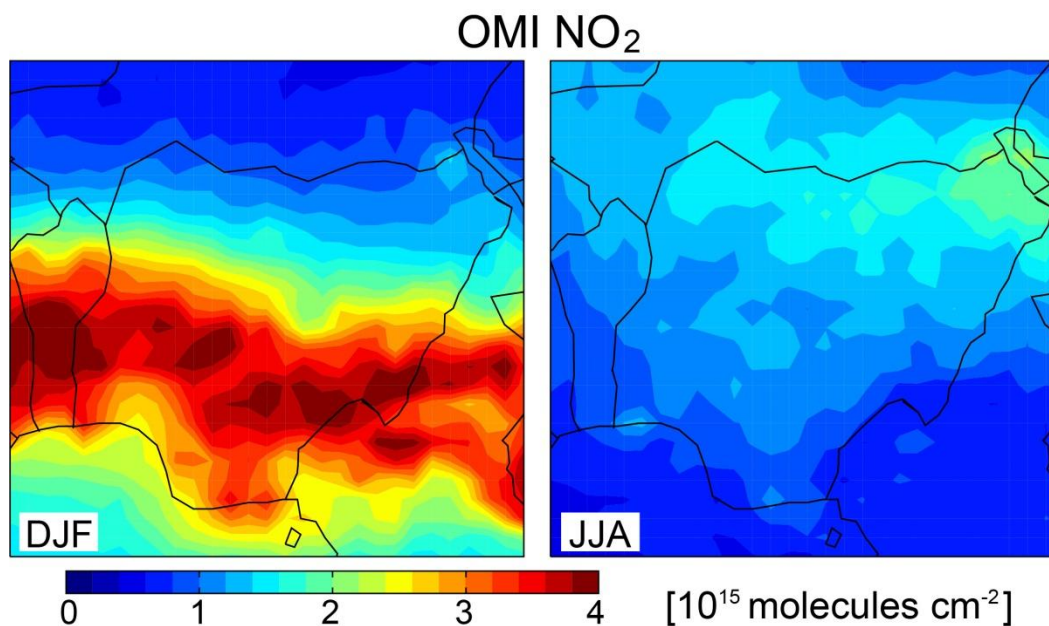
Figure 4.4: Seasonality of tropospheric NO_2 columns in Nigeria. Values are seasonal means for December-February and June-August 2005-2007 averaged on a 0.5×0.5^o grid.

boundary layer (<1 km) NMVOC and CO concentrations. GEOS-Chem uses RETRO (Schultz et al., 2007) as its default global inventory for anthropogenic NMVOC emissions, except for ethane which is from Xiao et al. (2008). We find that CO, ethane, propane, and acetone are well simulated. Other NMVOCs including higher alkanes and aromatics are underestimated several-fold, likely reflecting missing sources from vehicles and industry and consistent with other observations of elevated concentrations in Lagos (Baumbach et al., 1995, Hopkins et al,. 2009). Successful simulation of CO and short alkanes suggests that the model bias for NMVOCs reflects error in emissions rather than transport or dilution. We adjusted anthropogenic emissions throughout Nigeria by the corresponding factor bias and results are shown in **Figure 4.5**. The residual error is from chemical non-linearity and is within the uncertainty in the comparison.

Table 4.2: Annual emissions in Nigeria (2006)[a]

Species	Emission Inventory	Emissions
NO_x [Tg N a^{-1}]		**1.2**
Anthropogenic	Footnote *b*	0.21
Biofuel	Yevich and Logan (2003)	0.073
Open fires[c]	GFED v2	0.24
Soils	Footnote *d*	0.52
Lightning	Murray et al. (2012)	0.11
CO [Tg CO a^{-1}]		**27**
Anthropogenic	Footnote *e*	5.0
Biofuel	Yevich and Logan (2003)	5.3
Open fires[c]	GFED v2	17
NMVOCs [Tg C a^{-1}]		**6.4**
Anthropogenic + biofuel	Footnote *f*	5.7
Open fires	GFED v2	0.037
Biogenic	Footnote *g*	0.65
CH_4 [Tg a^{-1}]		**12**
Oil and Gas	Footnote *h*	5.5
Livestock	EDGAR v4.2	1.3
Waste	EDGAR v4.2	0.90
Wetlands	Picket-Heaps et al. (2011)	2.7
Other[i]	EDGAR v4.2	1.6

[a] Values used in the GEOS-Chem model, including corrections described in footnotes and in the text.

[b] Emissions in the standard GEOS-Chem model are 0.10 Tg N a^{-1} from the EDGAR v2.0 inventory and are increased here to 0.21 Tg N a^{-1} to include additional emissions from motorcycles and back-up generators (see Appendix).

[c] Open fire emissions of CO and NO_x in the standard GEOS-Chem model (6.2 Tg CO a^{-1} and 0.096 Tg N a^{-1}, respectively) are increased to improve agreement with AIRS CO and OMI NO_2.

[d] Emissions in the standard GEOS-Chem model are from Yienger and Levy (1995) and are increased here by 60% to improve agreement with OMI NO_2 in northern Nigeria. Fertilizer only accounts for 3% of soil NO_x emissions in Nigeria.

[e] Emissions in the standard GEOS-Chem model are 3.2 Tg CO a^{-1} from EDGAR v2.0 and are increased here to 5.0 Tg CO a^{-1} to include additional emissions from motorcycles and back-up generators (see Appendix).

[f] Includes ethane, propane, $\geq C_4$ alkanes, ethene, $\geq C_3$ alkenes, acetylene, benzene, toluene, xylenes, acetaldehyde, acetone, methyl ethyl ketone, and ethanol. Emissions in the standard GEOS-Chem model are 1.6 Tg C a^{-1} from RETRO and are increased here to 5.7 Tg C a^{-1} on the basis of AMMA aircraft observations (see text).

[g] Includes isoprene, acetone, ethene, and propene. Emissions in the standard GEOS-Chem model of 0.79 Tg C a^{-1} from MEGAN are adjusted here to 0.65 Tg C a^{-1} by decreasing emissions across the Sahel to match the HCHO and CHOCHO satellite data.

[h] Oil and gas emissions in the EDGAR v4.2 inventory are 1.7 Tg a^{-1} and are increased here to 5.5 Tg a^{-1} to match the levels observed by SCIAMACHY in southern Nigeria.

[i] Includes open fires, coal mining, biofuel, rice, and soils from EDGAR v4.2 (EC-JRC/PBL, 2011).
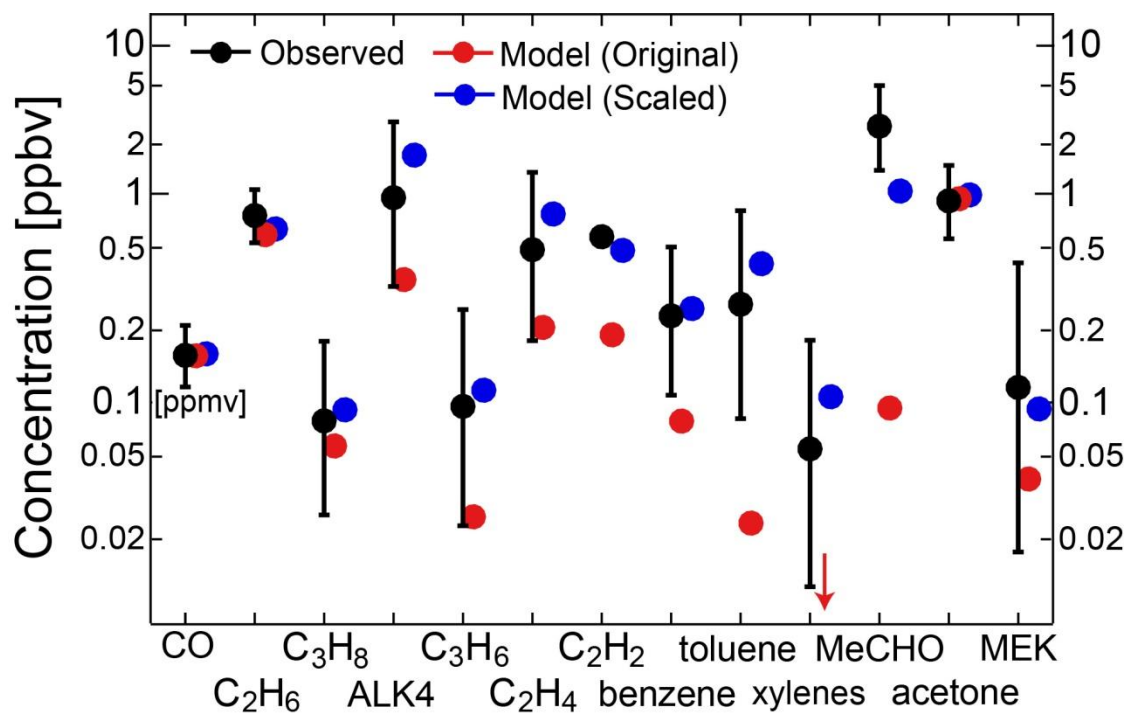
Figure 4.5: Concentrations of CO and NMVOCs over Lagos (< 1 km) on 8 August 2006 at 1530-1700 local time. Observations from the AMMA aircraft (black) are compared to GEOS-Chem results sampled at the time and location of the aircraft observations, using the standard GEOS-Chem emission inventories (red) and after scaling of emissions to correct for the bias (blue). Values are geometric means, with geometric standard deviations for the observations. Model points are offset for clarity. CO concentrations are ppmv. $C_2H_6 \equiv$ ethane, $C_3H_8 \equiv$ propane, ALK4 $\equiv \geq C_4$ alkanes, $C_3H_6 \equiv$ propene, $C_2H_4 \equiv$ ethene, $C_2H_2 \equiv$ acetylene, MeCHO $\equiv$ acetaldehyde, MEK $\equiv$ methyl ethyl ketone.

The resulting anthropogenic NMVOC emissions in Nigeria for 2006 are 5.7 Tg C a[-1]. From the stoichiometry of speciated emissions this translates into 7.6 Tg NMVOCs a[-1] (45 kg NMVOCs per capita). This can be compared to an estimated anthropogenic source of 23 Tg NMVOCs a[-1] from China (18 kg NMVOCs per capita) (Zhang et al., 2009).

Figure 4.6 shows the simulated annual GEOS-Chem atmospheric composition over Nigeria in 2006 for comparison to **Figure 4.3** sampled during the satellite overpass time. AIRS and SCIAMACHY averaging kernels have been applied to GEOS-Chem CO and CH_4, respectively. The model has a horizontal resolution of 2×2.5° while the observations in **Figure**

4.3 are on a 0.5×0.5° grid, so that fine-scale features in the observations can be diluted or

displaced in the model.

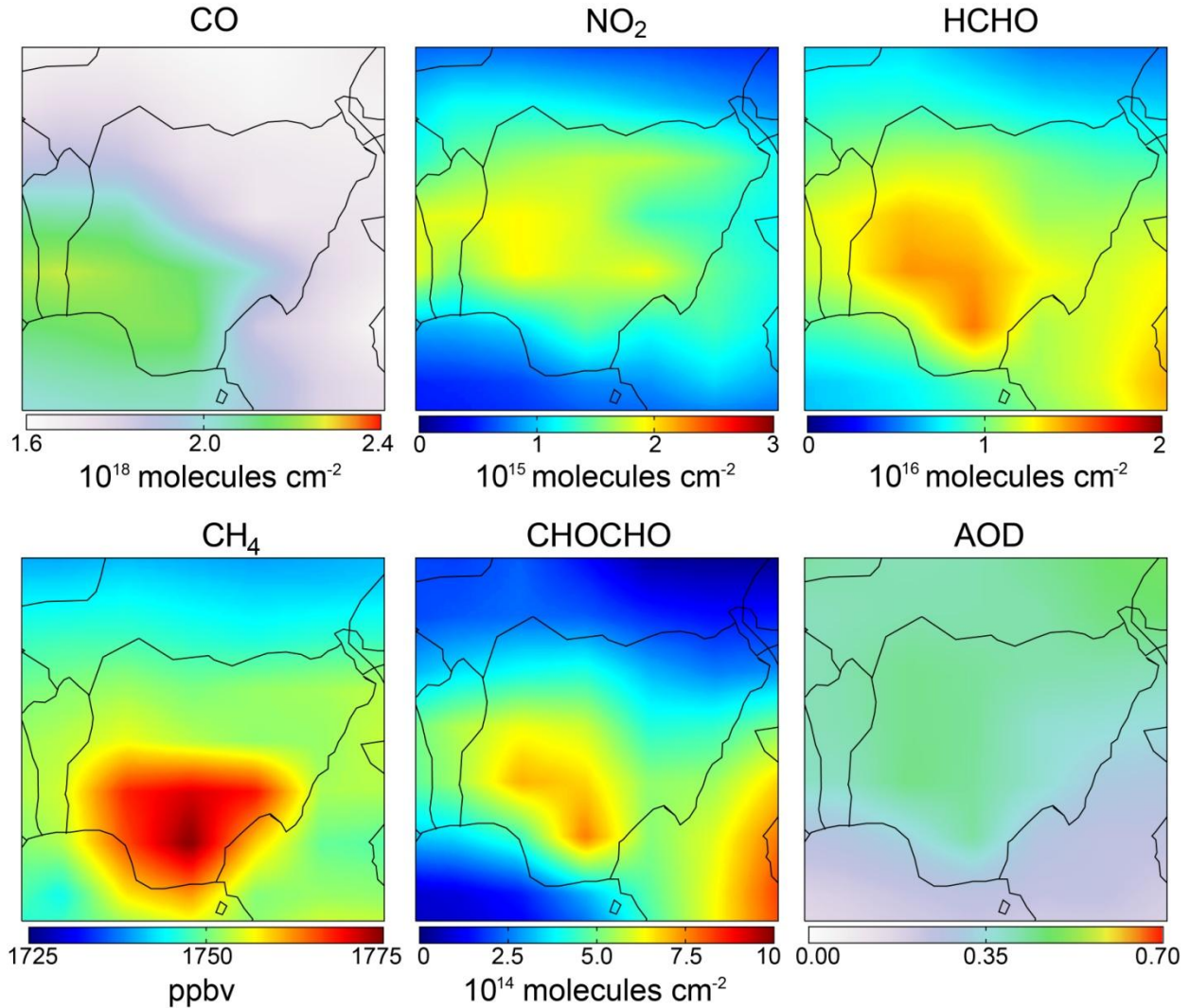**Figure 4.6**: GEOS-Chem simulation at 2×2.5° of the satellite observations in **Figure 4.3**. Values are annual means for 2006 and include total column CO weighted by the AIRS averaging kernels, tropospheric NO_2 column, HCHO column, column average CH_4 mixing ratios weighted by the SCIAMACHY averaging kernels, CHOCHO column, and AOD. The model is sampled during the satellite overpass time.

GEOS-Chem roughly reproduces the spatial distribution and magnitude of NO_2 and CO after increasing local open fire emissions of NO_x and CO (**Table 4.2**). The model does not reproduce the observed AOD hotspots in Lagos and the Niger Delta, and we attribute this to missing sources from road dust and anthropogenic organic aerosols.

The previously discussed increase of model anthropogenic NMVOC emissions to fit the AMMA data enables simulation of the observed OMI HCHO maximum over Lagos and the Niger Delta. The model background HCHO to the north is higher than observed and this possibly reflects an overestimate of biogenic NMVOC emissions. The model roughly reproduces the CHOCHO observations over Lagos but is too high in the Delta. Aromatics are the dominant anthropogenic source of CHOCHO (Liu et al., 2012), and were greatly increased in the model to match the AMMA aircraft data over Lagos (**Figure 4.5**). It may be that such an increase is not appropriate for the Delta as oil/gas emissions are dominated by alkanes. The CHOCHO and HCHO enhancement east of Nigeria is from oxidation of isoprene emitted in central Africa that is still too high after downscaling emissions there (**Table 4.2**).

The default anthropogenic inventory for CH_4 emissions in GEOS-Chem is EDGAR v4.2 but we find that it greatly underestimates the elevated CH_4 observed by SCIAMACHY in the Delta and across coastal Nigeria. These elevated levels are consistent in pattern with a large oil and gas source, likely reflecting extensive leakage. Reproducing the SCIAMACHY observations with GEOS-Chem, as shown in **Figure 4.6**, requires increasing Nigerian oil and gas emissions from 1.7 Tg a^{-1} in EDGAR v4.2 to 5.5 Tg a^{-1}.

4.5 Regional and global implications for ozone

In what follows we use GEOS-Chem with the Nigerian emissions of **Table 4.2** to examine regional and global implications for tropospheric ozone (O_3). **Figure 4.7** (top) shows mean surface daily maximum 8-hour average (MDA8) O_3 concentrations simulated for DJF and JJA in 2006. In DJF MDA8 O_3 in central Nigeria exceeds 80 ppbv. The high O_3 levels are coincident with the location of open fires (**Figure 4.3, 4.6**), but due to both open fires and coastal anthropogenic emissions. Omitting anthropogenic emissions in GEOS-Chem leads to equivalent O_3 levels in south-central Nigeria as a simulation without open fires. Coastal values are 60 ppbv in DJF and less than 40 ppbv in JJA. The low values in JJA reflect efficient ventilation (**Figure 4.2**). This is consistent with AMMA aircraft observations in the boundary layer over Lagos in August, which indicate a mean O_3 concentration of 30 ppbv; the model sampled along the AMMA flight tracks has a mean of 27 ppbv. The model is also consistent with MOZAIC (http://www.iagos.fr/) aircraft observations during ascents/descents at Lagos and Abuja airports. O_3 concentrations below 1 km are 40-60 ppbv in DJF and 20-30 ppbv in JJA in Lagos (Sauvage et al., 2005), while in Abuja O_3 averages 67 ppbv in DJF for observations in 2000-2004.

Nigeria is ventilated by deep convection throughout the year. Studies for the Southeast US have shown that interaction of convected NMVOCs with lightning NO_x produces elevated O_3 in the upper troposphere (Li et al., 2005; Cooper et al., 2006; Hudman et al., 2007, 2009) and one might expect similar behavior over Nigeria. To address this issue we evaluated GEOS-Chem with MOZAIC observations of NO and NO_y (defined as the sum of NO_x and its oxidation products) (Volz-Thomas et al., 2005) as well as O_3 (Thouret et al., 1998). NO_y observations over West Africa are available during the peak lightning season (April-September) in 2003. **Figure 4.8** shows mean cruise altitude (10-12 km) concentrations measured by MOZAIC together with
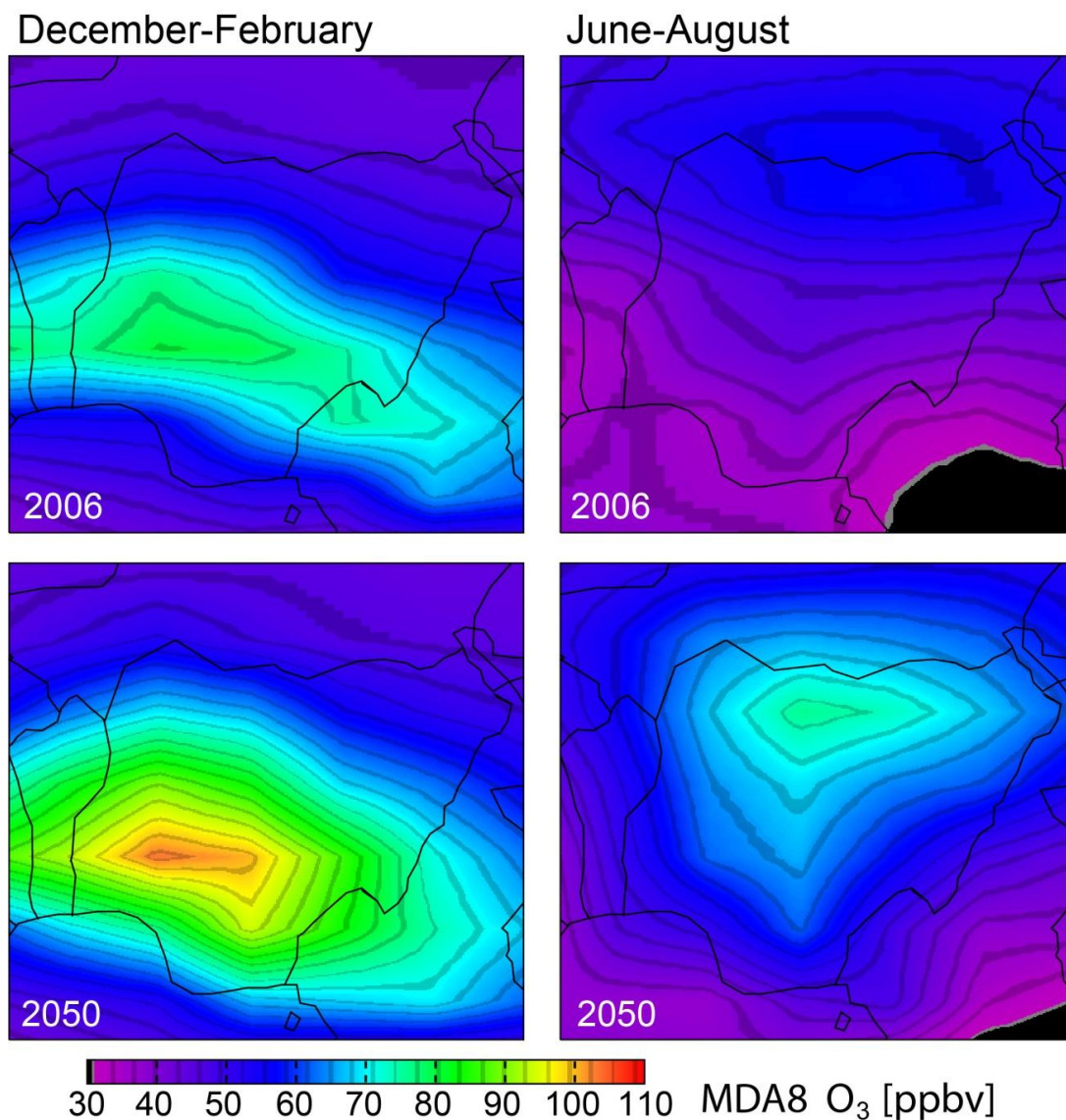
Figure 4.7: Mean daily maximum 8-hour average (MDA8) O_3 concentrations simulated by GEOS-Chem in surface air over Nigeria for December-February and June-August 2006 (top) and 2050 (bottom), assuming a 15-fold increase in Nigerian NO_x emissions from 2006 to 2050 (see text).

the corresponding model monthly averages (background). Observations of NO are only available

south of 14° N as the NO_y instrument measures NO for the first 30 min of each flight (Volz-

Thomas et al., 2005). GEOS-Chem captures the overall levels and latitudinal gradients of NO_y

the corresponding model monthly averages (background). Observations of NO are only available

south of 14° N as the NO_y instrument measures NO for the first 30 min of each flight (Volz-Thomas et al., 2005). GEOS-Chem captures the overall levels and latitudinal gradients of NO_y and O_3 concentrations. North of 30°N the observations are mainly in the stratosphere. Lightning contributes > 85 % NO and 60-70 % NO_y in GEOS-Chem south of Algeria. O_3 there is in the range 65-75 ppbv. Lightning enhances O_3 by 25 ppbv, while lofted anthropogenic NMVOCs enhance O_3 by 4 ppbv, as indicated by difference with sensitivity simulations including no lightning emissions and no Nigerian anthropogenic NMVOC emissions, respectively. The enhancement from lightning is larger than the 11-14 ppbv over the Southeast US (Cooper et al., 2006; Hudman et al., 2007).
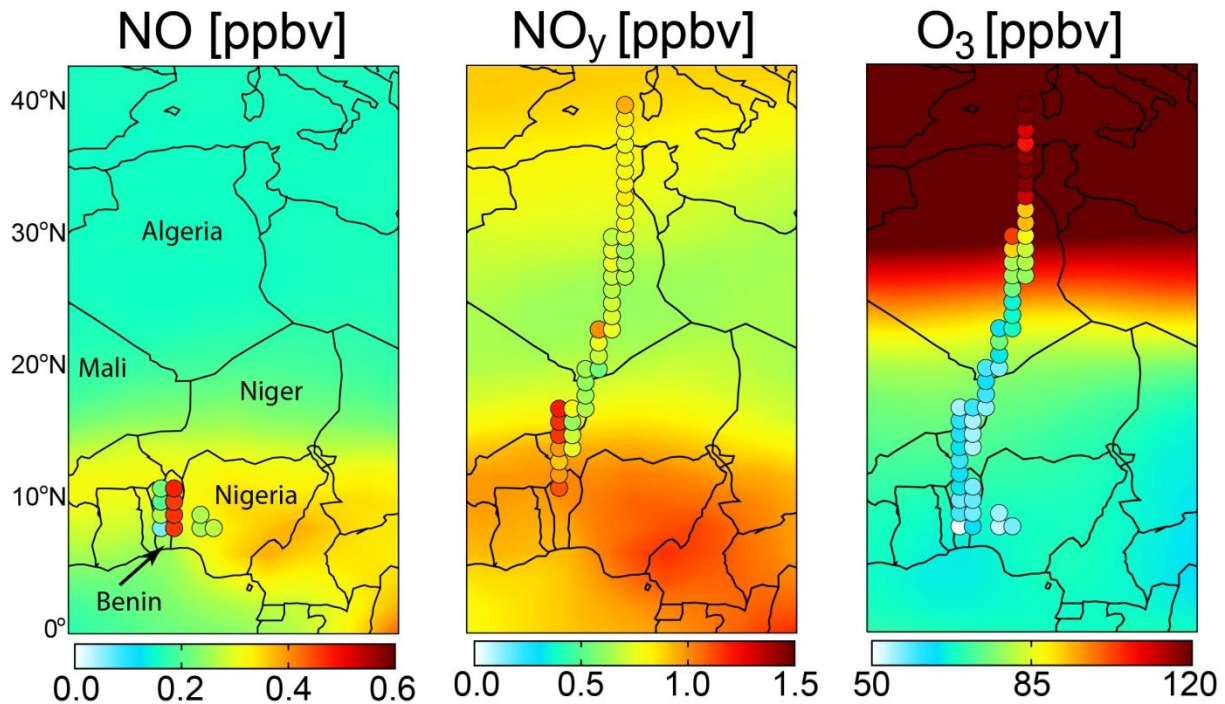

Figure 4.8: NO, NO_y, and O_3 concentrations at mean cruise altitude (10-12 km) over West Africa. Mean observations in April-September 2003 from MOZAIC (circles) are compared to corresponding GEOS-Chem values for 2006 (background). MOZAIC data are averaged on a 1×1° grid.

Nigeria has the potential to become the 13th largest world economy by 2050 if its current economic growth is sustained with a diversified economy, improved infrastructure, and strengthened institutions (PwC, 2013). Central to Nigeria's growth is development of its power sector. Current electricity production is 200 kWh per capita, which can be compared to 3 700 kWh per capita in China. The Nigerian government plans to grow the country's power sector with thermal power from natural gas in the short term and coal in the long term, with crude oil continuing to be mainly exported (GCFR, 2010). Current emerging economies Brazil, Russia, India, China, and South Africa (the so-called BRICS nations) had average electricity production of 2 100 kWh per capita in 2006. If Nigeria develops to a comparable level of electricity usage per capita by 2050 without emission controls we can estimate the corresponding NO_x emissions. Assuming a 2050 population of 400 million people (UN, 2013; PRB, 2012), a thermal efficiency of 30 %, and an average NO_x emission rate of 300 g NO_x GJ^{-1} for a 50:50 share in electricity from coal and natural gas with no emission controls (EPA, 1995), we derive a NO_x emission of 1.5 Tg N a^{-1}. This is 15 times higher than the 2006 EDGAR inventory value of 0.10 Tg N a^{-1} and higher than the 0.2-0.5 Tg N a^{-1} range of NO_x emissions in Nigeria projected by the Representative Concentration Pathways (RCP) scenarios for 2050 (van Vuuren et al., 2011). The RCP scenarios assume strict air pollution controls, which seems unlikely for Nigeria. NMVOC emissions from the power sector may increase in the future, but reduced leakage, venting and flaring of natural gas with the development of a local market may counteract this.

A 15-fold increase in Nigerian anthropogenic NO_x emissions by 2050 leads to a large increase in surface O_3, as shown by the bottom panel of **Figure 4.7**. The increase is displaced north of the coastal emissions by the prevailing winds in JJA (**Figure 4.2**). MDA8 O_3 exceeds 90 ppbv north of Lagos and the Delta in DJF. Nigeria may thus develop a serious O_3 air quality

problem in the future if economic development takes place without emission controls. Increasing NO_x emissions in Nigeria would also have significant climatic implications through changes in tropospheric oxidants (O_3, OH) on a global scale. NO_x emissions in the tropics are more efficient than emissions at mid-latitudes in affecting global O_3 and OH (Naik et al., 2007; Bowman and Henze, 2012). Bowman and Henze (2012) show that NO_x emissions in West Africa are amongst the most efficient in the world for driving radiative forcing by tropospheric O_3, likely reflecting deep convection in the WAM and consistent with our result of large O_3 sensitivity to NO_x in the upper troposphere over Nigeria.

4.6 Summary

Nigeria has a large and rapidly growing population, a massive oil/gas exploitation sector, and poorly functioning energy infrastructure. Little information is available on Nigerian air quality. Here we used an ensemble of satellite observations of atmospheric composition together with the GEOS-Chem model to better understand pollution sources and air quality in Nigeria and to make projections for the future.

Satellite observations of HCHO and CHOCHO indicate extremely high NMVOC emissions in the Lagos megacity and in the Niger Delta where oil and gas extraction is concentrated. HCHO is highest over the Delta while CHOCHO is highest over Lagos and downwind. The HCHO data imply considerable leakage of NMVOCs (mostly alkanes) from oil/gas extraction, and this is corroborated by satellite observations of CH_4. The CHOCHO data imply a large source of aromatic VOCs in Lagos, consistent with limited in situ data including an AMMA aircraft flight over Lagos. We estimate an anthropogenic NMVOC source of 5.7 Tg C a$^-$^{1} for Nigeria – higher on a per capita basis than China. We estimate a CH_4 source of 12 Tg CH_4

99

a^{-1}, 50 % higher than the standard EDGAR v4.2 inventory, likely reflecting extensive leakage from a poorly managed oil/gas production and distribution system.

Despite these extremely high NMVOC and CH_4 emissions, we find that other air quality-related emissions are not particularly high. Aerosol optical depths over Lagos and the Niger Delta are ~0.6 but localized; dust and organic aerosol appear to dominate. CO emissions are dominated by seasonal open fires. Anthropogenic NO_x emissions are much lower than in comparable urban/industrial areas of China or the US, reflecting the very inefficient power production system. The Lagos NO_x/NMVOCs ratio is considerably lower than in other megacities of the US or China.

Coastal Nigeria is ventilated by onshore flow year-round, and ventilation is further aided in JJA by convection during the West African Monsoon (WAM) over central Nigeria. However, south-central Nigeria is prone to pollution episodes in DJF due to restricted ventilation and the Harmattan inversion layer. GEOS-Chem simulations indicate mean surface MDA8 O_3 levels exceeding 90 ppbv in south central Nigeria in DJF, due to open fires and anthropogenic activity. MDA8 O_3 is less than 40 ppbv in JJA. Lightning NO_x enhances upper tropospheric O_3 over Nigeria by 25 ppbv.

Nigeria's rapid population growth and considerable fossil energy resources may have important future consequences for air quality and climate forcing. We estimate that future per capita economic development of Nigeria to the level of a BRICS nation will result in a 15-fold increase of anthropogenic NO_x emissions relative to present in the absence of emission controls. This could lead to very poor O_3 air quality (> 100 ppbv MDA8 O_3 in DJF) and significant climate forcing. On the other hand, a reduction of CH_4 fugitive emissions by using currently wasted CH_4 as a source of energy could abate the associated climate forcing.

References:

Akinlo, A. E.: Electricity consumption and economic growth in Nigeria: Evidence from cointegration and co-feature analysis, *J. Policy Model*., 31, 681-693, doi:10.1016/j.jpolmod.2009.03.004, 2009.

Ana, G. R. E. E., Sridhar, M. K. C., and Emerole, G. O.: Polycyclic aromatic hydrocarbon burden in ambient air in selected Niger Delta communities in Nigeria, *J. Air Waste Manage*, 62, 18-25, doi:10.1080/10473289.2011.628900, 2012.

Ashton-Jones, N.: The Human Ecosystem of the Niger Delta: An ERA Handbook, Environmental Rights Action (ERA), Ibadan, Nigeria, p. 137, 1998.

Assamoi, E-M., and Liousse, C.: A new inventory for two-wheel vehicle emissions in West Africa for 2002, *Atmos. Environ.*, 44, 3985-3996, doi:10.1016/j.atmosenv.2010.06.048, 2010.

Barletta, B., Meinardi, S., Rowland, F. S., Chan, C.-Y., Wang, X., Zou, S., Chan, L. Y., Blake, D. R.: Volatile organic compounds in 43 Chinese cities, *Atmos. Environ.*, 39, 5979-5990, doi:10.1016/j.atmosenv.2005.06.029, 2005.

Batello, C., Marzot, M., and Touré, A. H.: The Future is an Ancient Lake, FAO, Rome, Italy, 2004.

Baumbach, G., Vogt, U., Hein, K. R. G., Oluwole, A. F., Ogunsola, O. J., Olaniyi, H. B., and Akeredolu, F. A.: Air pollution in a large tropical city with a high traffic density – results of measurements in Lagos, Nigeria, *Sci. Total Environ*., 169, 25-31, 1995.

Boersma, K. F., Eskes, H. J., Veefkind, J. P., Brinksman, E. J., van der A, R. J., Sneep, M., van den Oord, G. H. J., Levelt, P. F., Stammes, P., Gleason, J. F., and Bucsela, E. J.: Near-real time retrieval of tropospheric NO_2 from OMI, *Atmos. Chem. Phys.*, 7, 2103-2118, doi:10.5194/acp-7-2103-2007, 2007.

Bowman, K., and Henze, D. K.: Attribution of direct ozone radiative forcing to spatially resolved emissions, *Geophys. Res. Lett.*, 39, L22704, doi:10.1029/2012GL053274, 2012.

CIESN (Center for International Earth Science Information Network), Gridded Population of the World, Version 3 (GPWv3) Data Collection, http://sedac.ciesin.columbia.edu/gpw/index.jsp, Columbia University, New York, 2005.

Cocks, T.: Will Nigerian boom babies feed prosperity or entrench poverty?, Reuters, http://www.reuters.com/article/2013/04/09/us-africa-summit-population-idUSBRE9380DH20130409, 9 April 2013, [Accessed 8 July 2013].

Cooper, O. R., Stohl, A., Trainer, M., Thompson, A. M., Witte, J. C., Oltmans, S. J., Morris, G., Pickering, K. E., Crawford, J. H., Chen, G., Cohen, R. C., Bertram, T. H., Wooldridge, P., Perring, A., Brune, W. H., Merrill, J., Moody, J. L., Tarasick, D., Nédélec, P., Forbes, G., Newchurch, M. J., Schmidlin, F. J., Johnson, B. J., Turquety, S., Baughcum, S. L.,

Ren, X., Fehsenfeld, F. C., Meagher, J. F., Spichtinger, N., Brown, C. C., McKeen, S. A., McDermid, I. S., and Leblanc, T.: Large upper tropospheric ozone enhancements above midlatitude North America during summer: In situ evidence from the IONS and MOZAIC ozone measurement network, *J. Geophys. Res.*, 111, D24S05, doi:10.1029/2006JD007306, 2006.

Duncan, B. N, Yoshida, Y., Olson, J. R., Sillman, S., Martin, R. V., Lamsal, L., Hu, Y., Pickering, K. E., Retscher, C., Allen, D. J., and Crawford, J. H.: Application of OMI observations to a space-based indicator of NO_x and VOC controls on surface formation, *Atmos. Environ.*, 44, 2213-2223, doi:10.1016/j.atmosenv.2010.03.010, 2010.

EC-JRC/PBL (European Commission, Joint Research Centre/Netherlands Environmental Assessment Agency PBL). Emission Database for Global Atmospheric Research (EDGAR), release version 4.2. http://edgar.jrc.ec.europa.eu, 2011.

EIA (US Energy Information Administration), Nigeria, http://www.eia.gov/countries/analysisbriefs/Nigeria/nigeria.pdf, Last Updated: October 16, 2012, [Accessed: 15 January 2013].

EPA (U.S. Environmental Protection Agency), Compilation of Air Pollutant Emission Factors, Volume 1: Stationary Point and Area Source, 5th Edition, Research Triangle Park, NC, January 1995.

Fadeyibi, I. O., Jewo, P. I., Opoola, P., Babalola, O. S., Ugburo, A., and Ademiluyi, S. A.: Burns and fire disasters from leaking petroleum pipes in Lagos, Nigeria: An 8-year experience, *Burns*, 37, 145-152, doi:10.1016/j.burns.2010.06.012, 2011.

Frankenberg, C., Aben, I., Bergamaschi, P., Dlugokencky, E. J., van Hees, R., Houweling, S., van der Meer, P., Snel, R., and Tol, P.: Global column-averaged methane mixing ratios from 2003 to 2009 as derived from SCIAMACHY: Trends and variability, *J. Geophys. Res.*, 116, D04302, doi:10.1029/2010JD014849, 2011.

Fu, T.-M.., Jacob, D. J., Palmer, P. I., Chance, K., Wang, Y. X., Barletta, B., Blake, D. R., Stanton, J. C., and Pilling, M. J.: Space-based formaldehyde measurements as constraints on volatile organic compound emissions in east and south Asia and implications for ozone, *J. Geophys. Res.*, 112, D06312, doi:10.10292/2006JD007853, 2007.

Fu, T.-M.., Jacob, D. J., Wittrock, F., Burrows, J. P., Vrekoussis, M., and Henze, D. K.: Global budgets of atmospheric glyoxal and methylglyoxal, and implications for formation of secondary organic aerosols, *J. Geophys. Res.*, 113, D15303, doi:10.1029/2007JD009505, 2008.

GCFR (Grand Commander in the Order of the Federal Republic): Roadmap for the Power Sector Reform, Federal Republic of Nigeria, http://www.nbet.com.ng/resources/power_sector_Roadmap_Full.pdf, August 2010, [Accessed: 28 May 2013].

Giglio, L., Descloitres, J., Justice, C. O., and Kaufman, Y. J.: An enhanced contextual fire detection algorithm for MODIS, *Remote Sens. Environ.*, 87, 273-282, doi:10.1016/S0034-4257(03)00184-6, 2003.

Gilman, J. B., Lerner, B. M., Kuster, W. C., and de Gouw, J. A.: Source signature of volatile organic compounds from oil and natural gas operations in northeastern Colorado, *Environ. Sci. Technol., 47,* 1297-1305, doi:10.1021/es304119a, 2013.

Hopkins, J. R., Evans, M. J., Lee, J. D., Lewis, A. C., Marsham, J. H., McQuaid, J. B., Parker, D. J., Stewart, D. J., Reeves, C. E., and Purvis, R. M.: Direct estimates of emissions from the megacity of Lagos, *Atmos. Chem. Phys.*, 9, 8471-8477, doi: 10.5194/acp-9-8471-2009, 2009.

Hudman, R. C., Jacob, D. J., Turquety, S., Leibensperger, E. M., Murray, L. T., Wu, S., Gilliland, A. B., Avery, M., Bertram, T. H., Brune, W., Cohen, R. C., Dibb, J. E., Flocke, F. M., Fried, A., Holloway, J., Neuman, J. A., Orville, R., Perring, A., Ren, X., Sachse, G. W., Singh, H. B., Swanson, A., and Wooldridge, P. J.: Surface and lightning sources of nitrogen oxides over the United States: Magnitudes, chemical evolution, and outflow, *J. Geophys. Res.*, 112, D12S05, doi:10.1029/2006JD007912, 2007.

Hudman, R. C., Murray, L. T., Jacob, D. J., Turquety, S., Wu, S., Millet, D. B., Avery, M., Goldstein, A. H., and Holloway, J.: North American influence on tropospheric ozone and the effects of recent emission reductions: Constraints from ICARTT observations, *J. Geophys. Res.*, 114, D07302, doi:10.1029/2008JD010126, 2009.

Hyman, E. L.: Fuel substitution and efficient woodstoves: Are they the answers to the fuelwood supply problem in northern Nigeria, *Environ. Manage.*, 18, 23-32, doi:10.1007/BF02393747, 1994.

Ikeme, J., and Ebohon, O. J.: Nigeria's electric power sector reform: what should form the key objectives?, *Energ. Policy*, 33, 1213-1221, doi:10.1016/j.enpol.2003.11.018, 2005.

Jaeglé, L., Martin, R. V., Chance, K., Steinberger, L., Kurosu, T. P., Jacob, D. J., Modi, A. I., Yoboué, V., Sigha-Nkamdjou, L., and Galy-Lacaux, C.: Satellite mapping of rain-induced nitric oxide emissions from soils, *J. Geophys. Res.*, 109, D21310, doi:10.1029/2004JD004787, 2004.

Kopacz, M., Jacob, D. J., Fisher, J. A., Logan, J. A., Zhang, L., Megretskaia, I. A., Yantosca, R. M., Singh, K., Henze, D. K., Burrows, J. P., Buchwitz, M., Khlystova, I., McMillan, W. W., Gille, J. C., Edwards, D. P., Eldering, A., Thouret, V. and Nédélec, P.: Global estimates of CO sources with high resolution by adjoint inversion of multiple satellite datasets (MOPITT, AIRS, SCIAMACHY, TES), *Atmos. Chem. Phys.*, 10, 855-876, doi:10.5194/acp-10-855-2010, 2010.

Kurosu, T. P.: OMI HCHO Readme File, http://www.cfa.harvard.edu/atmosphere/Instruments/OMI/PGEReleases/READMEs/OMHCHO_README.pdf, 1 May 2008, [Accessed: 1 August 2009].

Lerot, C., Stavrakou, T., De Smedt, I., Müller, J.-F., and Van Roozendael, M.: Glyoxal vertical columns from GOME-2 backscattered light measurements and comparisons with a global model, *Atmos. Chem. Phys.*, 10, 12059-12072, 2010.

Li, Q., Jacob, D. J., Park, R., Wang, Y., Heald, C. L., Hudman, R., Yantosca, R. M., Martin, R. V., and Evans, M.: North American pollution outflow and the trapping of convectively lifted pollution by upper-level anticyclone, *J. Geophys. Res.*, 110 D10301, doi: 10.1029/2004JD005039, 2005.

Liu, Z., Wang, Y., Vrekoussis, M., Richter, A., Wittrock, F., Burrows, J. P., Shao, M., Chang, C-C., Liu, S-C., Wang, H., and Chen, C.: Exploring the missing source of glyoxal (CHOCHO) over China, *Geophys. Res. Lett.*, 39, L10812, doi:10.1029/2012GL051645, 2012.

Maconachie, R., Tanko, A., and Zakariya, M.: Descending the energy ladder? Oil price shocks and domestic fuel choices in Kano, Nigeria, *Land Use Policy*, 26, 1090-1099, doi:10.1016/j.landusepol.2009.01.008, 2009.

Marais, E. A., Jacob, D. J., Kurosu, T. P., Chance, K., Murphy, J. G., Reeves, C., Mills, G., Casadio, S., Millet, D. B., Barkley, M. P., Paulot, F., and Mao, J.: Isoprene emissions in Africa inferred from OMI observations of formaldehyde columns, *Atmos. Chem. Phys.*, 12, 6219-6235, doi:10.5194/acp-12-6219-2012, 2012.

Marenco, A., Thouret, V., Nédélec, P., Smit, H., Helten, M., Kley, D., Karcher, F., Simon, P., Law, K., Pyle, J., Poschmann, G., Von Wrede, R., Hume, C., and Cook, T.: Measurement of ozone and water vapor by Airbus in-service aircraft: The MOZAIC airborne program, An overview, *J. Geophys. Res.*, 103, D19, 26 631-25 642, doi: 10.1029/98JD00977, 1998.

Martin, R. V., Fiore, A. M., and Van Donkelaar, A.: Space-based diagnosis of surface ozone sensitivity to anthropogenic emissions, *Geophys. Res. Lett.*, 31, L06120, doi:10.1029/2004GL019416, 2004.

Martonchik, J. V., Diner, D. J., Crean, K. A., and Bull, M. A.: Regional aerosol retrieval results from MISR, *IEEE Geosci. Remote*, 40, 1520-1531, doi: 10.1109/TGRS.2002.801142, 2002.

McMillan, W. W., Evans, K. D., Barnet, C. D., Maddy, E. S., Sasche, G. W., and Diskin, G. S.: Validating the AIRS Version 5 CO retrieval with DACOM *in situ* measurements during INTEX-A and -B, *IEEE Geosci. Remote*, 49, 2802-2813, doi: 10.1109/TGRS.2011.2106505, 2011.

Minga, A., Thouret, V., Saunois, M., Delon, C., Serça, D., Mari, C., Sauvage, B., Mariscal, A., Leriche, M., and Cros, B.: What caused extreme ozone concentrations over Cotonou in December 2005?, *Atmos. Chem. Phys.*, 10, 895-907, doi:10.5194/acp-10-895-2010, 2010.

Murray, L. T., Jacob, D. J., Logan, J. A., Hudman, R. C., and Koshak, W. J.: Optimized regional and interannual variability of lightning in a global chemical transport model constrained

by LIS/OTD satellite data, *J. Geophys. Res.*, 117, D20307, doi:10.1029/2012JD017934, 2012.

Naik, V., Mauzerall, D. L., Horowitz, L. W., Schwarzkopf, M. D., Ramaswamy, V., Oppenheimer, M.: On the sensitivity of radiative forcing from biomass burning aerosols and ozone to emission location, *Geophys. Res. Lett.*, 34, L03818, doi:10.1029/2006GL028149, 2007.

Obanijesu, E. O., Adebiyi, F. M., Sonibare, J. A., and Okelana, O. A.: Air-borne SO_2 pollution monitoring in the upstream petroleum operation areas of Niger-Delta, Nigeria, *Energ. Source. Part A*, 31, 223-231, 2009.

Oguejiofor, G. C.: Modeling of linear and exponential growth and decay equations and testing them on pre- and post-war-coal production in Nigeria: An operations research approach, *Energ. Source. Part B*, 5, 116-125, 2010.

Ologunorisa, T. E.: A review of the effects of gas flaring on the Niger Delta environment, *Int. J. Sust. Dev. World*, 8, 249-255, 2001.

Osuji, L. C., and Avwiri, G. O.: Flared gases and other pollutants associated with air quality in industrial areas of Nigeria: An overview, *Chem. Biodivers.*, 2, 1277-1289, doi: 10.1002/cbdv.200590099, 2005.

PRB (Population Reference Bureau), 2012 World Population Dataset, http://www.prb.org/pdf12/2012-population-data-sheet_eng.pdf, 2012, [Accessed: 13 July 2013].

PwC (Pricewaterhouse Coopers), http://www.pwc.com/en_GX/gx/world-2050/assets/pwc-world-in-2050-report-january-2013.pdf, World in 2050. The BRICs and beyond: prospects, challenges and opportunities, [Accessed: 26 April 2013].

Picket-Heaps, C. A., Jacob, D. J., Wecht, K. J., Kort, E. A., Wofsy, S. C., Diskin, G. S., Worthy, D. E. J., Kaplan, J. O., Bey, I., and Drevet, J.: Magnitude and seasonality of wetland methane emissions from the Hudson Bay Lowlands (Canada), *Atmos. Chem. Phys.*, 11, 3773-3779, doi:10.5194/acp-11-3773-2011, 2011.

Redelsperger, J.-L., Thorncroft, C. D., Diedhiou, A., Lebel, T., Parker, D. J., and Polcher, J.: African Monsoon Multidisciplinary Analysis (AMMA): An international research project and field campaign, *B. Am. Meteorol. Soc.*, 87, 1739–1746, doi:10.1175/BAMS-87-12-1739, 2006.

Rienecker, M. M., Suarez, M. J., Gelaro, R., Todling, R., Bacmeister, J., Liu, E., Bosilovich, M. G., Schubert, S. D., Takacs, L., Kim, G.-K., Bloom, S., Chen, J., Collins, D., Conaty, A., Da Silva, A., Gu, W., Joiner, J., Koster, R. D., Lucchesi, R., Molod, A., Owens, T., Pawson, S., Pegion, P., Redder, C. R., Reichle, R., Robertson, F. R., Ruddick, A. G., Sienkiewicz, M. and Woollen, J.: MERRA: NASA's Modern-Era Retrospective Analysis of Research and Applications, *J. Climate*, 24, 3624-3648, doi:10.1175/JCLI-D-11-00015.1, 2011.

Sauvage, B., Thouret, V., Cammas, J.-P., Gheusi, F., Athier, G., and Nédélec, P.: Tropospheric ozone over Equatorial Africa: regional aspects from the MOZAIC data, *Atmos. Chem. Phys.*, 5, 311-335, doi:10.5194/acp-5-311-2005, 2005.

Schultz, M.G., Backman, L., Balkanski, Y., Bjoerndalsaeter, S., Brand, R., et al.: REanalysis of the TROpospheric chemical composition over the past 40 years (RETRO) — A long-term global modeling study of tropospheric chemistry: Final Report, Jülich/Hamburg, Germany, August 2007.

Stavrakou, T., Müller, J.-F., De Smedt, I., Van Roozendael, M., van der Werf, G. R., Giglio, L., and Guenther, A.: Evaluating the performance of pyrogenic and biogenic emission inventories against one decade of space-based formaldehyde columns, *Atmos. Chem. Phys.*, 9, 1037-1060, doi:10.5194/acp-9-1037-2009, 2009.

Thouret, V., Marenco, A., Logan, J. A., Nédélec, P., and Grouhel, C.: Comparisons of ozone measurements from the MOZAIC airborne program and the ozone sounding network at eight locations, *J. Geophys. Res.*, 103, D19, 25695-25720, doi:10.1029/98JD02243, 1998.

UN (United Nations) Economic and Social Affairs, World Population Prospects: The 2012 Revision, http://esa.un.org/unpd/wpp/, New York, 2013, [Accessed: 13 July 2013].

Volz-Thomas, A., Berg, M., Heil, T., Houben, N., Lerner, A., Petrick, W., Raak, D., and Pätz, H.-W.: Measurements of total odd nitrogen (NO_y) aboard MOZAIC in-service aircraft: instrument design, operation and performance, *Atmos. Chem. Phys.*, 5, 583-595, doi:10.5194/acp-5-583-2005, 2005.

van Vuuren, D. P., Edmonds, J., Kainuma, M., Riahi, K., Thomson, A., Hibbard, K., Hurtt, G. C., Kram, T., Krey, V., Lamarque, J.-F., Masui, T., Meinshausen, M., Nakicenovic, N., Smith, S. J., and Rose, S. K.: The representative concentration pathways: an overview, *Climatic Change*, 109, 5-31, doi:10.1007/s10584-011-0148-z, 2011.

Warner, J. X., Wei, Z., Strow, L. L., Barnet, C. D., Sparling, L. C., Diskin, G., and Sachse, G.: Improved agreement of AIRS tropospheric carbon monoxide products with other EOS sensors using optimal estimation retrievals, *Atmos. Chem. Phys.*, 10, 9521-9533, doi:10.5194/acp-10-9521-2010, 2010.

Witte, J. C., Duncan, B. N., Douglass, A. R., Kurosu, T. P., Chance, K., and Retscher, C.: The unique OMI HCHO/NO_2 feature during the 2008 Beijing Olympics: Implications for ozone production sensitivity, *Atmos. Environ.*, 45, 3103-3111, doi:10.1016/j.atmosenv.2011.03.015, 2011.

Xiao, Y., Logan, J. A., Jacob, D. J., Hudman, R. C., Yantosca, R., and Blake, D. R.: Global budget of ethane and regional constraints on U.S. sources, *J. Geophys. Res.*, 113, D21306, doi:10.1029/2007JD009415, 2008.

Yevich, R., and Logan, J. A.: An assessment of biofuel use and burning of agricultural waste in the developing world, *Global Biogeochem. Cy.*, 17, 4, 1095, doi:10.1029/2002GB001952, 2003.

Yienger, J. J., and Levy II, H.: Empirical model of global soil-biogenic NO_x emissions, *J. Geophys. Res.*, 100, D6, 11447-11464, doi:10.1029/95JD00370, 1995.

Yurganov, L. N., McMillan, W. W., Dzhola, A. V., Grechko, E. I., Jones, N. B., and van der Werf, R.: Global AIRS and MOPITT CO measurements: Validation, comparison, and links to biomass burning variations and carbon cycle, *J. Geophys. Res.*, 113, D09301, doi:10.1029/2007JD009229, 2008.

Yurganov, L., McMillan, W., Grechko, E., and Dzhola, A.: Analysis of global and regional CO burdens measured from space between 2000 and 2009 and validated by ground-based solar tracking spectrometers, *Atmos. Chem. Phys.*, 10, 3479-2494, doi:10.5194/acp-10-3479-2010, 2010.

Zhang, Q., Streets, D. G., Carmichael, G. R., He, K. B., Huo, H., Kannari, A., Klimont, Z., Park, I. S., Reddy, S., Fu, J. S., Chen, D., Duan, L., Lei, Y., Wang, L. T., and Yao, Z. L.: Asian emissions in 2006 for the NASA INTEX-B mission, *Atmos. Chem. Phys.*, 9, 5131-5153, doi:10.5194/acp-9-5131-2009, 2009.

Appendix

GEOS-Chem Description

We use the GEOS-Chem chemical transport model (version 9-01-03, http://geos-chem.org) driven by GEOS-5 assimilated meteorological data from the NASA Global Modeling and Assimilation Office (GMAO). The GEOS-5 meteorological data have a native horizontal resolution of $0.5 \times 0.67°$ with 72 vertical pressure levels and 6-h temporal frequency (3-h for surface variables and mixing depths). We use data for year 2006 and degrade the horizontal resolution to $2 \times 2.5°$ for input to GEOS-Chem. All model results are for 2006 following one year of spinup for chemical initialization.

The simulations presented here include the standard GEOS-Chem representation of oxidant-aerosol chemistry as described for example by Mao et al. (2010). We added for this study chemical mechanisms for the oxidation of benzene, toluene, and xylenes (Calvert et al., 2002), and ethylene and acetylene (Saunders et al., 2003), as these are important reactive NMVOCs in Nigeria. We also conducted a separate GEOS-Chem simulation of CH_4 (Pickett-Heaps et al., 2011) for comparison with the SCIAMACHY CH_4 data.

Anthropogenic emissions of CO and NO_x in GEOS-Chem are from the EDGAR v2.0 inventory (Olivier et al., 1996) and biofuel NO_x and CO emissions are from the Yevich and Logan (2003) inventory. NO_x emissions from soils and fertilizer use are from Yienger and Levy (1995) as implemented by Wang et al. (1998). Open fire emissions are from GFED v2 with 8-day temporal resolution (van der Werf et al., 2006). We impose a cap of $1 \text{ g C m}^{-2} \text{ d}^{-1}$ on the biomass burn rate in central Africa to avoid spuriously high emissions. Anthropogenic NMVOC emissions, including biofuel use, are from the RETRO inventory (Schultz et al., 2007), except

ethane emissions which are from Xiao et al. (2008). Isoprene and biogenic acetone, ethene, and propene emissions are calculated with the MEGAN v2.1 inventory (Guenther et al., 2006) including modifications described in Marais et al. (2012). Lightning NO_x emission is as described by Murray et al. (2012).

Anthropogenic emission inventories for Nigeria do not properly account for motorcycles and diesel-powered backup generators (BUGs), which are important sources in Nigeria. Assamoi et al. (2010) developed a black carbon and organic carbon aerosol emission inventory for motorcycles in West Africa. Here we include these emissions and emissions of carbonyls, aromatic VOCs, NO_x, and CO using emission factors available for Vietnam (Oanh et al., 2012). We derive BUG emissions in Nigeria using the 2,400 MW installed capacity for 1999 estimated by the Nigerian Energy Commission (www.energy.gov.ng/) and emission factors from Gullet et al. (2006) and Sawant et al. (2007).

Further adjustment of emissions on the basis of the aircraft and satellite data over Nigeria is described in **Chapter 4** and **Table 4.2**.

References:

Assamoi, E-M., and Liousse, C.: A new inventory for two-wheel vehicle emissions in West Africa for 2002, *Atmos. Environ.*, 44, 3985-3996, doi:10.1016/j.atmosenv.2010.06.048, 2010.

Calvert, J., Atkinson, R., Becker, K. H., Kamens, R. M., Seinfeld, J. H., Wallington, T. J., and Yarwood, G.: The mechanisms of atmospheric oxidation of aromatic hydrocarbons, Oxford University Press, New York, 2002.

Guenther, A., Karl, T., Harley, P., Wiedinmyer, C., Palmer, P. I., and Geron, C.: Estimates of global terrestrial isoprene emissions using MEGAN (Model of Emissions of Gases and Aerosols from Nature), *Atmos. Chem. Phys.*, 6, 3181-3210, doi:10.5194/acp-6-3181-2006, 2006.

Gullet, B. K., Touati, A., Oudejans, L., and Ryan, S. P.: Real-time emission characterization of organic air toxic pollutants during steady state and transient operation of a medium duty diesel engine, *Atmos. Environ.*, 40, 4037-4047, doi:10.1016/j.atmosenv.2006.03.031, 2006.

Mao, J., Jacob, D. J., Evans, M. J., Olson, J. R., Ren, X., Brune, W. H., St. Clair, J. M., Crounse, J. D., Spencer, K. M., Beaver, M. R., Wennberg, P. O., Cubison, M. J., Jimenez, J. L., Fried, A., Weibring, P., Walega, J. G., Hall, S. R., Weinheimer, A. J., Cohen, R. C., Chen, G., Crawford, J. H., McNaughton, C., Clarke, A. D., Jaeglé, L., Fisher, J. A., Yantosca, R. M., Le Sager, P., and Carouge, C.: Chemistry of hydrogen oxide radicals (HO_x) in the Arctic troposphere in spring, *Atmos. Chem. Phys.*, 10, 5823–5838, doi:10.5194/acp-10-5823-2010, 2010.

Marais, E. A., Jacob, D. J., Kurosu, T. P., Chance, K., Murphy, J. G., Reeves, C., Mills, G., Casadio, S., Millet, D. B., Barkley, M. P., Paulot, F., and Mao, J.: Isoprene emissions in Africa inferred from OMI observations of formaldehyde columns, *Atmos. Chem. Phys.*, 12, 6219-6235, doi:10.5194/acp-12-6219-2012, 2012.

Murray, L. T., Jacob, D. J., Logan, J. A., Hudman, R. C., and Koshak, W. J.: Optimized regional and interannual variability of lightning in a global chemical transport model constrained by LIS/OTD satellite data, *J. Geophys. Res.*, 117, D20307, doi:10.1029/2012JD017934, 2012.

Oanh, N. T. K., Phuong, M. T. T., and Permadi, D. A.: Analysis of motorcycle fleet in Hanoi for estimation of air pollution emission and climate mitigation co-benefit of technology implementation, *Atmos. Environ.*, 59, 438-448, doi:10.1016/j.atmosenv.2012.04.057, 2012.

Olivier, J. G. J., Bouwman, A. F., van der Maas, C. W. M., Berdowski, J. J. M., Veldt, C., Bloos, J. P. J., Visschedijk, A. J. H., Zandveld, P. Y. J., and Haverlag, J. L.: Description of EDGAR Version 2.0: A set of global emission inventories of greenhouse gases and ozone-depleting substances for all anthropogenic and most natural sources on a per country basis and on 1×1° grid, Bilthoven, The Netherlands., 1996.

Picket-Heaps, C. A., Jacob, D. J., Wecht, K. J., Kort, E. A., Wofsy, S. C., Diskin, G. S., Worthy, D. E. J., Kaplan, J. O., Bey, I., and Drevet, J.: Magnitude and seasonality of wetland methane emissions from the Hudson Bay Lowlands (Canada), *Atmos. Chem. Phys.*, 11, 3773-3779, doi:10.5194/acp-11-3773-2011, 2011.

Saunders, S. M., Jenkin, M. E., Derwent, R. G., and Pilling, M. J.: Protocol for the development of the Master Chemical Mechanism, MCM v3 (Part A): tropospheric degradation of non-aromatic volatile organic compounds, *Atmos. Chem. Phys.*, 3, 161-180, doi:10.5194/acp-3-161-2003, 2003.

Sawant, A. A., Shah, S. D., Zhu, X., Miller, J. W., and Cocker, D. R.: Real-world emissions of carbonyl compounds from in-use heavy-duty diesel trucks and diesel Back-Up Generators (BUGs), *Atmos. Environ.*, 41, 4535-4547, doi:10.1016/j.atmosenv.2006.11.028, 2007.

Schultz, M.G., Backman, L., Balkanski, Y., Bjoerndalsaeter, S., Brand, R., et al.: REanalysis of the TROpospheric chemical composition over the past 40 years (RETRO) — A long-term global modeling study of tropospheric chemistry: Final Report, Jülich/Hamburg, Germany, August 2007.

Wang, Y., Jacob, D. J., and Logan, J. A.: Global simulation of tropospheric O_3-NO_x-hydrocarbon chemistry, 1. Model formulation, *J. Geophys. Res.*, 103, D9, 10713-10725, doi:10.1029/98JD00157, 1998.

van der Werf, G. R., Randerson, J. T., Giglio, L., Collatz, G. J., Kasibhatla, P. S., and Arellano, Jr., A. F.: Interannual variability in global biomass burning emissions from 1997 to 2004, *Atmos. Chem. Phys.*, 6, 3423-3441, doi:10.5194/acp-6-3423-2006, 2006.

Xiao, Y., Logan, J. A., Jacob, D. J., Hudman, R. C., Yantosca, R., and Blake, D. R.: Global budget of ethane and regional constraints on U.S. sources, *J. Geophys. Res.*, 113, D21306, doi:10.1029/2007JD009415, 2008.

Yevich, R., and Logan, J. A.: An assessment of biofuel use and burning of agricultural waste in the developing world, *Global Biogeochem. Cy.*, 17, 4, 1095, doi:10.1029/2002GB001952, 2003.

Yienger, J. J., and Levy II, H.: Empirical model of global soil-biogenic NO_x emissions, *J. Geophys. Res.*, 100, D6, 11447-11464, doi:10.1029/95JD00370, 1995.